UNIVERSITEIT VAN PRETORIA
UNIVERSITY OF PRETORIA
YUNIBESITHI YA PRETORIA

Ultra high-resolution climate simulations over the Stellenbosch wine producing region using a variable-resolution model

by
Belinda Roux

Submitted in partial fulfilment of the requirements
for the degree of

MASTER OF SCIENCE

in the
Faculty of Natural and Agricultural Sciences
University of Pretoria

April 2009

Ultra high-resolution climate simulations over the Stellenbosch wine producing region using a variable-resolution model

Belinda Roux

Supervisor: Dr. F.A. Engelbrecht
Department: Department of Geography, Geoinformatics and Meteorology
Faculty: Faculty of Natural and Agricultural Sciences
University: University of Pretoria
Degree: Master of Science

Summary

The study aims to generate a simulated, ultra high-resolution climatology over the southwestern Cape of South Africa, and in particular the Stellenbosch wine producing region, by the dynamical downscaling of observed synoptic-scale circulation. A variable-resolution global model, the conformal-cubic atmospheric model (CCAM), and a multiple-nudging strategy are applied in order to reach this goal. CCAM is employed in stretched-grid mode as a regional climate model (RCM) to simulate climate for the period 1976-2005 at four different spatial resolutions. Nudging from coarse-resoltion (2.5°in latitude and longitude), the model was first applied at a 60 km resolution over southern Africa in order to obtain a simulation of the synoptic-scale circulation over the region. Two higher resolution simulations, at 8 km and 1 km resolution, were obtained consecutively over the western and southwestern Cape, nudging from the 60 km and 8 km simulations, respectively. Finally, a 200 m simulation was performed over the Stellenbosch region. Because of the high computational requirements of high-resolution runs, each progressively higher resolution simulation is performed over a progressively smaller area of interest over which the spatial resolution is high. The simulations verify well against observed datasets, and generally capture the important climatic features over the area of interest. The 60 km CCAM simulation gives a good representation of the synoptic scale weather over southern Africa, with realistic seasonal circulation patterns and rainfall percentages as well as intra-annual rainfall totals over various regions. The mesoscale climate over the Western Cape of South Africa is captured by the 8 km simulation, especially with respect to seasonal variations in temperature and rainfall percentages - although the actual rainfall over the southwestern tip of the Western Cape is severely underestimated. The ultra high-resolution simulated diurnal cycle of temperature, relative humidity and screen level wind speed compared well against observations for the month of February. The CCAM climate simulations might not be accurate enough for some of the very sensitive studies of the wine industry, but it can have great value for the demarcation of areas which are climatically suited for viticulture and some more general viticultural studies. Ultra high-resolution climate parameter maps are presented for 1976-2005.

Ultra hoë -resolusie klimaat simulasies oor die Stellenbosch wyn produserende gebied deur gebruik te maak van 'n veranderlike-resolusie model

Belinda Roux

Promotor: Dr. F.A. Engelbrecht
Departement: Departement van Geografie, Geoinformatika en Meteorologie
Fakulteit: Fakulteit Natuur- en Landbouwetenskappe
Universiteit: Universiteit van Pretoria
Graad: Meester in Wetenskap

Opsomming

Hierdie studie poog om 'n gesimuleerde ultra hoë-resolusie klimatologie vir Suid Afrika se suidwes Kaap, en in besonder die Stellenbosch wyn produserende gebied, te genereer deur die dinamiese afskaling van waargenome sinoptiese sirkulasie. 'n Veranderlike-resolusie globale model, die konformies-kubiese atmosferiese model (CCAM) en 'n strategie van verskeie genestelde lopies is gebruik om hierdie mikpunt te bereik. CCAM word in gestrekte-rooster opstelling gebruik as 'n streeksklimaat model om die klimaat vir die periode 1976-2005 op vier verskillende ruimtelike resolusies te simuleer. 'n 60 km resolusie simulasie is aanvanklik oor suider Afrika geloop, genestel in 'n growwe resolusie (2.5°in lengte- en breedtegraad), om 'n simulasie van die sinoptiese sirkulasie oor die gebied te verkry. Twee hoër resolusie simulasies (8 km en 1 km) is opeenvolgend oor die wes- en suidwes Kaap geloop, onderskeidelik genestel in die 60 km en 8 km lopies. Laastens is 'n 200 m resolusie lopie oor die Stellenbosch gebied gedoen. Elke hoër resolusie simulasie is gedoen oor 'n toenemende kleiner area waarvan die ruimetlike resolusie hoog is oor die spesifieke gebied van belang - as gevolg van die hoë berekeningsvereistes van hoë-resolusie simulasies. Die simulasies vertoon goed teenoor waargenome datastelle en vang oor die algemeen die belangrike klimaatsverskynsels vas oor die area van belang. Die 60 km simulasie weerspieël die sinoptiese toestande oor suider Afrika in sirkulasie patrone sowel as seisonale en intra-jaarlikse reënval. Die mesoskaal klimaat oor die Wes-Kaap van Suid Afrika word goed saamgevat deur die 8 km simulasie, veral ten opsigte van die seisonale temperatuur en reënval persentasies, alhoewel die werklike reënval oor die suidwestelike punt van die Wes-Kaap erg onderskat word. Die ultra hoë-resolusie gesimuleerde daaglikse siklus van temperatuur, relatiewe vogtigheid en windspoed vir Februarie vertoon goed teenoor waargenome data. Die CCAM klimaat simulasies verskaf 'n goeie aanduiding van die klimaat oor die suidwes Kaap. Dit mag dalk nie akkuraat genoeg wees vir party uiters sensitiewe studies in die wynbedryf nie, maar dit het wel waarde om areas uit te lig wat volgens klimaat geskik is vir wynbou asook vir meer algemene wingerdkundinge studies. Ulra hoë-resolusie klimaat parameter kaarte is geproduseer vir 1976-2005.

I declare that the thesis that I hereby submit for the degree Master of Science in Meteorology at the University of Pretoria is my own work and has not previously been submitted by me for degree purposes at any other university or institution.

2009·04·30
DATE

Acknowledgments

Thank you to everybody that made this study possible.

1. My promoter Francois, for his support and excellent advice. You have taught me so much and I can always learn from you.
2. My wonderful husband Dawid, for all your love, understanding and support.
3. My parents for giving me the opportunity to study and setting a good example as well as the rest of my family and friends for their support.
4. For his patience and endless help with the model I would like to thank John McGregor at the CSIRO as well as Marcus Thatcher and the rest of the team there.
5. Albert Gazendam at the CSIR, for help with the computer cluster.
6. Christien Engelbrecht for supplying data and other administrative stuff she had to deal with.
7. My colleagues at the ARC-ISCW and especially Noelien, my "partner in crime".
8. Prof Rautenbach who gave me the opportunity to get into this project in the first place.
9. Most importantly to God, through Whom all things are possible.

Contents

List of Figures

Chapter 1

Introduction

1.1 Background

The southwestern Cape of South Africa is a major wine producing area for a variety of wines (Saayman, 2003), since its Mediterranean climate makes it the ideal location to grow a range of grapes. With its many wine farms it has become world-famous and have delivered numerous award-winning wines. The most important decision in wine quality is site selection (Smith and Whigham, 1999; Roberts, 1999). Thus, the availability of high quality climatological information at a high spatial resolution aids significantly in the site-selection of vineyards. Vineyards is the optimum spatial scale for climate monitoring for optimal cultivar choice for specific sites (Bonnardot et al, 2004).

Certain climatic conditions are required for the optimum physiological performance of vineyards, of which temperature is the most important climatic component when looking at indices to describe the viticultural potential of a region. Happ (1999) found that thermal indices based on hourly temperatures are sensitive discriminators of site differences. Their use should enable making better decisions in the process of selecting sites as well as the most suitable grape varieties to optimise flavour outcomes. Other climatic variables that also play a role are rainfall, humidity, sunshine duration and wind (Bonnardot et al, 2003). Another key concept is that of growing degree-days (GDD). This involves the heat summation (sum of all the degree days) above the physiological minimum of 10°C during the growing period of the grapevine (Winkler et al, 1974). Each degree a day averages above 10°C is considered a degree day. For example, if during a 24-hour period the average temperature is 17.5°C it will be equivalent to 7.5 degree days (17.5 minus 10). Higher temperatures, lower relative humidity, and higher wind speeds are detrimental to the vines (Happ, 1999). The wine industry is also interested in finding homogeneous areas with respect to soil, climate and topography. This is generally known as terroir.

There are a number of ways to obtain a high-resolution climatology for an area. One method is to spatially interpolate station data to a high-resolution grid. In the case of temperature, data features such as elevation, slope, aspect and distance to the oceans can be statistically incorporated in such an interpolation process. Examples of high-resolution climate data sets developed in this way are the South African Atlas of Agrohydrology and -Climatology (Shulze, 1997; 2007) and the recently constructed climate data set for the Western Cape by Joubert (2007). However, it is inevitable that the relatively low density of station data will impact negatively on such an interpolation. This is true in particular for variables such as relative humidity, hourly temperatures and wind speed and direction, which is not measured at the same density as minimum and maximum temperature and rainfall. As an alternative, a dynamic regional model may be used to simulate the climate for a large variety of variables at high resolution in both space and time.

A high resolution observed climatology is not available over the wine producing areas of South Africa since the weather station network is not dense enough and stations with long records are rare. Although satellite observations seem like a good alternative to station data, this is not available at a high enough spatial resolution for a long enough period to be used to define climate. Therefore, a project was initiated to apply a high-resolution numerical atmospheric model to simulate the meso-scale and micro-scale climates of wine producing areas in South Africa, in order to identify the ideal locations for vineyards, and more particularly, vine cultivars. Using a numerical model to simulate climate has the advantage of obtaining information of the complete range of variables required for the demarcation of wine-producing areas, at a high spatial resolution and with a continuous distribution in space. However, in order to be of use in vineyard location, the climate simulations need to be of ultra high resolution (spatial resolution of 1 km or higher). Simulations at such high resolution is unexplored in climate modelling and need to be verified thoroughly against observations before being applied.

In 2003 a project was initiated to use a fine resolution atmospheric model to simulate climate, where long observational records are absent, in order to identify the ideal locations for vineyards, and more particularly locations for vine cultivars, within the South African wine producing areas. The first model simulations were performed over the Stellenbosch region for the February months of 2000-2005, using the Regional Atmospheric Modelling System (RAMS) developed by the University of Colorado State in the USA. The simulations were performed at the Laboratoire de Météorologie Physique in France under supervision of Prof. S. Cautenet during three visits undertaken by Dr. V. Bonnardot and Ms. C. du Preez respectively. Although RAMS is well suited for ultra high-resolution simulations (e.g. Tremback and Walco, 2004) and good results were obtained using the model in the current project (Bonnardot et al 2002; Du Preez 2007) alternative models were considered for the project due to the time consum-

ing process and the high costs involved by running RAMS. The conformal-cubic atmospheric model (CCAM) developed by the Australian Commonwealth and Scientific Industrial Research Organisation (CSIRO) was found to be the most suitable and cost-effective model to be used for this purpose. A comparison between the two models indicated that CCAM had similar skill to RAMS, but could be completed at a much shorter time.

1.2 Regional Climate Modelling

The main method to simulate climate is by using global circulation models (GCMs) which gives a three-dimensional representation of the atmosphere (Giorgi et al, 1991; Engelbrecht and Rautenbach, 2000). Unfortunately GCMs have computational requirements which quickly become prohibiting with increasing spatial resolution. There are important meso-scale meteorological phenomena such as tropical cyclones and orography-induced rainfall patterns which cannot be adequately parameterized as subgrid-scale processes at the coarse spatial resolution employed by GCMs. This results in the need to employ high resolution regional models to simulate mesoscale phenomena (McGregor et al, 1993; McGregor 1997; Engelbrecht and Rautenbach, 2000).

Regional climate models (RCMs) provide a computationally feasible alternative to GCMs. RCMs simulate climate at high resolution over an area of interest, whilst being forced with GCM data at its lateral boundaries, or alternatively over the regions where the RCM has low resolution (in the case of variable-resolution global models). RCMs can improve climate simulations at the regional scale, especially in coastal regions and areas with complex topography (McGregor 1997; Wang et al, 2004). In South Africa, they can be very useful in areas such as the Little Karoo and South Coast where the topography of the area cause increased rainfall at high slopes and rain shadows in other places. Areas which are prone to sea breezes such as the Namibian and Natal coast as well as areas of steep topography such as the Darkenberg ranges (where catabatic and anabatic winds occur) can also benefit from the improved resolution of a mesoscale model. Another area where a RCM can be useful is on the escarpment where the interaction of synoptic and mesoscale circulation can lead to heavy thunderstorms (Engelbrecht and Rautenbach, 2000; Engelbrecht et al, 2002). An important prerequisite for a successful RCM simulation, is that the GCM in which it is nested should give a realistic description of the synoptic scale circulation (McGregor, 1997).

RCMs have been used successfully to simulate the main features of southern African climate at a regional scale, and also to obtain projections of future climate over the region. The CSIRO Division of Atmospheric Research limited-area model (DARLAM) was used to perform climate simulations for January and July over the SADC region. Nine separate model simulations were performed for both January and July (Engelbrecht et al, 2002). The same model was used

to obtain projections of future climate over southern Africa for the 2030s and 2060s (Olwoch et al, 2008). High-resolution 30 year simulations of present and future climate over southern Africa were obtained using CCAM (Engelbrecht, 2005, 2009; Reason et al, 2006). Ten years of present-day and ten years of future climate over southern Africa were also simulated using NCAR Mesoscale Model (MM5) and UK Met Office PRECIS (Providing REgional Climates for Impacts Studies) regional climate model (Tadross et al, 2005; Reason et al, 2006). In all these RCM studies over southern Africa, the models were typically applied at spatial resolutions of about 0.5°, which is a resolution about five times higher than that of a typical GCM. Note, however, that a resolution of 0.5° is considerably lower than the ultra high-resolution simulations that are needed to be of use in vineyard location.

1.3 The Conformal-cubic atmospheric model

CCAM is regarded as a state-of-the-art RCM. It makes use of an efficient semi-implicit semi-Lagrangian technique to solve the atmospheric equations and also includes a comprehensive range of physical parametrization schemes (McGregor and Dix, 2001; McGregor, 2005). CCAM currently makes use of the hydrostatic approximation. The hydrostatic approximation fundamentally consists of neglecting the vertical acceleration term in the vertical momentum equation (Engelbrecht et al, 2007).

CCAM is a global circulation model, but it can be used as an RCM when applying it at high spatial resolution over an area of interest by running the model in stretched-grid variable-resolution mode (e.g. McGregor and Nguyen, 2003; Engelbrecht et al, 2009). Variable-resolution global modelling is an extremely flexible method of dynamic downscaling, essentially requiring only sea-surface temperatures (SSTs) and possibly far-field winds from the host model or host analysis (e.g. McGregor and Dix, 2001; Wang et al, 2004; Engelbrecht et al, 2009). A more detailed description of the model is provided in Chapter 2.

CCAM has been used for a number of studies in South Africa. Engelbrecht (2005) has used CCAM to obtain simulations of climate and climate change over Southern Africa for the periods 1975-2005 and 2070-2100, applying the model as an RCM at a horizontal resolution of about 60 km over southern Africa. The observed regional characteristics of the maximum and minimum temperature and rainfall distribution over southern Africa were well-represented in the present-day CCAM climate simulation (Engelbrecht, 2005). The model also simulated the intra-annual cycle in rainfall and circulation over the region well (Engelbrecht et al, 2009). CCAM has been applied at even higher (15 km) spatial resolution over southern Africa, for the purpose of short-range weather forecasting (Rautenbach et al, 2005; Potgieter, 2006). For the the short-range forecasts verified by Potgieter (2006), it was found that CCAM outperforms 24-hr persistence forecasts over a four-day integration period (Potgieter, 2006).

1.4 Objectives of the research

As discussed in section 1.1, site location is of primary importance in wine production. For the optimum location of vineyards and grape varieties, high-resolution climate data is required. However, the spatial density of weather stations is too low and the length of data records too short in order to sufficiently describe the meteorological variables used in determining vineyard location over the southwestern Cape of South Africa. This study therefore aims to use an RCM to simulate the climate of the southwestern Cape, and the Stellenbosch wine producing region in particular, at ultra-high spatial resolution. In order to reach this goal, the study had the following objectives:

To simulate climate of the southwestern Cape at a spatial resolution high enough to be used in the site location of vineyards.

In order to reach this objective, it was necessary to follow a multiple-nudging approach, where synoptic-scale reanalysis data was dynamically downscaled over the wine producing regions of the southwestern Cape. The coarsest resolution simulation had a resolution 60 km over southern Africa, was nudged within observed reanalysis data, and was used to force an 8 km simulation over the Western Cape. The latter simulation was used to force 1 km simulation over the southwestern Cape, in which a 200 m simulation over the Stellenbosch wine producing region was nudged. All the simulations were performed for the 30 year period 1976-2005. The simulations were performed on a powerful computer cluster of the Council for Scientific and Industrial Research (CSIR) in South Africa.

To verify the climate simulations against observations

The model simulation of synoptic-scale circulation and rainfall patterns was verified against observed and reanalysis data. The simulation of meso-scale climatological patterns was compared against gridded data of the Climatic Research Unit (CRU), whilst point-verification was performed for the 1 km and 200 m simulations, by comparing these against available station data.

To use the high-resolution CCAM simulations to obtain a description of the meso- and micro-scale climate of the Stellenbosch wine-producing area.

Once model biases were identified and model strenghts were determined, the gridded fields for a number of model variables, and additional derived variables, were constructed in order to describe climate of the Stellenbosch wine producing region at high spatial resolution.

Determine the value of the simulated climate data for the demarcation of wine producing regions.

Based on the verification results and the high-resolution climate fields, the value of the simulated climate data in demarcating sites for vineyard location was evaluated.

1.5 Organisation of the report

The literature review (Chapter 2) commences with a overview of viticulture in South Africa, including aspects such as the location of the vineyards and the main wine grape varieties found in the country. It is followed by a discussion on the concept of terroir as well as viticultural requirements, from which it becomes apparent that temperature and humidity are two of the most important climatic variables influencing the quality of the grapes and consequently the wine. The two main approaches of regional climate modelling are examined, namely nested limited-area modelling and variable resolution global modelling. This is followed by a discussion of history and status quo of regional climate modelling in South Africa. Chapter 2 ends with a discussion of CCAM and describes the climate modelling experiments performed to date in South Africa using this model.

In Chapter 3 the observed data used in the verification of the model simulations are described. This entails the National Center for Environmental Prediction (NCEP) reanalysis data used to verify the synoptic-scale (60 km) simulation over southern Africa; the CRU data used for verification of the meso-scale (8 km) simulation, and the weather station data used for verification of the ultra high-resolution (1 km and 200 m) simulations. The various model configurations over southern Africa and the southwestern Cape are discussed, with emphasis on the nudging techniques used to perform the simulations at different spatial resolutions ranging from 60 km to 200 m. The chapter concludes with a description of the computing infrastructure at the CSIR, which was essential for successfully performing the simulations.

The climate simulations at the different spatial resolutions are verified in Chapter 4. The chapter commences with an overview of model verification. The 60 km simulation is then verified by comparing the simulated rainfall to observed CRU data and the simulated circulation patterns to NCEP reanalysis data. After an inter-comparison between the 8 km and 60 km simulations, the 8 km simulation is verified against CRU observed data in terms of rainfall, temperature, relative humidity and 10 m wind speed. The 1 km resolution simulation is examined with regard to the simulated monthly-averaged diurnal variation in a temperature as well as the monthly rainfall totals. The simulation is compared for a number of locations against the long-term average observations obtained from weather station data. A more in depth comparison is made for February,

a month of great importance for the wine industry, by considering and comparing temperature, wind speed, and relative humidity of the 200 m simulation as well as the 1 km simulation. In conclusion a number climate parameter maps that may be of value for the demarcation of vineyards are presented. Conclusions on the ultra high-resolution climate simulations and applications for the site-location of vineyards are presented in Chapter 5.

Chapter 2

Literature review

2.1 Viticulture in South Africa

2.1.1 Climate of the southwestern Cape

The southwestern Cape consists of a mixture of coastal plains and folded mountains, which mostly exceed 600 m in altitude (Schulze, 1996; Du Preez, 2006). For the purpose of this discussion the "Western Cape" refer to the Provence and the "southwestern Cape" is the south-western part of Western Cape. "The domain" refers to the focus area of the high resolution study (around False Bay, Cape Town and Stellenbosch) and have dimensions of around 18°E-19°E and 33.6°S-24.5°S. Table Mountain is to the west of Cape Town, with a top height of over 1000 m above sea-level. To the east of the domain the Drakenstein Mountains (Near Paarl and Stellenbosch) and the Hottentots-Holland Mountains (to the east of False Bay) are to be found - both with a highest point of more than 1500 m above sea-level. In between Table Mountain and the ranges to the east is a wide area of low altitude, known as the Cape Flats. Due to the mountainous nature of the southwestern Cape, there is a great variety in the meso-scale climate (Kruger, 2004). The Atlantic ocean surrounds the southwestern Cape to the west and south, with False Bay to the south and Table Bay to the west of the Cape Flats. There is a significant difference in sea surface temperatures between Table Bay and False Bay, caused by the cold Benguela current and warm Agulhas current, respectively (Bonnardot et al, 2002; Du Preez, 2006). Figure 2.1 shows the topography of the southwestern Cape.

The southwestern Cape is a winter rainfall area that is marked by warm, dry summers and cool, wet winters. The average annual rainfall is 600 mm with most of the rain occurring from May to September. The rainfall occurs mainly due to frontal depressions. Heavy orographic rains occur at the Hottentots-Holland and Drakenstein ranges, and can exceed 1500 mm a year (Schulze, 1996). In Cape Town, June is the month with the highest average monthly rainfall (93 mm) and the driest month is November with 14 mm (SAWS Climate data,

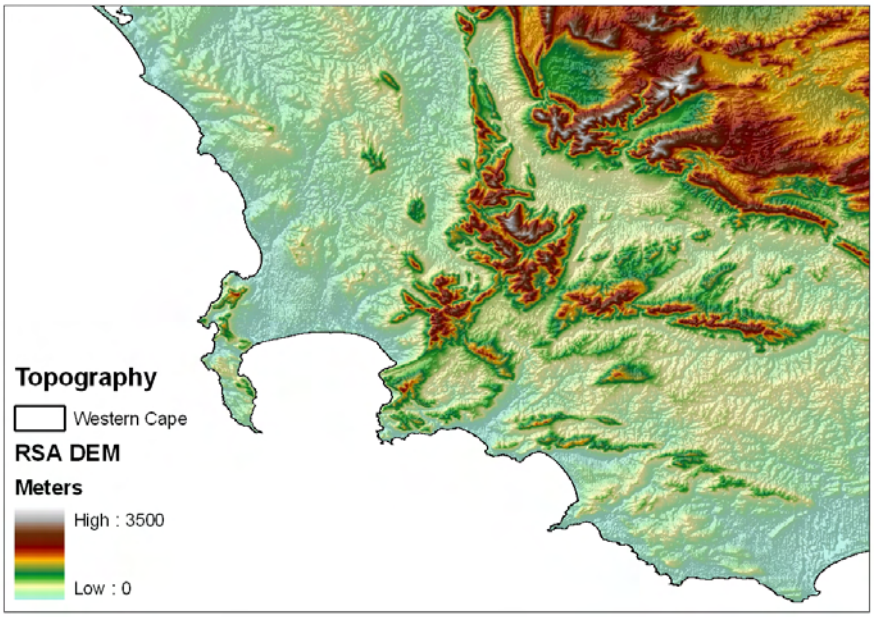

Figure 2.1: Topography of the Western Cape (created from DEM data by Dawie van Zyl, from the ARC-ISCW)

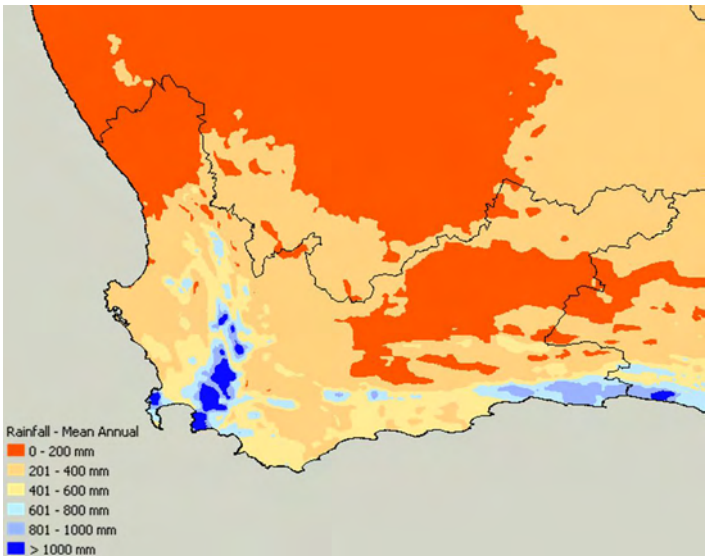

Figure 2.2: Average annual rainfall of the Western Cape (adopted from AGIS, 2007)

2003). Figure 2.2 indicates the average annual rainfall for the Western Cape as adopted from the Natural Resource Atlas from the Agricultural Geo-reference Information System (AGIS, 2007). The underlying climate data of the Atlas is obtained form the ARC weather station network. The relatively high rainfall totals over the areas of high topography can clearly be seen.

The cool ocean has a moderating effect on the average temperature of the south-western Cape (Schulze, 1996). This can be seen in the maps of the annual average maximum and minimum temperature over the Western Cape (adopted from the AGIS Natural Resource Atlas, 2007). The mean minimum temperatures along the coastline are warmer than the inland minimum temperatures, and vary between 4°C and 8°C in the focus area, while temperatures fall below 2°C in other places in the Western Cape (Figure2.3). At the same time, the annual(?) mean maximum temperatures along the coast are between 25°C and 29°C, while some inland temperatures exceed 35°C. The areas of high topography are also cooler than their surroundings (Figure 2.4). The slope aspect has a significant effect on temperature as well. Northerly and westerly aspects are warmer because they receive more direct radiation during the middle and latter part of the day (Bonnardot et al, 2004). The average January minimum and maximum temperatures for Cape Town are 16°C and 26°C, respectively, while the average July temperatures are 7°C and 18°C, respectively (SAWS Climate data, 2003).

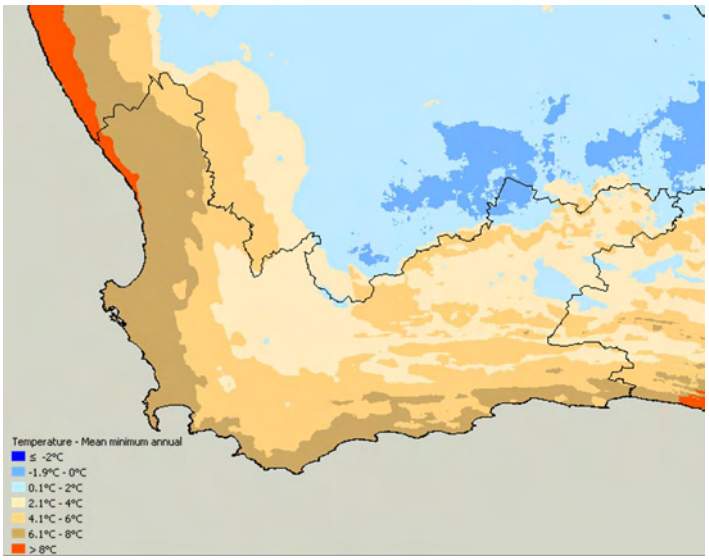

Figure 2.3: Average annual minimum temperature for the Western Cape (adopted from AGIS)

In winter the frontal depressions are accompanied by north-westerly winds that turn south-westerly as the front pass. During summer the southeaster brings subtropical air which is associated with fair weather. The Cape southeaster is a dominant feature in summer. It blows strongly for several days without interruption (Schulze, 1996). Usually between April and August, in the case of strong anticyclonic flow over the interior plateau, a hot, dry, squally wind can occur off the interior across the coastal regions. This is known as a berg wind, and is accompanied by a sharp increase in temperatures (Van Rooy, 1936; AMS, 1986). At the mesoscale, a sea breeze often forms in summer during calm and sunny days, accompanied by a (usually weaker) land breeze during the night. It blows from the ocean to the land an is a result of the difference in the sea and land temperatures, when the sea surface temperatures are colder than the adjacent land (Defant, 1951; Clarke, 1955). The cool, moist air that accompany the sea breeze is an important feature for the wine industry and a number of studies have been performed on this subject (e.g Bonnardot et al, 2002; Du Preez, 2007).

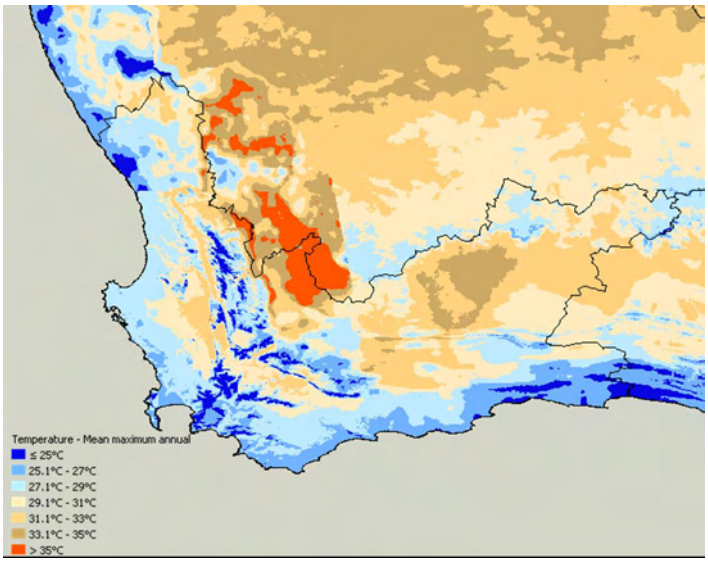

Figure 2.4: Average annual maximum temperature for the Western Cape (adopted from AGIS)

2.1.2 Location of the wine producing regions

Viticulture in South Africa instigated at the southwestern extremity of the continent, where after it gradually spread inland along the coastal mountain ranges as well as northwards in irrigation schemes as far as the Orange River (Saayman, 2003). The South African Wine Information and Statistics (SAWIS) reported that, in 2006, South African wine grape vineyards covered a total area of 102 146 hectares. Figure 2.5 shows the location of the wine regions in South Africa. The Western coastal zone (Stellenbosch, Paarl, Malmesbury, Worcestor, Robertson) is regarded as the region which focuses on the production of high quality wines (Saayman, 2003). Some of the most well-known wines produced here are Chenin Blanc, Cabernet Sauvicnon, Shiraz, Merlot, Chardonnay, Colombard, Sauvignon Blanc and Pinotage.

The focus of the study will be on the Stellenbosch district, a renowned wine producing area. It is located on the border of the Cape Metropole (Kleynhans & Opperman, 2005). The first wine routes in South Africa were developed in Stellenbosch in 1971. Currently, the wine routes represent more than 300 wine and grape producers in the Stellenbosch area and is regarded as one of the biggest tourist's attractions in the Western Cape (Saayman, 2003).

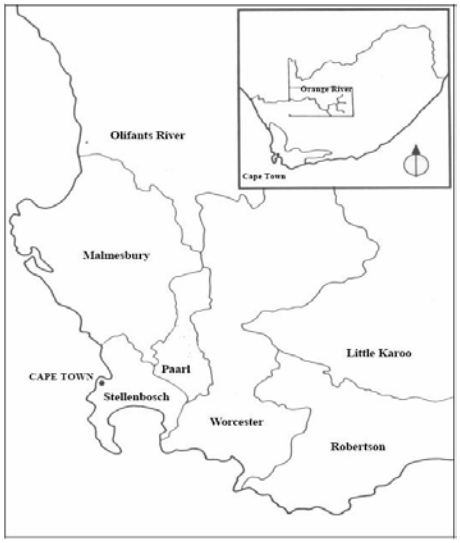

Figure 2.5: Wine regions of South Africa (adopted from SAWIS, 2007)

2.1.3 Wine grape varieties

In 1999, the percentages of winelands in South Africa covered by white and red varieties were approximately 70% and 30%, respectively. Throughout the years the area covered by red varieties increased so that, in 2006, the red varieties comprise 44.9% of the total area covered by wine grape vineyards (SAWIS). A short discussion on eight of the main varieties planted in South Africa is given below.

Chenin Blanc

Also known as Steen, Chenin Blanc is the most widely planted variety in South Africa. It is a white wine grape variety from the Loire valley of France. Chenin Blanc has a high acidity which causes it to be it very versatile; everything from sparkling wines to dry table wines and desert wines can be made from this grape (LaMar, 2002; Robinson, 2006). The versatility, vigorous growth and good wind resistance of Chenin Blanc have made it a popular variety in South Africa (Robinson, 1986). It does well in climates which are usually too warm for the many vinifera types. Chenin Blanc can grow in various soil types and is resistant to many diseases although it is susceptible to bunch rot and sun burn. It has a tendency for early bud break and late ripening. Although it can produce very bland, neutral wines if the vine's natural vigour is not controlled, careful viticultural practices can result in excellent wine (LaMar, 2002).

Cabernet Sauvignon

Cabernet Sauvignon is a red variety and the second most planted variety in South Africa (SAWIS). The berries have a thick skin and thus results in wines that can be high in tannin, the ingredient that provides structure and very good aging abilities. Although believed to be an ancient wine, recent studies have shown the Cabernet Sauvignon is a cross between Cabernet Franc and Sauvignon Blanc (LaMar, 2003; Robinson, 2006). The toughness of the skin makes the grapes fairly resistant to disease and spoilage. It can even withstand some autumn rains with little damage. Cabernet Sauvignon is a mid to late season ripener. Although it is the most stubborn yielder of any variety grown in SA (Robinson, 1986), quality wines are produced on well-drained soils which are not too fertile and in moderately warm, semi-arid regions providing a long growing season (LaMar, 2003).

Colombard

Colombard is a white variety that originated in the Charente district of France. It was traditionally used to make Cognac. Colombard grows effortlessly in warm, dry vineyards, producing large quantities of fairly crisp wine. The vine is very vigorous, buds early and is a medium-late ripener. It does not suffer particularly from any serious diseases or susceptibilities (Robinson, 1986). Colombard has a high acidity and is suitable to cool fermentation, which resulted in an increase in plantings in South Africa since 1970. A well-balanced and really appealing young wine can be made due to the high acidity which is complemented by a distinctly flowery perfume (Robinson, 1986).

Shiraz

Shiraz, a red variety from the North Rhône, is one of the few varieties that demonstrate a strict relationship between how severely it is pruned and the eventual quality of the wine (Robinson, 1999). Its vines are relatively productive, although a lower yield is required to make quality wines. Shiraz is resistant to most pests and diseases, although it is sensitive to *coulure* (berries not forming or falling off as soon as they form) (Robinson, 1986). *Coulure* manifest during spring and is triggered by periods of cold, cloudy, rainy weather or unseasonably high temperatures. Shiraz buds fairly late but is a mid-season ripener (LaMar, 2003). It performs best on poor soil (Robinson, 1986). Shiraz requires heat to become fully ripe but if it is left past its optimal ripening stage it can quickly loose some of its aroma and acidity (LaMar, 2003; Robinson, 1999).

Sauvignon Blanc

Sauvignon Blanc is a white variety that produces distinctive wines all over the world (Robinson, 1999). It makes wines that can be enjoyed young and is recognized easily (Robinson, 1986). It is important to manage the canopy by pruning and thinning leaves to direct the plants' energy towards ripening the fruit as unrestrained growth and over-cropping can result in neutral-tasting, uninteresting wines. Sauvignon Blanc has a tendency to diseases such as powdery mildew and black rot; hence production levels are irregular in humid climates. It has a high acidity and can also produce good dessert wines when allowed to hang past the normal ripeness point for dry table wines also known as a noble rot (LaMar, 2005). Sauvignon Blanc is prone to the escalating effects of botrytis which concentrate the evident sweetness but also have a propensity to damp the natural aroma (Robinson, 1986).

Chardonnay

Chardonnay is a rich white variety with a delicate aroma. Its delicacy allows it to absorb the influences of vinification technique and appellation of origin (LaMar, 2005). Chardonnay has a combination of relatively high alcohol and low acidity content. It yields well and ripens and buds early. Chardonnay can be produced in the hot as well as the cooler wine regions, although frost is a hazard in the cooler regions due to the early budding. It is fairly hardy apart from its susceptibility to powdery mildew and botrytis (Robinson, 1986). Chardonnay is quite versatile, producing a range of dry white wines, sparkling wines and sweet white wines (Robinson, 1999). Chardonnay oxidizes easily, which makes it sensitive to winemaking techniques. The flavour of Chardonnay is dramatically affected by soil, climate and vineyard practices due to its black canvas quality (LaMar, 2005).

Merlot

Merlot, a red variety from Bordeaux, is an early maturing wine. It also ripens early but is susceptible to fungal diseases such as rot and *coulure* (Robinson, 1999). Merlot is a productive vine which can adapt to a range of different micro climates and soil types (Robinson, 1986). However, it thrives in cold soils, particularly ferrous clay. The soil should be well drained as water stress is important to the vine (Clarke, 2001). Merlot's vine growth is moderately vigorous and must sometimes be pruned to prevent over-cropping. This is often followed by cluster thinning a few weeks later (LaMar, 2003). Merlot has great blending capabilities but can also make fascinating varietal wines. It has fewer tannins, a higher sugar content and lower malic acid than Cabernet Sauvignon (Robinson, 1986). One characteristic of Merlot is that it can over ripen quickly once it gets to its initial ripeness level (Clarke, 2001).

Pinotage

Pinotage is a unique South African red variety. It came into being in 1925, when Professor Abraham Izak Perold crossed Pinot Noir and Cinsaut. Under ideal cultivation conditions, Pinotage has the intrinsic capacity and adaptability to produce high grape yields. It is moderately susceptible to diseases and an early mid season ripener. In areas with an annual rainfall higher than 500 mm per year Pinotage vines do well under dryland conditions and with supplementary irrigation where the rainfall is less than 500 mm per year. Pinotage is well acclimatized in both cooler and warmer regions. The best soils for the growing of quality Pinotage grapes are poor to medium potential sloping hillsides with a medium to good water retention capacity (Du Toit & Joubert, 2005). Pinotage grows easily and produce high sugars relatively early. It shows best quality when produced from well-pruned vines that is allowed to ripen well (Robinson, 1986).

2.2 Viticultural requirements

2.2.1 Terroir

There is a great deal of controversy regarding the concept of terroir. Most wine experts believe that it is the ultimate factor in determining the quality of wine, although there are skeptics that dismiss it as a marketing tale. The general consensus however, is that factors such as climate, soil and viticultural practices greatly influences the quality of wine. An example of the influence of such factors is given by Van Leeuwen et al in the statement that berry composition and vine behaviour are significantly affected by climate and soil (Van Leeuwen et al, 2004). In South Africa, there is currently a growing attentiveness of the effect of terroir on the quality of wine, to such an extend that this is regarded as a dominant site factor when buying land in the Stellenbosch district (Kleynhans & Opperman, 2005).

The exact definition of terroir is also a point of dispute. The components that are usually included are micro-scale climate, soil type, geology, aspect, altitude, vineyard management practices, vinification practices and the human history (what people were traditionally doing) of the land. Some people are of the opinion that only factors such as soil and topography (Grogan, 2001) should be included in the definition of terroir, whilst others give it a much wider application by also including predominantly climate as well as some of the other components mentioned above (Carey et al, 2002; Moran, 2001; Smith & Wigham, 1999). In South Africa it is widely accepted that terroir is the relationship between climate, topography and soils determining grape and wine quality (Kleynhans & Opperman, 2005). According to Robinson, terroir is the environmental and growing conditions which determine the quality of grapes (Smith & Whigham,

1999; Robinson, 1996). Van Leeuwen et al (2004) claims that climate, soil and cultivar are the three main components of terroir.

This study will make use of the definition of a viticultural terroir as given by Winetech: "A viticultural terroir can be defined as a unit of the earth's biosphere that is characterised by relatively homogeneous topographical, pedological and climatic features, which find expression through interaction with the vine and vintner, resulting in a distinct wine with an identifiable origin" (Winetech, 2007).

2.2.2 Climate variables relevant to the viticulture

The quality of the grapes is fundamental to the quality of wine, and the quality of grapes in turn is determined by the environmental and growing conditions (Smith, 2002). Climate is a dominant factor in determining wine quality and style (Smart, 2002).

Temperature is a significant determinant of plant growth as well as fruit flavour results (Happ, 1999). High temperatures cause the sugar and potassium contents to rise and the malate contents to be lower (Carey et al, 2002; Gladstones, 1992). Temperature also influences ripeness and by selecting, fermenting, and blending certain batches of grapes with suitable ripeness and flavours, wine makers can have better control over the product (Smith & Whigham, 1999). The optimal mean temperature for physiological ripening and the synthesis of colour, flavour and aroma compounds is 20-22°C during the month of ripening (Carey et al, 2002; Gladstones, 1992). As mentioned in Chapter 1, the heat summation above a threshold value of 10°C during the growing period of the grapevine is called the growing degree-days (GDD). For a vineyard site, the minimum heat accumulation required in the growing season is 1093 GDD (Bonnardot et al, 2004).

In the event of limited soil water supply, the relative humidity will have an effect on the photosynthetic rate (Carey et al, 2002; Champagnol, 1984). Warm and wet conditions can set off pest and diseases such as mildew and fungus (Smith & Whigham, 1999) while warm and dry conditions result in high berry PH values (Carey et al, 2002; Gladstones, 1992).

Air circulation averts high temperatures and relative humidity from developing in the vineyards (Carey et al, 2002). However, strong winds can injure the grapevine in spring and early summer (Carey et al, 2002; Hamilton, 1989). Prevailing winds along the row direction during the ripening phase will cause leaves and bunches to dry sooner, which will reduce the possibility of fungal infections (Du Toit & Joubert, 2005). Exposure to the sea-breeze will also result in al cooling of vineyards, consequently enhances grape quality (Kleynhans & Opperman, 2005).

Exposure to solar radiation can have a positive or negative effect on the grapevine. The ripening process will be stimulated where grapes are exposed to direct sunlight (Du Toit & Joubert, 2005). Grapes also produce poly phenols (biochemical precursors to flavour and colour compounds) to protect them from UV light. The poly phenols have a positive influence on the wine quality as they provide flavour and colour to the grapes, which are important for wine quality (Smart, 2002). On the other hand, sunburn can damage varieties such as Chenin Blanc (LaMar, 2002).

Thus, climate variables such as temperature, relative humidity, wind speed and radiation have direct impacts on growth and characteristics of vineyards and thereby inherently contribute to define the terroir of a specific location. Note however, that it is not only the long-term averages of these variables but also their extremes that are relevant for the viticulture.

2.3 Regional climate modelling

GCMs are based on the laws of momentum, mass and energy conservation applied to the atmosphere, and have become the primary tool to simulate climate. In order to obtain projections of future climate, it is also important to project the future oceanic state. This is feasible through the coupling of GCMs to ocean models. To such a coupled systems are referred to as ocean-atmosphere global circulation models (OAGCMs). GCMs are computationally expensive to integrate, and when coupled to an ocean model the resulting OAGCM is about twice as expensive to run as the GCM. The largest international modelling groups can at present manage OAGCM climate simulations at spatial resolutions of about 2.5° in the horizontal (IPCC, AR4). At these resolutions, important meso-scale meteorological phenomena such as tropical cyclones and orography-induced rainfall cannot be adequately parametrized as subgrid-scale processes. This results in the need to employ high resolution RCMs to spatially resolve and simulate mesoscale phenomena more adequately (Giorgi et al, 1991; McGregor et al, 1993; McGregor 1997; Engelbrecht and Rautenbach, 2000). RCMs are typically integrated at resolutions about five times higher than that of OAGCMs. This can achieved by clustering the RCM grid points over a regional area of interest. Two primary methods of regional climate modelling have evolved, namely nested climate modelling (limited-area climate modelling) and variable resolution global modelling. In both these approaches the RCM needs to be supplied with some form of boundary forcing by the relevant GCM or OAGCM.

Regional climate modelling is often referred to as dynamic downscaling. One disadvantage of this approach is that even at the higher resolution of these models convective rainfall can't be resolved explicitly, and needs to be parameterised. These parameterisation schemes are thought to be an important source of uncertainty within RCM simulations (Tadross et al, 2006). As an alternative

to dynamic downscaling, it is also possible to obtain high resolution simulations and projections of climate by statistically downscaling GCM projections. This approach is fundamentally based on finding statistical relationships between the observed large-scale circulation fields and the relatively higher resolution observations of variables such as rainfall. One disadvantage of the statistical approach is that it relies on the availability of high quality observational data sets of sufficient resolution and spanning a sufficiently long period in order for the statistical relationships to be found. However, variables such as relative humidity, wind speed and hourly rainfall are often observed at spatial resolutions much lower than those of minimum and maximum temperature and 24 hr rainfall totals. Most statistical downscaling studies over South Africa have indeed been limited to the latter variables (e.g. Hewitson and Crane, 2006) and methodologies to downscale variables such as wind speed, relative humidity and their extremes have not been developed and tested. In the present study, the spatial resolution of the climatology needed to define terroir is higher than that of the observational network of the relevant variables, implying that dynamic downscaling is the only viable option to obtain a simulated climatology of sufficiently high resolution.

2.3.1 Nested climate modelling

The traditional and most widely applied approach of regional climate modelling is that of nested modelling, where a higher resolution limited-area model is integrated over an area of interest, while receiving information at its lateral boundaries from a GCM. This is usually obtained via a one-way nesting technique (McGregor, 1997; Wang et al, 2004). One-way nesting allows the coarse resolution model to provide data to the nested RCM, but data from the nested RCM is not allowed to interact with the GCM in return (McGregor et al, 1993). A relaxation zone (e.g. Davies, 1976) is typically applied at the lateral boundaries of the limited area model in order to describe the forcing of the GCM and how this depletes as on moves deeper within the limited-area model domain.

A main advantage of high-resolution limited-area modelling is that orographic forcing can be described more adequately at higher resolution. Such models are therefore capable to describe the regional rainfall patterns in more detail than the host GCM. Meso-scale circulation patterns can also be better resolved and simulated. Nested climate-modelling is unfortunately also associated with a number of problems. The spurious reflection of atmospheric waves may occur at the lateral boundaries of the nested model, where model resolution changes from that of the coarse resolution GCM to the much higher resolution of the RCM (McGregor, 1997). Spurious rainfall can also be produced near the boundaries due to the intermittent supply of boundary data from the GCM. Tropical divergent circulation can be generated and maintained because of the way the gravity inertia waves behave in the tropics (McGregor, 1997).

It should also be noted that the nested climate model's synoptic-scale circulation should be consistent with that of the forcing GCM, and that the RCM is supposed to improve on the meso-scale features of the simulated climate. Clearly, if the GCM simulation of synoptic-scale features is inadequate, it would be meaningless to perform downscaling of these simulations using an RCM. Ideally the circulation of the RCM should feed back into the GCM, through a two-way interaction approach. However, two-way interaction is technically cumbersome to achieve, especially when the architectures of the GCM and RCM are different (e.g. McGregor, 1997; Wang et al, 2004). Variable resolution global models provide an easier approach to achieve high resolution simulations over an area of interest that are interactive with the simulations over the areas of coarser resolution (e.g. McGregor, 1997).

2.3.2 Variable-resolution climate modelling

A fairly new approach of achieving dynamic downscaling of coarse resolution GCM or OAGCM simulations is through the use of variable-resolution GCMs. In this approach a global stretched-grid is used to provide high resolution over the area of interest, with the resolution gradually decreasing as one moves away from the area of interest. (Fox-Rabinovitz et al, 2005). Variable-resolution stretched-grid GCMs have no artificial lateral boundaries, and thereby avoids many of the problems associated with nested modelling, such as reflection of waves at the lateral boundaries (McGregor, 1997). The technique is highly flexible. A variable resolution model essentially needs only sea surface temperature (SST) forcing from a host model or reanalysis data (e.g. Engelbrecht et al, 2009), although wind-nudging may be used if the resolution in the far-field is too coarse (McGregor and Dix, 2001; Wang et al, 2004; Engelbrecht et al, 2009). With the variable resolution modelling approach, self-consistent two-way interactions between global and regional scales of motion can be achieved which are an inherent advantage of this approach (Fox-Rabinovitz et al, 2005).

In 2001 a project was initiated to compare the performance of variable-resolution general circulation models (GCMs) from different centers/groups in Australia, Canada, France and the United States (Fox-Rabinovitz et al, 2005) in simulating climate. The project was called the Stretched-Grid Model Intercomparison Project, phase-1 (SGMIP-1). Climate simulations were produced at high resolution over a large part of North America, for the 12-year period of 1987 - 1998. The models were forced with the NCEP weekly analysis of SST and sea-ice distributions. It was found that, in terms of temporal and spatial diagnostics, there were a good comparison between the multi-model ensemble results and both observations and reanalysis (Fox-Rabinovitz et al, 2005). The observed features of global circulation are well preserved within the variable-resolution global model runs and regional biases for time averaged model products are within the uncertainties of the available reanalysis. Results have shown that all the models display similar performance in simulating climate, with a high pattern correlation of about 0.8 between the mean observed annual precipitation

and the corresponding means simulated by the various models. Interestingly, the ensemble mean has a higher correlation coefficient as well as a lower root mean square error than any of the individual models (Fox-Rabinovitz et al, 2005).

2.3.3 Atmospheric modelling in South Africa

The first numerical weather prediction (NWP) model in South Africa (Triegaardt, 1965) was developed in the 1960s by a group of scientists from the Council of Scientific and Industrial Research (CSIR) and the South African Weather Bureau (SAWB) (today called the South African Weather Service, SAWS). By the 1980's a locally developed, state-of-the-art, five-level, split-explicit, hydrostatic primitive-equation model for hemispheric prediction existed at the CSIR (Riphagen, 1984). The performance of the model was comparable to international standards (Riphagen and Burger, 1986; Riphagen and Van Heerden, 1986) and an excellent foundation for local numerical modeling was in place. Unfortunately policy changes at the CSIR and SAWB in the mid 1980's resulted in a rapid decline in local numerical model development activities. For almost two decades the study field was largely dormant in South Africa, until the recent development of a dynamical core and numerical solution procedure for a new nonhydrostatic model at the University of Pretoria by Engelbrecht et al (2007).

Despite the lack of support for local numerical model development, a couple of international models have been applied in South Africa. The South African Weather Service (SAWS) has been producing daily weather forecasts from locally running the ETA model of the National Centers of Environmental Prediction (NCEP) from since 1992. In 2006 this modelling system was replaced with the Unified Model (UM) of the United Kingdom Meteorological office. They also provide seasonal forecasts from using the ECHAM 4.5, the European Center-Hamburg model version 4.5 (Landman et al, 2005).

Case studies of severe thunderstorms over South Africa were conducted at SAWS using the ETA model (De Coning & Adam, 2000; De Coning et al, 2000). The University of Witwatersrand applied the Regional Atmospheric Modelling System (RAMS) in the 1980's and 1990's to conduct sensitivity studies (Crimp et al, 1998; Crimp et al, 1997). The dynamics of heavy rainfall events have also been investigated using high resolution limited-area models (Singleton et al, 2006). At the University of Pretoria (UP) seasonal forecasts and sensitivity studies to explore the ocean-atmosphere interaction have been performed using the CSIRO Mark II general circulation model.

Regional climate modelling in South Africa commenced with the use of the the regional climate model DARLAM (Division of Atmospheric Research Limited Area Model) to perform climate simulations over southern Africa (Joubert et al, 1999; Engelbrecht et al, 2002). High-resolution climate simulations for the

SADC region were performed using the limited-area model DARLAM, nested within the CSIRO Mark II GCM. In these experiments, present and future mid-summer and mid-winter climate were simulated for two 10-year periods (Engelbrecht et al, 2002; Olwoch et al, 2007*)*. A general rise in temperature over South Africa was projected as well as increased rainfall over the western and central parts of the country (related to an increase in atmospheric pressure over the eastern parts). The changes in tick distributions and east coast fever over sub-Saharan Africa were simulated by a predictive species model using input from these climate simulations (Olwoch et al, 2003; Reason et al*,* 2006; Olwoch et al, 2008).

For the last decade or so the University of Cape Town (UCT) applied the NCAR Mesoscale Model (MM5) for climate simulations. One of the most extensive regional climate modelling studies performed to date over southern Africa is that of Tadross et al (2005). The 5th generation PSU/NCAR mesoscale model MM5 and the PRECIS model of the UK Hadley Centre were used to dynamically downscale two 10-year periods (control and future) of southern African climate (Tadross et al*,* 2005; Reason et al*,* 2006). The global climate was simulated under the A2 Special Report on Emissions Scenario (SRES) by the HadAM3 GCM. The MM5 simulations were run at 50 km resolution, and the PRECIS at 0.44 degrees. The output from both models were regridded to 0.5 degrees for comparison. The two models showed broadly consistent changes for the subcontinent as a whole. In the future climate, drier conditions were simulated over the tropical western part of the subcontinent during October to December, with the MM5 extending the area to the south up to the Northern Cape of South Africa. Wetter conditions to the east and drier conditions in the west and over the tropics in the north were simulated for the period of January to March (Tadross et al*,* 2005). In another study the potential climatic impacts were assessed when the vegetation map of southern Africa is altered from an estimated natural state to present day conditions. The regional climate model MM5 was used for this study and it was found that the September to November (SON) and December to February (DJF) surface climate was significantly impacted by the change in vegetation (MacKellar et al, 2008).

Since 2002 there has been intensive research into atmospheric modelling at UP. CCAM was used to perform 30-year current and future climate simulations over southern Africa as part of an intensive climate change study (Engelbrecht 2005; Engelbrecht et al*,* 2009). Climate simulations for the period 1975 - 2005 and 2070 - 2100 (A2 scenario) were performed at a horisontal resolution of 0.5 degrees. The future climate is simulated to have an intensification of the subtropical high pressure belt south of the continent during winter, with a subsequent southward displacement of the frontal rain bands. More prominent mid- and upper- level high pressure systems are simulated during spring and autumn over central and eastern southern Africa, resulting in generally lower rainfall totals over this area. Enhanced moisture advection to the north of the highs leads to

increased rainfall over northern Mozambique. Parts of Namibia, Botswana and the central and western interior of South Africa are also expected to experience more rainfall during these seasons, due to the enhanced southwards moisture advection along the western periphery of the anomalously strong highs. Summer is simulated to become wetter over the southeastern subcontinent, as a result of increase cloud bands over the area as the Indian Ocean High is simulated to intensify over the south-western Indian Ocean (Engelbrecht et al, 2009).

2.4 The Conformal-Cubic Atmospheric Model

CCAM is formulated on a conformal-cubic grid, derived by the projection of a cube's panels onto the earth's surface. This grid was developed by Rancic et al. (1996). It is isotropic except for eight singular vertices (McGregor, 2005). The model is formulated in terms of the hydrostatic primitive equations cast on the conformal-cubic grid (McGregor, 2005). When the C48 grid is used for the simulations (48 x 48 grid points on each panel), the model has a quasi-uniform resolution of about 208 km over the globe (McGregor, 2005). The model typically runs with 18 pressure-sigma levels in the vertical. By making use of the Schmidt (1977) transformation, CCAM may also be applied in variable-resolution stretched-grid mode. With this transformation the primitive equations are unchanged, although the map factors have altered values (McGregor, 2005). High resolution may be obtained over the area of interest by running the model in variable-resolution mode, with the resolution decreasing as one moves away from the area of interest.

CCAM is a hydrostatic model with two-time-level semi-implicit time differencing. Semi-Lagrangian advection with bi-cubic horizontal interpolation is used in the model. The grid is unstaggered, but improved dispersion characteristics are obtained by reversibly transforming the winds to/from C-staggered locations before/after gravity wave calculations (McGregor, 2005). Mountain resonances are avoided by making the time differencing weakly implicit through off-centering (Rivest et al, 1994). Global *a posteriori* conservation of mass and moisture is also utilized by CCAM (McGregor, 2005).

The physical parameterizations of CCAM are quite extensive. These include a mass-flux cumulus convection scheme from the CSIRO, which contains the evaporation of rainfall and downdrafts. Long- and short- wave radiation is parameterised by the GFDL parameterisation of Schwarzkopf and Fels (1991), with interactive cloud distributions diagnosed from liquid and ice-water content (Rotstayn, 1997). A stability-dependent boundary layer is employed, with non-local vertical mixing. The gravity wave drag is parameterised as well. A Canopy scheme with six layers of soil temperatures (Gordon et al, 2002) and moisture (solved using the Richarson equation) as well as three layers of snow is also used (Engelbrecht et al, 2009).

CCAM has been applied widely in the field of regional climate modelling. As mentioned in Section 2.3, it has been used to simulate climate at a high resolution over a large part of North America for 12 years as part of an international Stretched-Grid Model Intercoparison Project (Fox-Rabinovitz et al, 2005). CCAM has also been used in a lot of studies in Australasia and Asia. Climate change simulations over Australia was performed for a 140 year and two 20 year periods at a resolution of about 65 km (McGregor et al, 2002). Two CCAM runs for 1979-1989 and 1980-1989 were produced to study the effect that a large inland lake on Australian climate could have (Hope et al, 2004). CCAM has also taken part in the regional model intercomparison project (RMIP) over Asia (Fu et al, 2005). The Tasmanian precipitation and potential evapotranspiration resulting from an enhanced greenhouse scenario were estimated using a 30 year present and 30 year future climate simulation (Nunez and McGregor, 2007). CCAM has also been used to simulate Fiji's climate at a resolution of 8 km for the years 1975 - 1984. It was found that CCAM has good skill simulating the annual cycles of maximum and minimum temperatures and rainfall. The observed intra annual and inter annual variability as well as the influence of the El Niño phenomena were also captured by the model (Lal et al, 2008). CCAM has been used in a number of studies in South Africa as well, as mentioned in the Chapter 1 and the previous section.

Chapter 3

Observed data and design of the modelling experiment

3.1 Observed data for verification purposes

3.1.1 NCEP/NCAR Reanalysis data

Global analysis of atmospheric fields is produced in a collaborative project between the National Centers for Environmental Prediction (NCEP) and the National Center for Atmospheric Research (NCAR). This data set (called "reanalysis" data) is constructed from quality controlled observational data such as land-surface, ship, rawinsonde, pibal, aircraft and satellite data. It is assimilated using a state-of-the-art analysis/forecast system to create a database that is as complete as possible (Kalnay et al, 1996; Kistler et al, 2001).

The NCEP/NCAR Reanalysis data has a spatial resolution of 2.5° in both longitude and latitude and is available at the surface and on 17 pressure levels. Data is available at 6-hourly time-intervals for the period 1948 to present. Monthly means as calculated for the period of 1976-2005 for the variables sea-level pressure, 850hPa and 500hPa geopotential heights and the 200hPa horizontal wind are used in this study for the purpose of model verification at the synoptic-scale. The changes in the observational system over the years have been found to impact on the data. An important influence is the addition of satellite data during 1978, resulting in a significant improvement in the quality of the data set, especially over the southern hemisphere where other observations are sparse. Pre-1979 NCEP/NCAR re-analysis data has reduced interannual variability compared to the post-1978 data and should be used with care (Tennant, 2004). For example, the trend in average temperature was found to be less than 0.2 degrees Celcius per decade (over the last five decades) at most weather stations considered by Kruger and Shongwe (2004), whilst trends in rainfall were statistically insignificant over the last century for most weather stations considered

by Kruger (2006).

3.1.2 CRU data

High-resolution gridded data obtained from the the Climatic Research Unit (CRU) is also used for verification purposes in this study. The CRU CL 1.0 data set is used to verify the 60 km resolution simulation of yearly rainfall and intra-annual variation in rainfall over southern Africa. This data set has a horizontal resolution of 0.5° on a latitude-longitude grid. It comprises of a mean monthly surface climatology for the 30-year period of 1961-1990 (New et al, 1999). Many regional features of southern African rainfall rainfall patterns are well captured in this CRU data set, and a number of regional modelling studies over southern Africa have relied on this data set for the purpose of model verification (e.g. Engelbrecht et al., 2002; Tadross et al., 2006; Engelbrecht et al., 2009).

The CRU CL 2.0 data set is used to perform the verification of the 8 km simulations. It is a mean monthly climatology for the 30-year period of 1961-1990 with a spatial resolution of 10' (New et al, 2002). The variables used in this verification are rainfall, temperature, relative humidity and 10 m wind speed. The CRU CL 1.0 climatology is used for the 60 km verification as the resolution of this dataset coincide with the 60 km simulation whilst the CL 2.0 is used for the 8 km verification for the same reason. Note that both the CRU CL 1.0 and CRU CL 2.0 climatologies are for the period 1961-1990, whilst the CCAM simulations are for the period 1976-2005. The 10' CRU data is only available for the period 1961-1990, which necessitates the use of this period for defining observed climate. The 0.5° observed climatology is therefore consistently obtained for the same period, although another CRU data set at this resolution is available for the period 1901-2000. Since the resolution of this dataset is too coarse for the verification of the 8 km simulation, this dataset is not used in the study. Although the model climatology is calculated over a different 30 year period, it may be argued that climatological features should be very similar for the two periods under consideration - as there is an overlap of 15 years between the two periods, and because observed trends in southern African climate have been found to be relatively small over the last five decades (Kruger and Shongwe, 2004; Kruger, 2004).

3.1.3 ARC weather station data

The 1 km and 200 m simulations are of a much higher resolution than is defined by the observational network over the southwestern Cape. The verification of the simulations are therefore problematic, and can not be performed using gridded observed data as for the 60 km and 8 km simulations. The approach followed in the study is to perform point verifications against weather stations that are located within the area of interest. For this purpose, data from the Agricultural Research Council (ARC) of South Africa is used. Within the ARC,

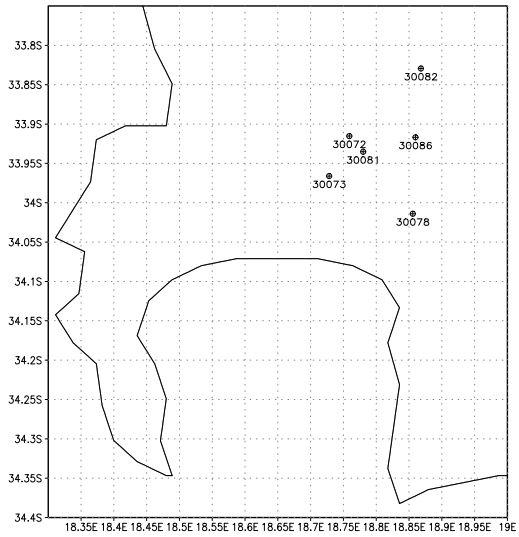

Figure 3.1: Location of stations used in high resolution verification

the Agrometeorology Division at the Institute for Soil, Climate and Water maintains a weather station network of about 500 stations throughout South Africa.

Only data from stations which are located within the area of interest, and which have been operational for at least 10 years, are used in the verification of the 1 km and 200 m simulations. A number of 6 stations satisfying these conditions are available for model verification. The location of these stations within the area of interest are shown in Fig.3.1. The stations used are Goedehoop (30072); Jacobsdal (30073); Alto (30078); Bonfoi (30081); Le Bonheur (30082) and Nietvoorbij (30086). The simulated climatological monthly diurnal temperature cycle and climatological monthly rainfall totals of the 1 km simulation are verified against four stations (Goedehoop, Alto, Bonfoi and Le Bonheur) for each month of the year. There are unfortunately no more ARC stations available with a complete dataset for all the months for the five year period used in this verification (1995-1999). For the 1 km and 200 m February verifications, the temperature, relative humidity and wind speed for all six ARC stations are used. Ten consecutive years of hourly February temperature data were available (1996-2005) for all six stations and are therefore used in the verification. Unfortunately the other two variables had very big gaps after 2000, and only a five year period (1996-2000) were used in the verification of the February relative humidity and wind speed.

3.2 Computing Infrastructure

The CCAM code is computationally efficient and flexible in the sense it can be implemented and compiled on computing infra-structures ranging from a single PC to to computer clusters and vector-based supercomputers. The ultra-high resolution simulations performed in this study are computationally so expensive that a computer cluster with some parallel processing capabilities was found to essential in order for the simulations to be performed within a reasonable time frame. Fortunately, advances have been made in cluster computing in South Africa with the recent establishment of the Meraka Institute within the CSIR in South Africa. Two powerful computer clusters have been constructed within the Meraka Institute. These include the Center for High Performance Computing and the C4 cluster. In order to perform the simulations required for the Winetech project, CCAM has been is installed on the Opteron master of the C4 cluster at the CSIR Meraka Institute. The following is a description of what Opteron encompass (Gazendam, 2008):

RAM: 4GB per cluster node (46 cluster nodes)

Processor: 2 x dual-core AMD Opteron 2.6GHz (thus 184 CPU cores in the cluster)

HDD: Ample free space on each cluster node, and several 100GB of shared storage space available

Compiler: GCC and PGI. The Intel compiler is available for academic purposes also.

OS: Linux (Redhat)

All the software required for CCAM to run was not present and the Intel Ifort compiler as well as some NetCDF libraries needed to be installed before the code could compile.

The 60 km simulation was completed on a single processor. The 8 km simulation was performed using the Message Passing Interface (MPI) version of the CCAM code. This implies that various processors are used to simultaneously perform calculations required to advance the model from one time-step to the next, exchanging information between the different processors where necessary. The 1 km and 200 m were performed using an “embarrassingly parallel” approach, with each monthly simulation initialised and performed on an individual basis. More information on the computational requirements of each different resolution run and the strategy followed to complete the simulations within a reasonable time frame is provided in the next section.

3.3 Configuration of the model over South Africa

3.3.1 Nudging techniques

CCAM is formulated on the conformal-cubic grid, derived by projecting the panels of a cube onto the surface of the earth (McGregor, 1995). High resolution over a specific area of interest can be obtained by stretching the grid, using the Schmidt stretching factor (e.g. McGregor, 2005). In this particular study the C48 grid is used, where every panel has a total number of 48 x 48 gridpoints. The number of gridpoints used per panel is constant, so that increased resolution is effectively obtained by clustering 48 x 48 grid points over a relatively small area of interest, with the remaining panels covering relatively larger areas. The panel of the cube opposite to the "high-resolution" panel covers the largest area and has the lowest resolution. In order to obtain ultra-high resolution over the relatively small area of the Stellenbosch wine producing region, the model was integrated with the high resolution panel located over progressively smaller areas of interest, having resolutions of about 60 km; 8 km; 1 km and 200 m, respectively. Each higher resolution simulation is nudged within the previously performed lower resolution run. A simulation with 60 km resolution over southern Africa was performed first, and was nudged within NCEP Reanalysis wind and SST data in the far-field. A simulation with 8 km over the Western Cape of South Africa was performed next, and was nudged within the 60 km simulation outside the area of high (8 km) resolution. The 1 km simulation (covering the southwestern Cape) was similarly nudged within the 8 km simulation, and was in turn used to force a 200 m simulation (covering an area of about $10\,km^2$ over the Stellenbosch wine producing region). The nudging is performed from the fourth level in the vertical (about 900 hPa) upwards, from the edges of the high resolution panel outwards. Figure 3.2 gives a graphical representation of variously stretched grids having resolution of 60 km (a), 8 km (b), 1 km (c) and 200 m (d), respectively. The coast line representations are from a relatively low resolution NCAR-dataset.. The actual model coastline and land-sea mask are of much higher resolution.

3.3.2 Synoptic-scale (60 km) simulations over southern Africa

As a first step in downscaling climate over the southwestern Cape, a simulation having 60 km resolution over southern Africa was performed. Having a Schmidt stretching factor of 3.3, the resolution of this C48 simulation is as coarse as 700 km in the far field. To compensate for the coarseness of the far field resolution, the technique of wind nudging is employed over that area. NCEP reanalysis data obtained from CMAR (the CSIRO Marine and Atmospheric Research centre) is used for this purpose. (The 60 km simulation was run continuously for the period 1976-2005 on a single processor at the CSIR and took approximately 30 days to be completed). The purpose of performing the 60 km simulation forced by reanalysis data, is to obtain a climate simulation over southern Africa with daily

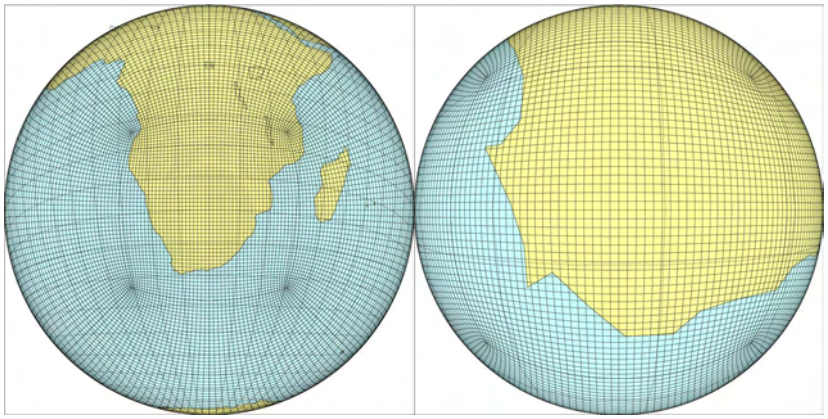

(a) 60 km resolution run (b) 8 km resolution run

(c) 1 km resolution run (d) 200 m resolution run

Figure 3.2: High-resolution panels of the 60 km, 8 km, 1 km and 200 m simulations.

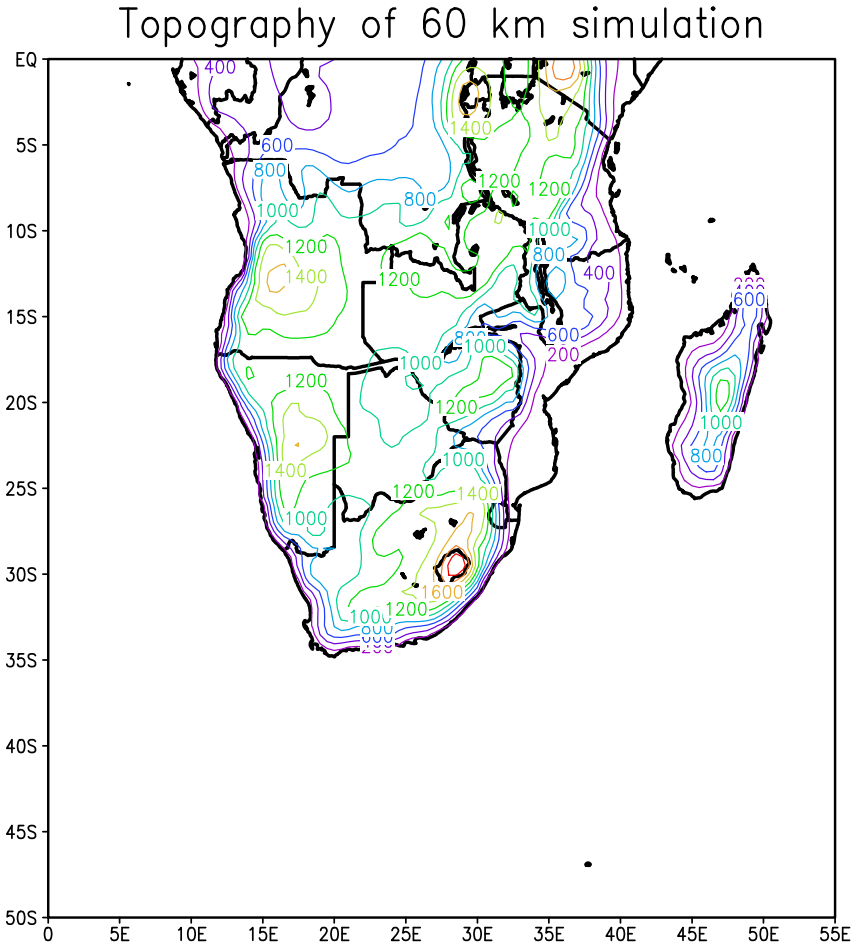

Figure 3.3: The topography of the 60 km simulation over Southern Africa

synoptic-scale circulation patterns that are consistent with observations, but which also contain some meso-scale features of the region's climate. The CSIRO provided additional boundary forcing data such as topography, vegetation, soil and SSTs that were incorporated into the model to perform the run.

Figure 3.3 illustrates the topography of the 60 km simulation. This topographic dataset is quite good for Southern Africa, but would be insufficient if one is interested in the effects of the topography of the south-western Cape on the mesoscale climate of that area. The plateau in South Africa with a height of more than 1000 m as well as the steep gradient of the eastern escarpment (part of the Drakensberg Mountains) can be seen. The highest point in southern Africa is in Lesotho, with a height of more than 1600 m. The east and southeast

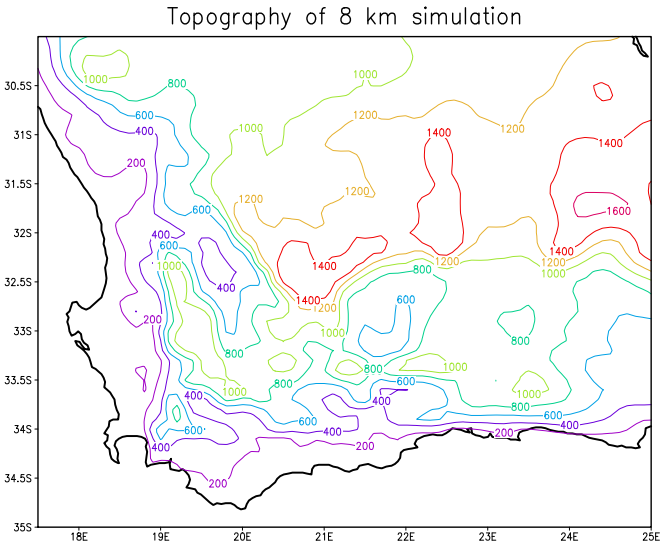

Figure 3.4: The topography of the 8 km simulation over the Western Cape

coast of South Africa are quite narrow. Tropical East Africa also has some high elevation and Madagascar has got topography that slopes up to more than 1000 m.

3.3.3 *Mesoscale (8 km) simulations over the Western Cape*

After completion of the 60 km resolution simulation, the 8 km resolution simulation was performed. Note that all the simulations of different resolution runs performed in the study employ the same number of grid points (18 x 6 x 48 x 48). This result from the 18 vertical levels, 6 panels of the conformal-cubic grid and 48 x 48 gridpoints on each panel. However, the 8 km simulation is considerably more expensive than the 60 km run. This stems from the necessity to reduce the model time step as the resolution decreases, in order to satisfy the constraints of numerical stability and accuracy. The 8 km simulation was performed using a time step of 3 minutes. Because the 8 km resolution simulation was also performed continuously, it was essential to complete this run using the MPI version of the CCAM code, in order for the run to be completed within a reasonable time frame. It took approximately 8 hours to complete a month-long 8 km simulation on a single processor, implying that it would have taken four months to complete the 8 km simulation on one processor. However, with the MPI settings using six processors at a time, it was possible to complete the 30-year climate simulation at 8 km resolution within one month. Note that this mesoscale simulation has a resolution of 8 km over the Western Cape, but as one moves away from this area the resolution rapidly becomes coarser. This results from a strong Schmidt stretching factor of 24.75. The 8 km run is there-

fore nudged within the 60 km simulation to compensate for the coarse resolution outside the area of interest, and to ensure that the simulation is consistent with the synoptic-scale forcing of the 60 km simulation. The topography of the 8 km resolution have much more detail over the Western Cape than the 60 km topography. Figure 3.4 show the topography of the 8 km resolution run over the Western Cape.

3.3.4 Micro-scale (1 km) over the southwestern Cape

A different strategy was followed in order to perform the 1 km simulations. The runs require the use of a time step of 30 s in order to obtain numerical accuracy and stability in the semi-implicit semi-Lagrangian discretization of the hydrostatic atmospheric equations used in CCAM. It may be noted that in explicit discretizations of the fully-elastic atmospheric equations, the Courant-Friedrich Levy (CFL) criterion requires a much smaller time step of about 3 s. Thus, the high computational efficiency of the CCAM code makes it a practical option to obtain climate simulations within a reasonable time-frame. Equivalent simulations based on the use of an explicit model (such as RAMS) would take at least ten times longer to complete. Still, even using the MPI formulation of the code, a 30-year simulation at 1 km resolution using six processors would take about six months to complete. For practical reasons the 1 km simulations were therefore not performed continuously. The 30-year period was divided into monthly segments, and each month was simulated individually by initializing from the corresponding 8 km field and from nudging the 1 km simulation within the relevant 8 km forcing fields. This approach was thought to be sufficient for the 1 km simulations, where the area of interest is relatively small, and the forcing through nudging within the 8 km simulation should be the dominant effect. In the 8 km and 60 km simulations, however, it was thought prudent to perform the runs continuously to allow for evolution of the soil moisture field in the simulations.

The 1 km simulation was therefore performed on an individual-month basis for the period 1976 - 2005 on single processors, using an “embarrassingly-parallel” approach. The 1 km simulation has a Schmidt factor of 198 and each simulation was initialised from and nudged within the output of the 8 km run. A 1 km simulation of one month in lenght took approximately 2 days to complete on a single processor. Between 15 and 30 processors from the C4-cluster were used to complete the 360 simulations (12 months x 30 years) within in a reasonable time. The 1 km runs were completed in less than two months due to the availability of processors. The focus of this micro-scale simulations is the southwestern Cape and False Bay area. The very fine topography dataset used in this run can be seen in Figure 3.5. This should result in a much improved local climate simulation, compared to the 8 km simulation over the same area as the great influences of topography should be simulated. The mountains of the southwestern Cape receive heavy orographic rainfall in comparison with the rest of the area as evident from the observed rainfall map in Chapter 2. The fact

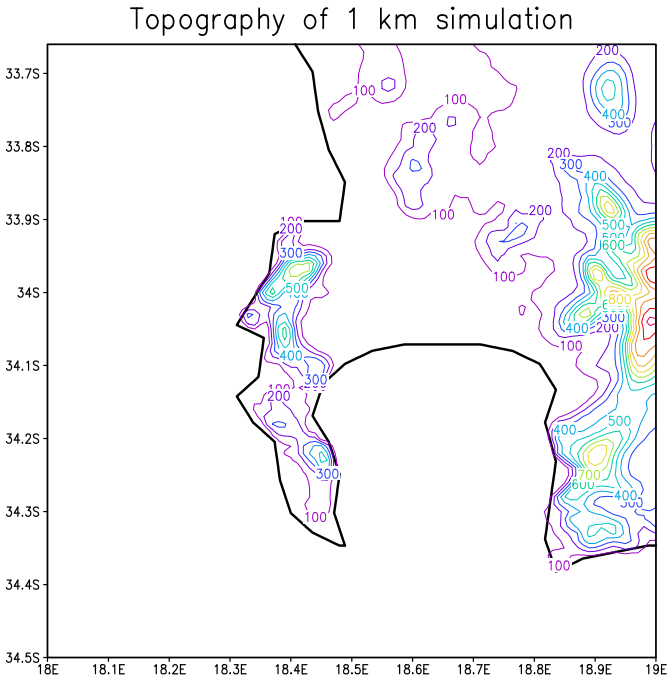

Figure 3.5: Topography over and around the high-resolution panel of the 1 km simulations

that the boundary of the high resolution domain cuts through the mountains should not cause spurious effects, because of the variable-resolution stretched-grid approach applied in the downscaling. This implies that the area of high resolution does not abruptly stop at that point (as would have been the case in limited-area modelling), but the resolution gradually becomes coarser as one moves away from the high resolution panel.

3.3.5 Ultra-high (200 m) simulations overt the Stellenbosch region

Lastly, the 200 m simulations were performed on an individual-month basis, following a similar approach as for the 1 km runs. That is, each monthly simulation was performed on a single processor and initialized from and nudged within the corresponding 1 km simulation. The time-step used was a mere 3 seconds, making the 200 m simulations relatively expensive. Each monthly simulation at 200 m resolution took about 2 weeks to complete on a single processor. The 200 m simulation have a Schmidt factor of 990. It may be noted that the convective parameterisation is not changed when moving to the higher resolutions. A convective time scale of 20 minutes is used in the model, so for the higher resolution runs with smaller timesteps a fractional adjustment is applied during each time step.

The focus of this ultra-high simulation is on the Stellenbosch wine producing region. In order to exploit the ultra-high resolution, the input data such as soil, topography and vegetation also had to be on a very fine scale. This input data was constructed at the ARC and incorporated into the model's surface scheme at the CSIRO. The topography, soil and vegetation were obtained from the ARC Institute for Soil, Climate and Water (ISCW). The soil data was interpolated from the Pedology division's soil datasets and vegetation was extracted from LandSat2000. The topography was extracted from a digital elevation model (DEM), which has a resolution of about 30 m (but was interpolated to the model grid of 200 m resolution). Figure 3.6 gives a representation of the topography over the Stellenbosch wine producing area. The actual dimensions of the ultra high 200 m resolution area is 33.79°S - 33.89°S and 18.79°E - 18.89°E.

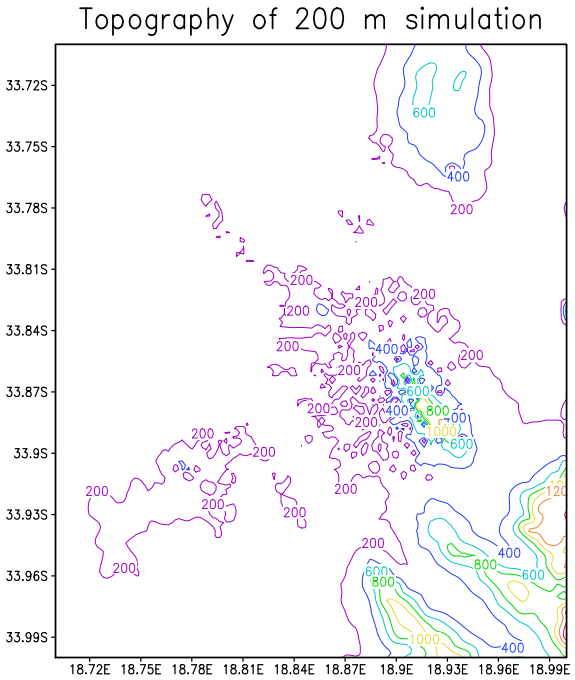

Figure 3.6: Topography over and around the high-resolution panel of the 200 m simulations

Chapter 4

Verification of model simulations

4.1 Introduction to model verification

An atmospheric model gives a representation of the atmospheric conditions over a certain area. The aim of any model is thus to simulate the actual weather or climate as accurately as possible. However, no model is perfect, and each model has its own biases that result from the approximations made in simulating the very complex climatic system. Therefore, before a model could be used for a certain climate study it is necessary to validate the model over the region. This process tests the accuracy and skill of the model to give a reasonable representation of the atmospheric conditions for the purpose of which the model is used. In this study the model is validated on different time and spatial scales. In order for the downscaling to the micro-scale to be successful, the first condition is that the model should provide a satisfactorily simulation of the synoptic-scale climatology of southern Africa and the southwestern Cape in particular. The 60 km simulation was therefore verified with the emphasis om the simulation of the synoptic-scale circulation over southern Africa. This was achieved by comparing the simulated seasonal circulation and rainfall cycles over southern Africa to against the observed cycles described by NCEP Reanalysis and CRU data. The simulated intra-annual rainfall cycle is subsequently compared against the observed cycle described by CRU over 10 subregions of the domain. The 8 km simulation of meso-scale climatological features over the southwestern Cape, such as the seasonal temperature, rainfall, wind speed and relative humidity cycles was verified against observed CRU data. How well the model simulates climatological features as a function of the fine-scale topography is of particular importance in this part of the verification.

The ultimate aim of the verification procedure is to determine whether the high-resolution model simulations are of sufficient quality to be of use for decision

making in the viticultural industry. It should be noted that the verification of the ultra-high resolution climate simulations are problematic, in the sense that the observation network is of a lower spatial resolution. In fact, as pointed out in Chapter 1 the need for ultra-high simulation climate simulation for the wine-industry stems from the fact that an observed climate of sufficiently high resolution is not available. The strategy followed to verify the ultra-high resolution simulations (1 km and 200 m) is to compare them against point data available from automatic weather stations. The model's ability to simulate the diurnal cycle of climatic variables such as temperature, relative humidity and wind speed is of particular interest, as these variables are all important for the viticulture to some extent. Unfortunately automatic weather stations occurring within the area of interest and having long, good quality data records are scarce. For each station the longest possible period of available data was used for verification, which turned out to be typically a period of 5 to 10 years.

4.2 Verification of synoptic-scale (60 km) simulations

4.2.1 Annual rainfall totals over southern Africa

The observed CRU climatological rainfall totals over South Africa (Figure 4.1 a) indicate a pronounced west-east gradient in rainfall over South Africa. Parts of the east coast receive more than 1000 mm per year on the average, whilst less than 100 mm falls along the west coast. The Namibian coast is an arid region, and it may be noted that a zonal band of dry conditions stretches from this region towards Mozambique, between 25° S and 15°S. The tropics are wet with much of the region receiving an average rainfall higher than 1600 mm, although parts of East Africa are significantly drier. CCAM simulates the west-east gradient in rainfall over South Africa satisfactorily, although rainfall over Lesotho is overestimated rather severely. The simulation of rainfall totals over this region are problematic in dynamic models, and seem to be related to the steep topography of this region (e.g. Engelbrecht et al, 2002; Christensen et al, 2007). The features of the extremely dry Namibian coast, wet tropics, relatively dry East Africa and the band of drier conditions from 25° S to 15°S are simulated remarkably well by the model. Rainfall totals over the Mozambique coast and eastern South Africa are overestimated, however, the model in general simulates rainfall totals realistically. Overall the model gives an excellent representation of the synoptic-scale distribution and amplitude of annual rainfall over tropical and southern Africa.

In the study performed by Engelbrecht (2009), a similar comparison was made between CCAM simulations and the CRU dataset. In that study, SSTs from the CSIRO Mk3 OAGCM were forced to drive the high-resolution CCAM simulations over southern and tropical Africa. In the resulting model simulation, it was found that the model captured many of the observed rainfall pattern's

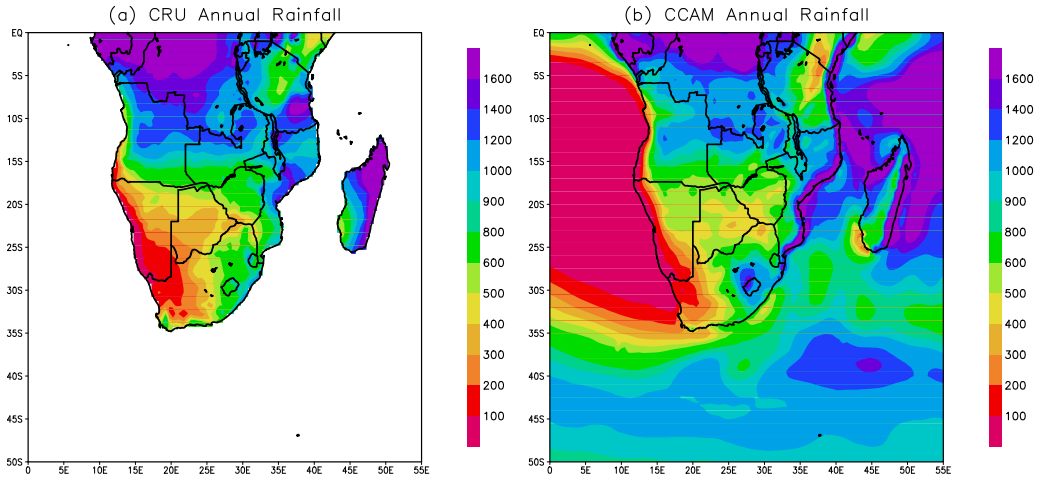

Figure 4.1: Annual rainfall for CRU-observed (a) and CCAM-simulated (b) over Southern Africa

regional features, but rainfall totals over the southern DRC, northern Zambia, western Tanzania and the Mozambican coast line were overestimated severely (Engelbrecht et al 2009). It may be noted that the current simulation of yearly rainfall over southern Africa is more realistic than those of Engelbrecht et al (2009). The fact that nudging the present simulations within NCEP reanalysis data as in the present study should indeed be expected to lead to an improvement of the model simulation, as realistic synoptic-scale forcing is prescribed compared to the OAGCM simulations where the model should generate its own synoptic-scale circulation climatology. An improved and more recent version of the CCAM code used in this study are probably an additional reason for the improved simulations.

4.2.2 Seasonal rainfall cycle over southern Africa

The seasonal rainfall pattern over southern Africa is depicted by means of rainfall percentages (the percentage of the annual rainfall that occur during the specific season), following Engelbrecht et al (2009). During austral winter (JJA), most of the continent receives less than 10 percent of its annual rainfall. Important exceptions are the southwestern Cape and the Cape south coast in South Africa, which receive up to 60 % and 40 % of their yearly rainfall, respectively. The southwestern Cape is a winter rainfall area, whilst the Cape south coast is an all year round rainfall region (Figure 4.2 a). The model correctly simulates the relatively high rainfall percentages over these regions and the drier subcontinent to the north (Figure 4.2b) . Much of the tropics also receive more than 10 % of the yearly rainfall during JJA, along the southern boundary of the Inter Tropical Convergence Zone (ITCZ) which is located in Northern Hemisphere at

this time. This is simulated satisfactorily by CCAM (Figure 4.2 b).

During spring (SON), the rainfall percentages start to increase over the subcontinent, especially over the eastern parts of South Africa and the tropics (Figure 4.2 c). The ITCZ moves to the south of the equator during these months, and much of tropical Africa south of the equator receives between 30 and 40 % of its annual rainfall. The model simulates the onset of the rainy season during SON over both the tropics and eastern South Africa well. The pattern and amplitude of rainfall percentages is well captured in the model simulation (Figure 4.2 d). An exception is Namibia and western South Africa, where the model somewhat overestimates rainfall percentages. The SON simulation of the current CCAM simulation is to a large extend similar to that obtained by Engelbrecht et al (2009). CCAM does, however, simulate the rainfall percentages over northern subcontinent a bit more realistic. It is expected since the simulations of Engelbrecht et al (2009) are forced with the SST of an OAGCM.

During summer (DJF) the southward displaced Inter Tropical Conversion Zone (ITCZ) induces a band of high rainfall percentages over the central parts of southern Africa (Figure 4.2 e). Over South Africa, a west-east gradient in rainfall percentages exists. Note in particular the low rainfall percentages over the southwestern Cape. The tropics receive most of its rainfall in SON, and the rainfall percentages between 5° S and the equator are higher in SON than in DJF, while the rest of central southern Africa receive most of its rainfall in DJF. CCAM satisfactorily simulates the band of high rainfall percentages over the central subcontinent. However, it underestimates rainfall percentages over northern Namibia, southern Angola and northern Botswana. This occurs in association with the overestimation of rainfall percentages over this region during SON. The model correctly simulates the low rainfall percentages over the southwestern Cape, but somewhat overestimates rainfall percentages over central South Africa (Figure 4.2 f) and underestimates rainfall percentages over eastern South Africa. The steepness of the observed west-east gradient in DJF rainfall percentages is as a result not fully represented in the model simulation.

During MAM the ITCZ moves northwards, and drier conditions set in over the eastern and central parts of southern Africa. Rainfall percentages are relatively high over the western parts of South Africa, Namibia and Angola (Figure 4.2 g). The reduced rainfall in autumn is satisfactorily simulated by CCAM. The model does simulate the relatively high rainfall percentages over the western subcontinent, although the amplitude of the pattern is shown to be lower than observed (Figure 4.2 h).

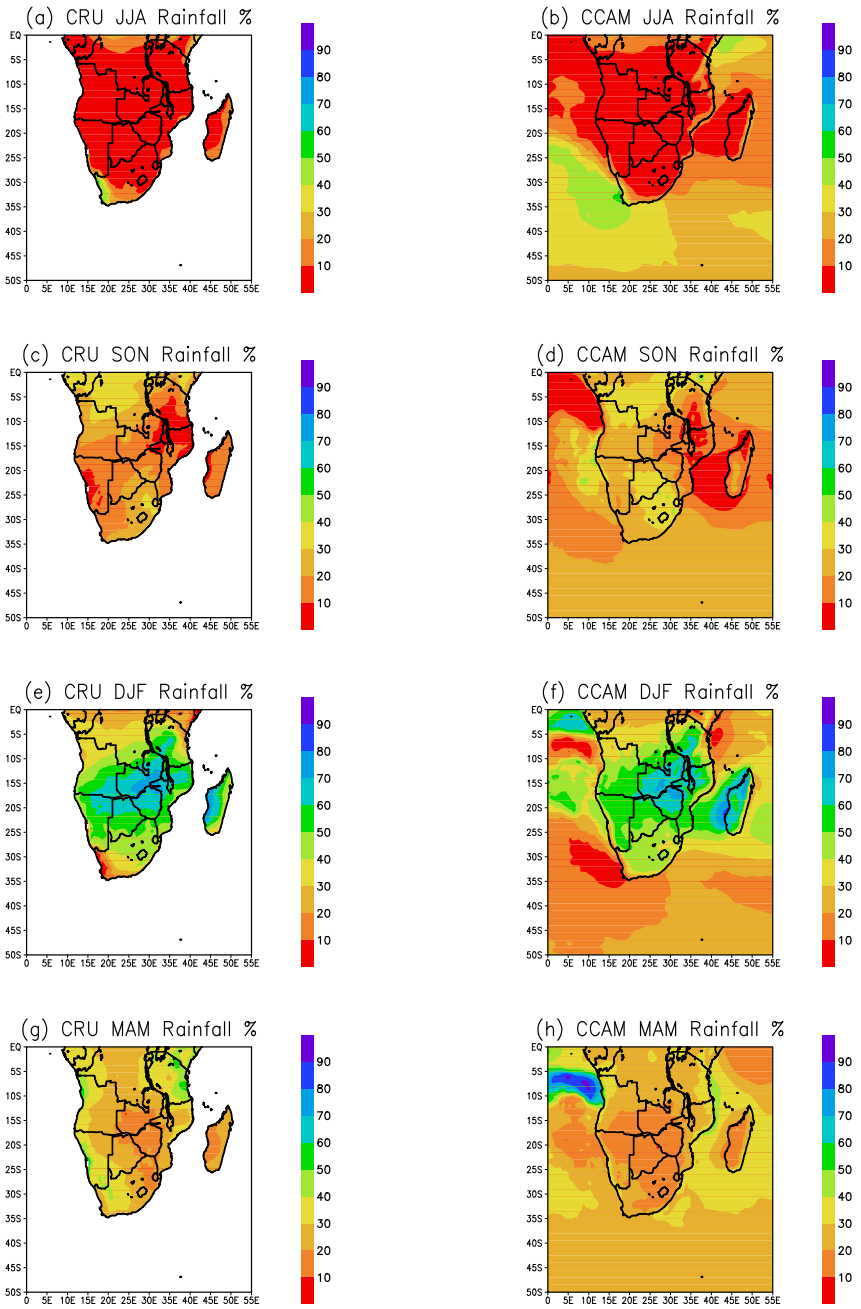

Figure 4.2: CRU-observed (left) and CCAM-simulated (right) seasonal rainfall expressed as a percentage of the annual totals for JJA (panels a and b); SON (panels c and d); DJF (panels e and f) and MAM (panels g and h)

4.2.3 Seasonal circulation cycle over southern Africa

Sea level pressure

Figure 4.3 shows the seasonal sea level pressure of the "observed" NCEP/NCAR Reanalysis fields (Kalnay et al, 1996) and the 60 km CCAM climate simulation.

Winter is characterized by by the presence of the subtropical high-pressure belt over South Africa, with the centers of two strong anticyclones, the Atlantic Ocean High (AOH) and Indian Ocean High (IOH), located over the oceans to the west and east of South Africa, respectively. A strong meridional pressure gradient to the south of the country and the presence of the ITCZ to the north can be detected by the lower pressures just south of the equator (Figure 4.3 a). CCAM captures the mean sea-level pressure pattern satisfactorily. Seen overall the amplitude of the mean sea level pressure is also simulated well, although pressure is underestimated over eastern South Africa. The amplitude and southern extent of the trough over the tropics are somewhat overestimated (Figure 4.3 b). The latitude position of the IOH and AOH are captured very well by CCAM. This accurate representation of the synoptic scale circulation provides the opportunity to successfully downscale to a higher resolution over the southwestern Cape.

During SON, a heat trough forms over the subcontinent in response to the southward advancing solar radiation. The IOH and AOH both weaken, and so does the meridional pressure gradient south of the subcontinent.(Figure 4.3 c). The model overestimates the intensity of the continental trough over the subcontinent, and also extends it too far southwards over South Africa. However, the weakening of the IOH and AOH as well as weakening of the meridional pressure gradient south of the subcontinent are simulated satisfactorily (Figure 4.3 d).

During the austral summer period (DJF) the continental trough widens and pressure drops over the whole subcontinent, in response to the enhanced solar heating. The trough is most intense over northern Namibia. The band of anomalously low pressure stretches eastward over the Indian Ocean (IO) and Madagascar. Both the IOH and AOH weaken, and the IOH undergoes a clear shift southwards (Figure 4.3 e). However, it extends a ridge westward to the eastern interior of South Africa. CCAM correctly simulates the continental trough to be most intense over northern Namibia. The weakening of the anticyclones and southern shift of the AOH are also captured well. However, the intensity of the wide band of lower pressure over the subcontinent and IO are overestimated in general. The intensity of the ridge that extends from the AOH to eastern South Africa is underestimated. (Figure 4.3 f).

The pressure over southern Africa starts to increase again during MAM, especially over the eastern parts of South Africa. The subtropical high pressure

belt intensifies over the oceans in the subcontinent. (Figure 4.3 g). CCAM captures these features well, however, the intensity of the northward displaced continental trough is still overestimated (Figure 4.3 h).

850 hPa and 500 hPa circulation anomalies

The 850 hPa and 500 hPa seasonal circulation anomalies, calculated relative to the respective annual long term means, are shown in Figure 4.4. The contours indicate the 850 hPa anomalies whilst the shades are for the 500 hPa anomalies. During JJA the region of maximum solar radiation is situated the Northern Hemisphere, and results in positive geopotential height anomalies at the 500 hPa geopotential level, from the equator to about 15° S. Negative anomalies of the 500 hPa geopotential heights occur over the rest of the domain, and increase in strength towards the south (Figure 4.4 a). This is the result of the relatively low tropospheric temperatures that prevail during the austral winter, through hydrostatic balance. The geopotential heights of the 850 hPa level over the subcontinent is anomalously high, as a result of the prevailing subtropical high pressure belt. South of the continent, the negative 850 hPa geopotential height anomalies are indicative of the eastward passage of the mid-latitude cyclones (Taljaard 1976; Engelbrecht et al, 2009). The model captures the JJA all these features well, although the 850 hPa geopotential height anomalies over central southern Africa and the southern Mozambique Channel are overestimated (Figure 4.4 b).

The 850 hPa geopotential heights over the subcontinent becomes anomalously low during SON over central southern Africa as the austral summer, with its consequential heat, approaches. The region of the largest negative 850 hPa anomalies over the central subcontinent reveals the deepening of the continental trough during SON (Figure 4.4 c). The orientation and strength of the region of negative 850 hPa geopotential anomalies over southern Africa, as well as the general geopotential anomaly distribution over the area of interest, are captured very well by CCAM. The anomalously high 500 hPa geopotential heights that occur over central southern Africa are also captured, but CCAM incorrectly extends the area of positive 500 hPa anomalies to Madagascar (Figure 4.4 d).

During the austral summer period (DJF) anomalously low 850 hPa geopotential heights occur over the central parts of southern Africa, as a result of the intense solar heating. The band of anomalously low pressure stretches eastward over the Indian Ocean (IO) and Madagascar (Figure 4.4 e). CCAM captures this pattern well, although the negative pressure anomalies over central southern Africa are overestimated compared to the reanalysis data - and even more so east of the country in the southern Mozambique Channel. The anomalously high geopotential heights of the 500 hPa over South Africa and the southern

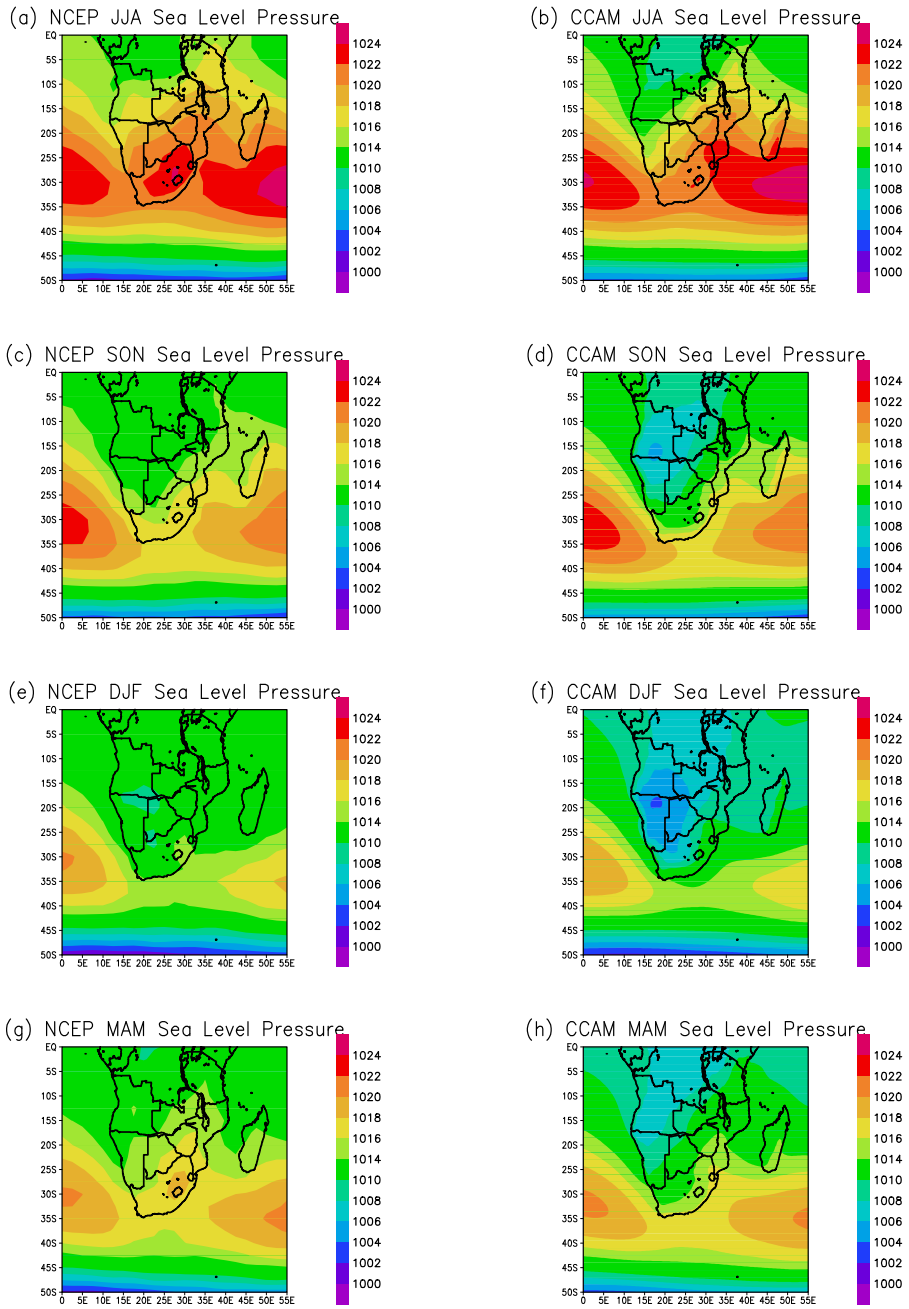

Figure 4.3: NCEP Reanalysis (left) and CCAM-simulated (right) seasonal sea-level pressure (hPa) for JJA (panels a and b); SON (panels c and d); DJF (panels e and f) and MAM (panels g and h).

oceans as well as the anomalously low geopotential heights of that level over the tropical subcontinent are almost perfectly captured by CCAM (Figure 4.4 f).

Negative sea-level pressure anomalies still persist in MAM over the subcontinent and surrounding oceans, although less in magnitude compared to in DJF (not shown). In contrast to this, the 850 hPa geopotential heights have with negative anomalies only over the tropical subcontinent, northern IO and northern AO. Positive anomalies are to be found over southern Africa in response to the strengthening of the subtropical high pressure belt during MAM. These features of the 850 hPa circulation are well represented in the CCAM simulation. Both the observed and simulated 500 hPa geopotential height anomalies are positive through domain but less in magnitude than in DJF, partially in response to the solar radiation that decreases during MAM.

200 hPa wind

The seasonal anomalies in the 200 hPa wind field calculated relative to the annual long-term mean are displayed in Fig.4.5. In winter (JJA) the circumpolar westerlies expand northward, intensify and displace the upper tropical easterlies equator ward (Tyson and Preston-Whyte, 2000). Indeed, the 200 hPa anomalies show anomalously strong westerly flow is present over the central subcontinent (Figure 4.5 a). The CCAM field resembles the observed field very closely. This is a result of the global wind nudging that is performed at all pressure levels greater than and equal to 500 hPa (Figure 4.5 b).

During spring (SON) the region of maximum anomalous westerly flow is located further to the north over the tropics, and the anomalies are smaller in magnitude (Figure 4.5 c). This pattern is mirrored in the model representation the flow (Figure 4.5 d).

As shown in Figure 4.5 e, summer is marked by anomalous easterly flow between 35°S and 5° S at the 200 hPa pressure level. The close correspondence between the CCAM and NCEP wind fields illustrates the success of the wind-nudging performed. (Figure 4.5 f).

The 200 hPa wind anomalies are relatively small in autumn (MAM). Anomalously easterly flow prevails south of the subcontinent (Figure 4.5 g). There is close correspondence between the NCEP Reanalysis and simulated CCAM 200 hPa wind anomalies (Figure 4.5 h).

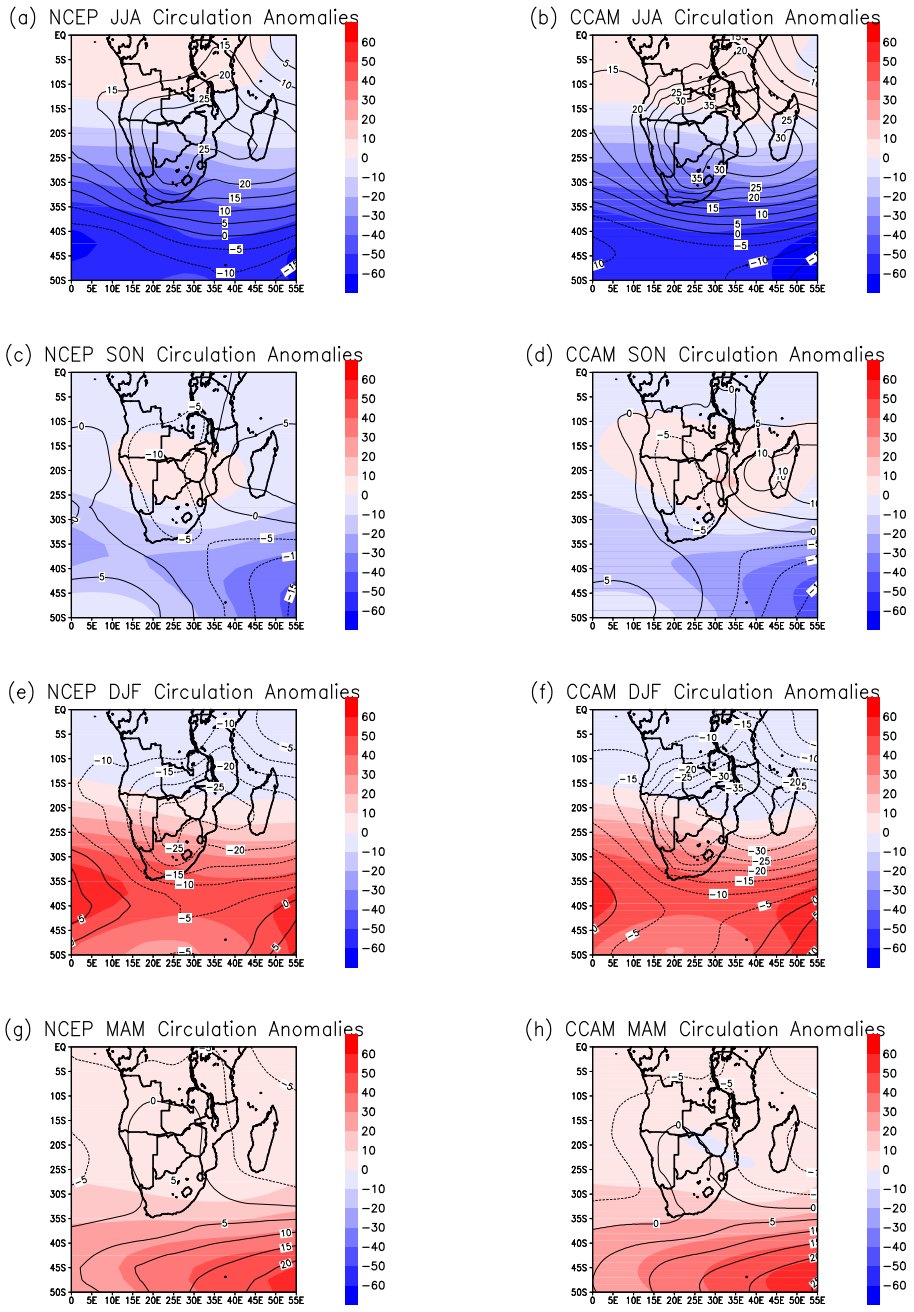

Figure 4.4: NCEP Reanalysis (left) and CCAM-simulated (right) seasonal circulation anomalies for JJA (panels a and b); SON (panels c and d); DJF (panels e and f) and MAM (panels g and h) for the 850hPa (contours) and 500hPa (shaded) levels. Anomalies are calculated relative to the respective annual long-term means and are given in geopotential meters (gpm)

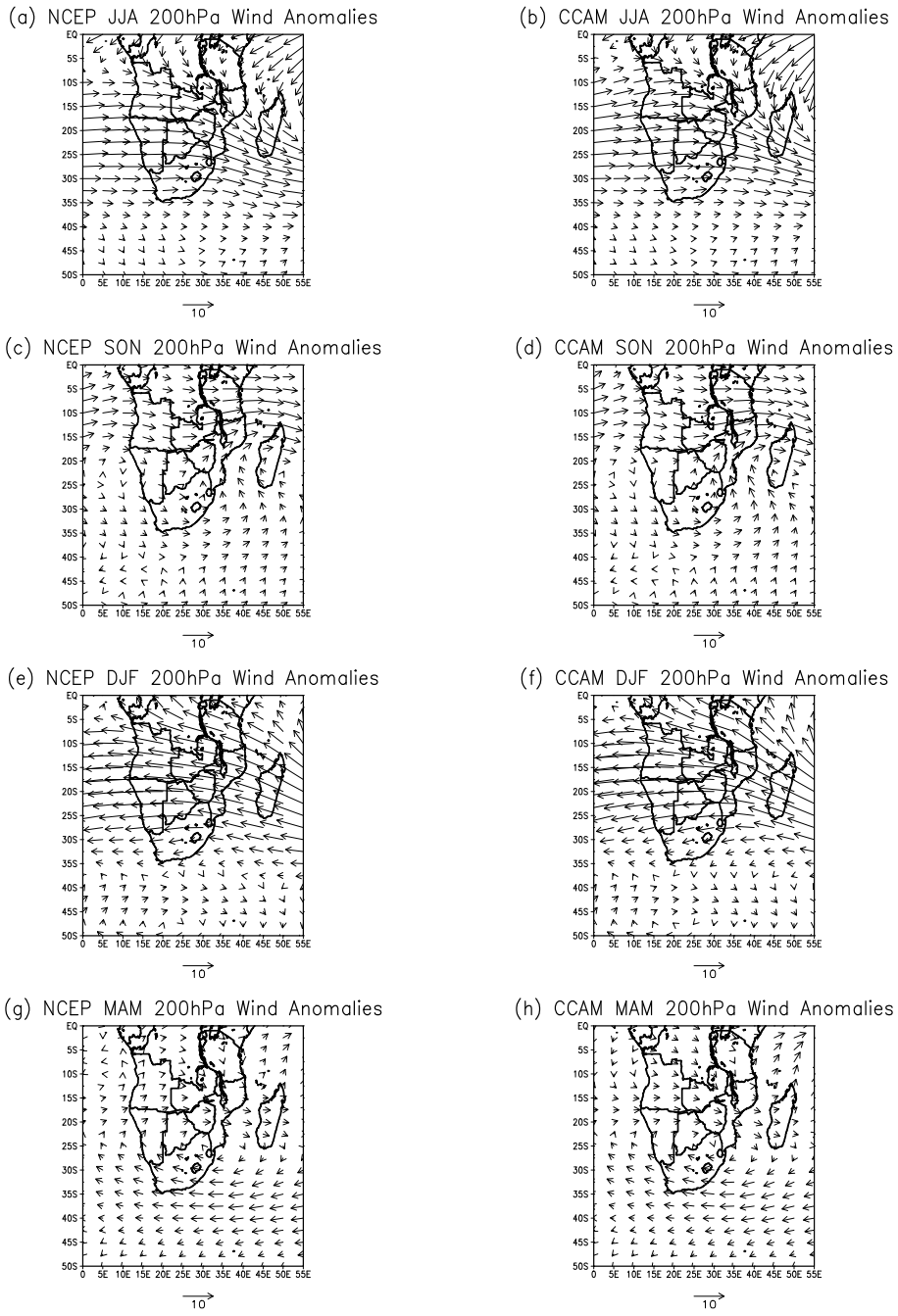

Figure 4.5: NCEP Reanalysis (left) and CCAM-simulated (right) 200hPa wind anomalies for JJA (panels a and b); SON (panels c and d); DJF (panels e and f) and MAM (panels g and h). Anomalies are calculated relative to the respective annual long-term means and are given in m/s

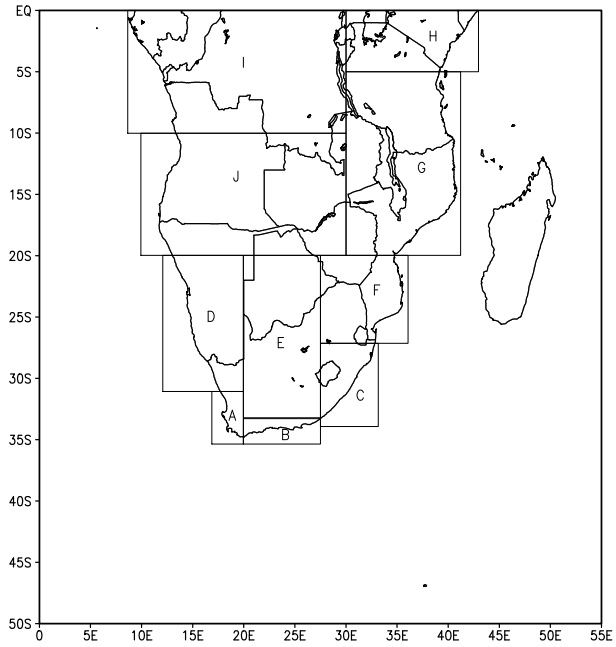

Figure 4.6: Locations of the different regions used in the intra-annual rainfall validation

4.2.4 Intra-annual rainfall cycle over various regions over southern and tropical Africa

The intra-annual rainfall cycle over the subcontinent is verified against observations over ten different subregions, following Engelbrecht et al (2009). Figure 4.6 show the subregions used for the intra-annual rainfall verification, and their precise longitudinal and latitudinal boundaries are given in Table 4.1.

The south-western Cape (Region A) is a winter rainfall region, with relatively high rainfall between April and September and a maximum in June. Interestingly, the observed rainfall in August is also slightly higher than in July (Figure 4.7 a). CCAM underestimates the rainfall during winter quite severely and does not simulate the slight increase of rainfall in August, but captures the fact that the rainfall peaks in June. The modeled monthly totals of Engelbrecht et al (2009) compared much better over the southwestern Cape than the current simulation, although the simulated presented here displays a similar pattern of intra-annual variation.

The Cape south coast (Region B) is a year-round rainfall area. March is the month which receive the most rainfall, followed by August. December is the driest month over this region, with less than 1.3 mm/day. January and July is

Table 4.1: Locations of the regions used for the intra-annual rainfall verification

Number	Region	Latitude	Longitude
A	South-western Cape	-35^{o}S to -31^{o}S	17^{o}E to 20^{o}E
B	Cape south coast	-35^{o}S to -33.5^{o}S	20^{o}E to 27^{o}E
C	Eastern South Africa	-34^{o}S to -27^{o}S	27^{o}E to 33^{o}E
D	Western subcontinent	-31^{o}S to -20^{o}S	12.5^{o}E to 20^{o}E
E	Central subcontinent	-33.5^{o}S to -20^{o}S	20^{o}E to 27^{o}E
F	North-eastern SA, S Zimbabwe and S Mozambique	-27^{o}S to -20^{o}S	27^{o}E to 36^{o}E
G	N Mozambique and Tanzania	-20^{o}S to -5^{o}S	30^{o}E to 41^{o}E
H	East Africa	-5^{o}S to 0^{o}S	30^{o}E to 43^{o}E
I	Northern subcontinent	-10^{o}S to 0^{o}S	8.5^{o}E to 30^{o}E
J	Subtropical subcontinent	-20^{o}S to -10^{o}S	10^{o}E to 30^{o}E

the other two relatively dry months with an average rainfall of about 1.4 mm/day (figure 4.7 b). The model simulates this variability in the intra-annual rainfall remarkably well. In the simulations done by Engelbrecht et al (2009), this region proved to be problematic for the model with a poor correlation between the observation and simulation. The current run is forced with NCEP "observed" data, with cause better circulation simulation and consequently improve the rainfall pattern.

Region C is a summer rainfall region with the onset of the rainy season in September and it continue through until April. CCAM gives a good representation of the cycle, but overestimate the rainfall from October to December quite severely (Figure 4.7 c). Engelbrecht et al (2009), simulated the rainfall over this region much more accurately, with just a slight overestimation in December.

The western subcontinent receives the majority of its rainfall between January and April, with the rainfall maximum occurring in February (Figure 4.7 d). Again the model overestimates the rainfall in the last three months of the year. The model does not simulated the rainfall peak in February and the model simulated more rainfall in latter part of the year (November and December) than in January and February. Engelbrecht et al (2009) overestimate the rainfall from May to January, but correctly simulates the peak in February.

The rainfall cycle of the central subcontinent (Region E) is similar to eastern South Africa (Region C), although the amount of rainfall is less over the central subcontinent (Figure 4.7 e). There's an observed rainfall peak in February, which is not picked up by the current CCAM simulation. The model also indicates a similar pattern as simulated in Region C and October, November and December is again overestimated extensively. The February rainfall peak is simulated by Engelbrecht et al (2009), but the simulation also overestimates the amount of rainfall during the summer months severely.

Region F is a summer rainfall region, with a maximum in February (Figure 4.7 f). This pattern is represented in the model simulation. The model somewhat overestimates rainfall over the region. It correctly simulates the rainfall maximum to occur in February, however, the intensity of this rainfall peak is overestimated. Engelbrecht et al (2009) found similar results over this region.

Region G is another summer rainfall area, with the onset of the rainy season in October and the end in May (Figure 4.7 g). CCAM simulates the rainfall for this region remarkably well.

East Africa (Region H) has rainfall maxima in April and November, in association with the northward and southward pass of the ITCZ over this region during April and November, respectively. The model underestimate this maximum in April, and just slightly overestimate it in November (Figure 4.7 h), unlike the simulations done by Engelbrecht et al (2009), which overestimated both maxima quite severely. In the current simulation, the rainfall for October is also overestimated.

Region I (the northern subcontinent) have maxima during March and November, which are also due to the north/south movement of the ITCZ. This time the rainfall of both months are underestimated by the model, but not to a great extend. Overall CCAM simulate the intra-annual rainfall variability of this region very good (Figure 4.7 i).

The subtropical subcontinent is a summer rainfall area which receives almost no rainfall during the winter (from May to September). Both the pattern and rainfall amount are simulated very accurately by the model (Figure 4.7 j).

4.3 Verification of the mesoscale (8 km) simulations

4.3.1 Comparison of the 8 km and 60 km simulations

The 8 km simulation provides much more detail over the Western Cape than the 60 km simulation. This is illustrated by the comparison of the average screen temperature between the 60 km simulation (Figure 4.8 a) and the 8 km simulation (Figure 4.8 b). The topography used in each simulation are shown in black contours over the figures. The broad patterns of temperature maxima to the north and west of the domain and the cooler south and east are consistent in the two simulations, but the 8 km simulation show much more detail. The finer topography of the 8 km simulation is one of the greatest influencing factors in the improved simulation as the 60 km run interpolates/averages between points spaced far apart. Local variations is often ignored by the 60 km simulation, as it is smaller than the grid on which the calculations is performed (60 km).

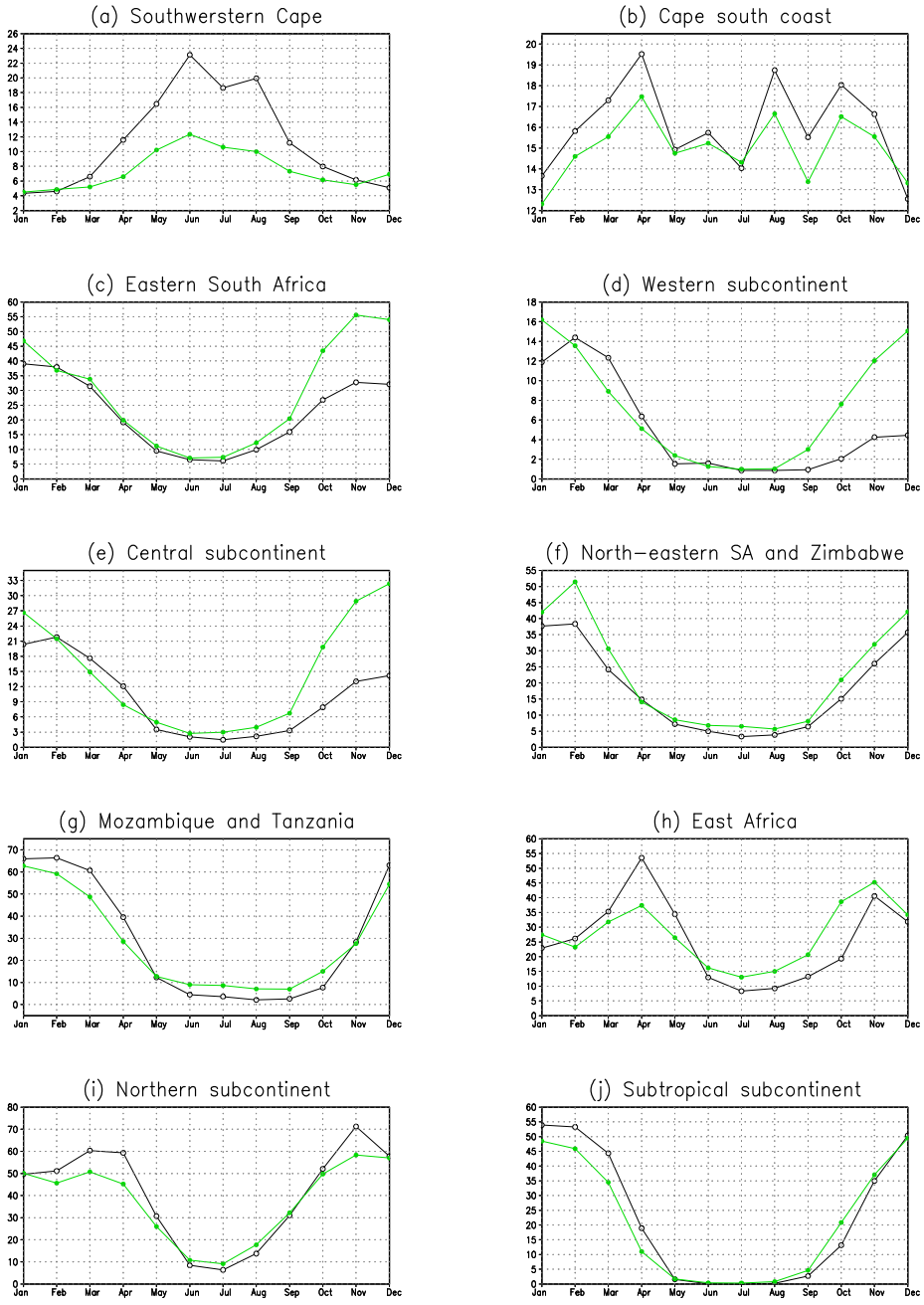

Figure 4.7: CRU observed (black) and CCAM simulated (green) monthly rainfall totals (mm/day)*10 over different regions of the subcontinent

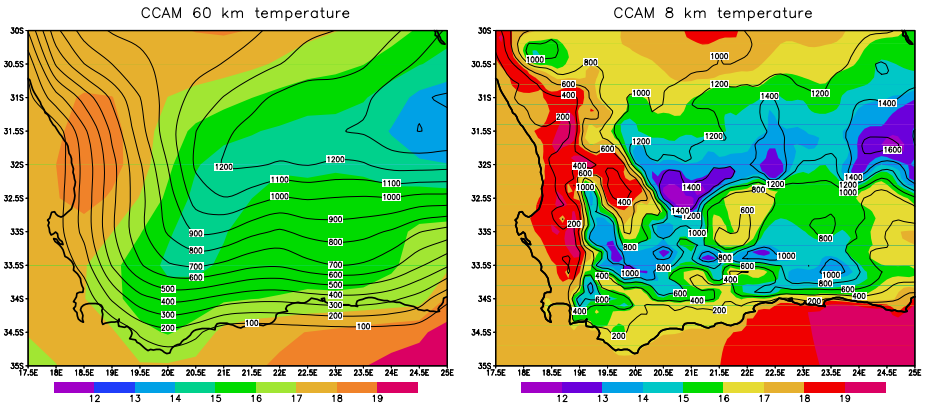

Figure 4.8: Topography (contours) and average screen-height temperature (shades) for February 2000 - a comparison between CCAM 60 km simulation (a) and 8 km simulation (b).

The areas of high topography is cooler than the surrounds. The south-easterly winds that are predominant in summer together with the occasional bergwinds in winter contributes to the warm temperatures to the west on the off-wind side of the mountains (due to the adiabatic heating). All these features can clearly be seen in the 8 km simulation, with its improve resolution and topography over the Western Cape.

4.3.2 Yearly and seasonal rainfall

Yearly rainfall

There is a distinct west-east gradient in the annual rainfall over the northern part of the western Cape, with the north western side of the area receiving less than 200 mm of rain per year and the eastern parts more than 400 mm (Figure 4.9). The highest rainfall occur along the southern coastal areas. Orographic forcing is responsible for two distinct rainfall maxima: the Cape Peninsula (the region west of the mountain ranges stretching from Franschoek northwards) and the coastal area between 22° E and 25° E both have a yearly rainfall in excess of 700 mm. The CCAM 8 km simulation of yearly rainfall captures the observed west-east gradient over the northern part of the province. The far northwest is simulated to be drier than observed. The presence of relative rainfall maxima over the Cape Peninsula and the southern coastal area between 22°E and 25°E are captured, however, rainfall totals over these regions are severely underestimated (Figure 4.9).

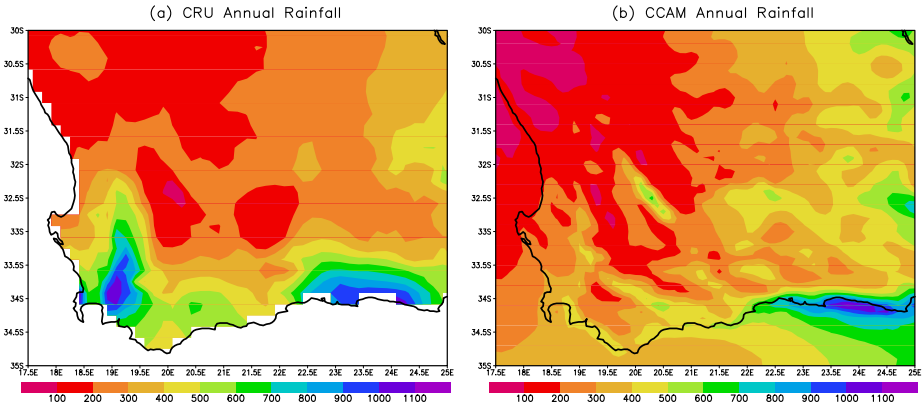

Figure 4.9: CRU observed (a) and CCAM simulated (b) yearly rainfall over the Western Cape

Seasonal rainfall

The southwestern Cape with its Mediterranean climate receives the majority of its rainfall during winter with a profound west-east gradient in rainfall percentages. The area west of the mountain ranges that stretches from the Franschoek northwards receives 40 % or more of its annual rainfall during JJA. The southern coastal areas receive 20 % or more of its annual rainfall, from where rainfall percentages decrease northwards to less than 10 % in the far north (Figure 4.10 a). CCAM simulates the general JJA pattern of rainfall percentages well. The area of orography induced high rainfall percentages in the far west is captured although percentages are slightly underestimated. The low rainfall percentages (less than 10 %) in the north stretches further to the south in the simulation than in observations. (Figure 4.10 b).

During Spring (SON) rainfall percentages range between 10 and 30 % over the region (Figure 4.10 c). The southern coastal areas receive up to 30 % of its annual rainfall during SON, from where percentages decrease towards the northwest. The model simulates the range of rainfall percentages well, and captures the occurrence of maximum percentages over the southern coastal areas. However, the gradient in rainfall percentages is simulated to occur from west-east, rather from the southeast to northwest as observed (Figure 4.10 d). Interestingly, it may be noted that the southern coastal areas with its high annual rainfall never receives much more than 30 percent of its rainfall in a season, indicating its year-round rainfall quality.

Summer is marked with a reversal in the gradient of rainfall percentages, with a marked east-west gradient occurring over the area of interest. The far western parts receive less than 10 % of its annual rainfall during DJF, while the north-

eastern corner of the domain receive up to 40 percent (Figure 4.10 e). This pattern is again captured satisfactorily by CCAM, although the model generally overestimates the summer rainfall percentages in the east.

The southern and western coastal areas receive close to 30 % of their annual rainfall during MAM, with even higher percentages (up to 45 %) occurring over the remainder of the area of interest. The model simulates the rainfall percentages occurring over the coastal areas during MAM well, but simulates relatively lower (rather than higher) percentages over the interior areas. This underestimation is related to the overestimation of rainfall percentages over this region during DJF

Intra-annual rainfall variability

Figure 4.11 shows the comparison between the 60 km and 8 km intra-annual rainfall variability over the southwestern Cape (Region A). In the simulated intra-annual rainfall, the 8 km simulation produces slightly less rainfall than the 60 km simulation. From the annual rainfall graphs it is clear that in both simulations, the rainfall is extensively underestimated by the model over the southwestern Cape. Both the 60 km and 8 km resolution simulations show the same intra-annual rainfall pattern. The intra-annual rainfall cycle is captured by the model to some extend, with the maximum rainfall occurring in June, but the second maxima in August is not quite there. The model also simulates a higher rainfall in December than in November, which is not captured in the observations.

4.3.3 Yearly and seasonal temperature

Yearly temperature

The average annual screen-height temperature over the Western Cape ranges between 12°C and 19°C (Figure 4.12 a). CCAM shows a remarkable coherence with the observations (Figure 4.12 b), indicating that the model correctly simulates the dependency of temperature on height. In the CCAM simulations, "screen-height" is at 2 m. The topography used of the 8 km simulation is shown in black contours over the CCAM figure. The areas of high topography are noticeably cool in both the model and observations. The highest temperatures occur along the west coast, adjacent coastal areas and in the valleys, in both the model and observations. The model captures the topographic forcing of the temperature well. CCAM somewhat overestimates the intensity of both the warmest and coolest areas, and the southeastern part of the domain is simulated to be somewhat cooler than observed. Generally the model gives an excellent representation of the average annual temperature.

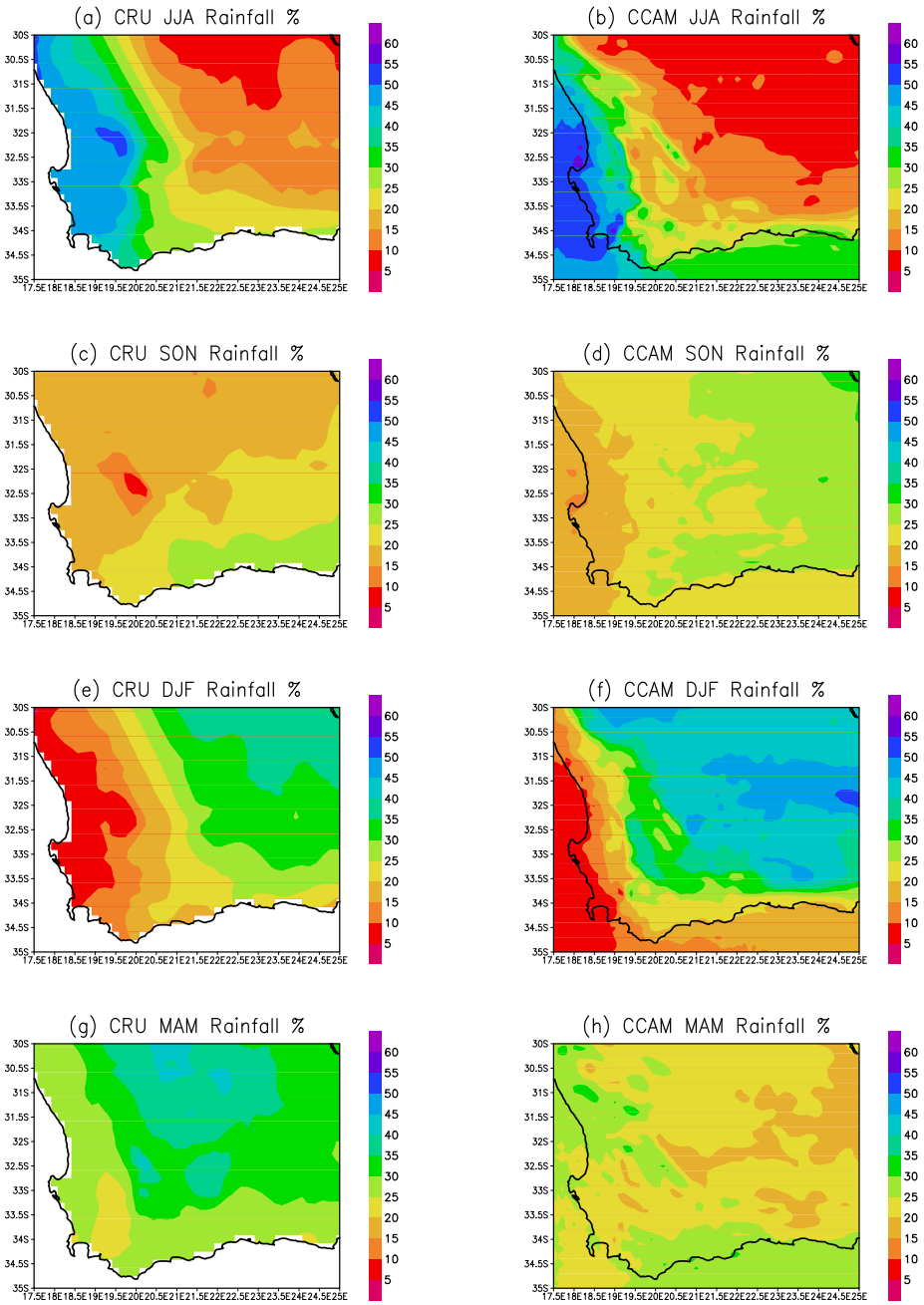

Figure 4.10: CRU observed and CCAM simulated seasonal rainfall percentages over the Western Cape for JJA (panels a and b); SON (panels c and d); DJF (panels e and f) and MAM (panels g and h)

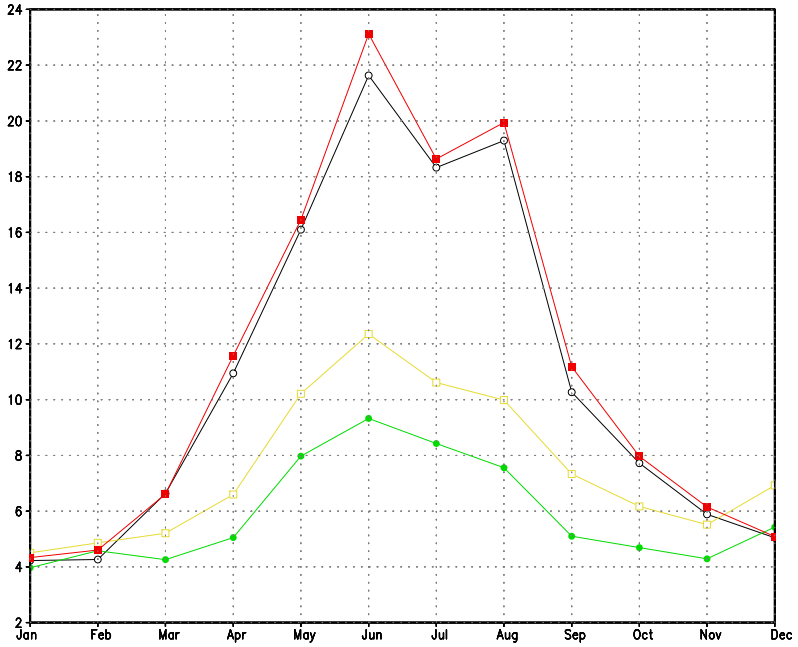

Figure 4.11: Comparison between simulated 60 km (yellow); simulated 8 km (green); CRU 0.5^o(red) and CRU 10' (black) intra-annual rainfall cycle ((mm/day)*10) over the south-western Cape

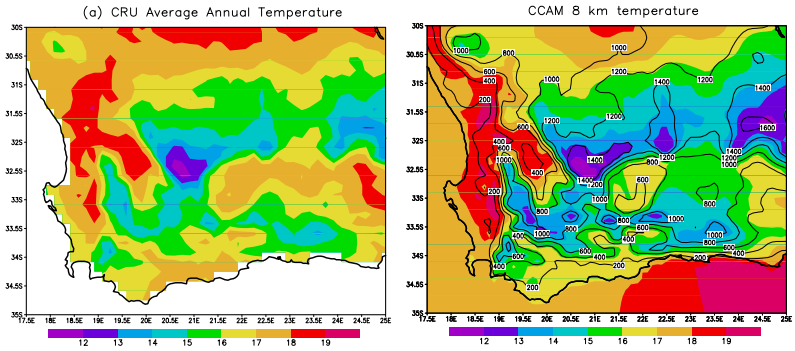

Figure 4.12: CRU observed (a) and CCAM simulated (b) annual temperature over the Western Cape

Seasonal Temperature

During winter coastal temperatures are relatively warm compared to the rest of the domain, due to the moderating effects of the ocean. The coldest temperatures occur on the high grounds, in particular over the central interior regions of the area of interest. The observed winter temperature pattern is well simulated by CCAM (Figure 4.13 b), although the model overestimates the magnitude of the temperature minima over the central interior regions (Figure 4.13 a).

The western Cape starts to warm up in Spring (SON), but as in winter the same pattern of cooler temperatures at the areas of high elevation is evident (Figure 4.13 c). The magnitude of the temperatures are in general accurately simulated by CCAM, with a slight underestimation of temperatures over the southeastern parts of the domain (Figure 4.13 d).

During summer the western Cape warms up with the majority of the area being in the twenties. The northern parts of the domain and the Breederivier valley (to the west of the Cederberg Mountain, at about 32°S and 19.7°E) receives the highest temperatures with average temperatures in excess of 24°C (Figure 4.13 e). CCAM satisfactorily simulates this pattern, although the model overestimates the magnitude of the temperature along the west coast (Figure 4.13 f).

Autumn (MAM) has got the same temperature range and broad pattern as Spring (SON). The west coast and the Breederivier valley are warmer than the rest of the domain and the high altitude areas are colder than their surroundings (Figure 4.13 g). This is accurately captured by the model (Figure 4.13 h).

4.3.4 Yearly and seasonal 10 m wind speed

Yearly wind speed

The observed CRU 10 m wind speed over the Western Cape appears much smoother than the observed rainfall and temperature fields. This results from the fact that there are significantly fewer stations reporting wind speed in the area than there are reporting temperature and rainfall. Nevertheless, some important characteristics of the average wind field can be deduced. The highest average wind speeds occur over the Cape Peninsula and the southwestern part of the area of interest, and decreases gradually towards the northern parts (Figure 4.14 a). CCAM gives a much more detailed presentation of the average annual wind speed. The simulated wind speed is of the same order of magnitude as the observations, but the influence of topography is clearly visible over the central mountainous areas (Figure 4.14 b). It is not clear whether the apparent

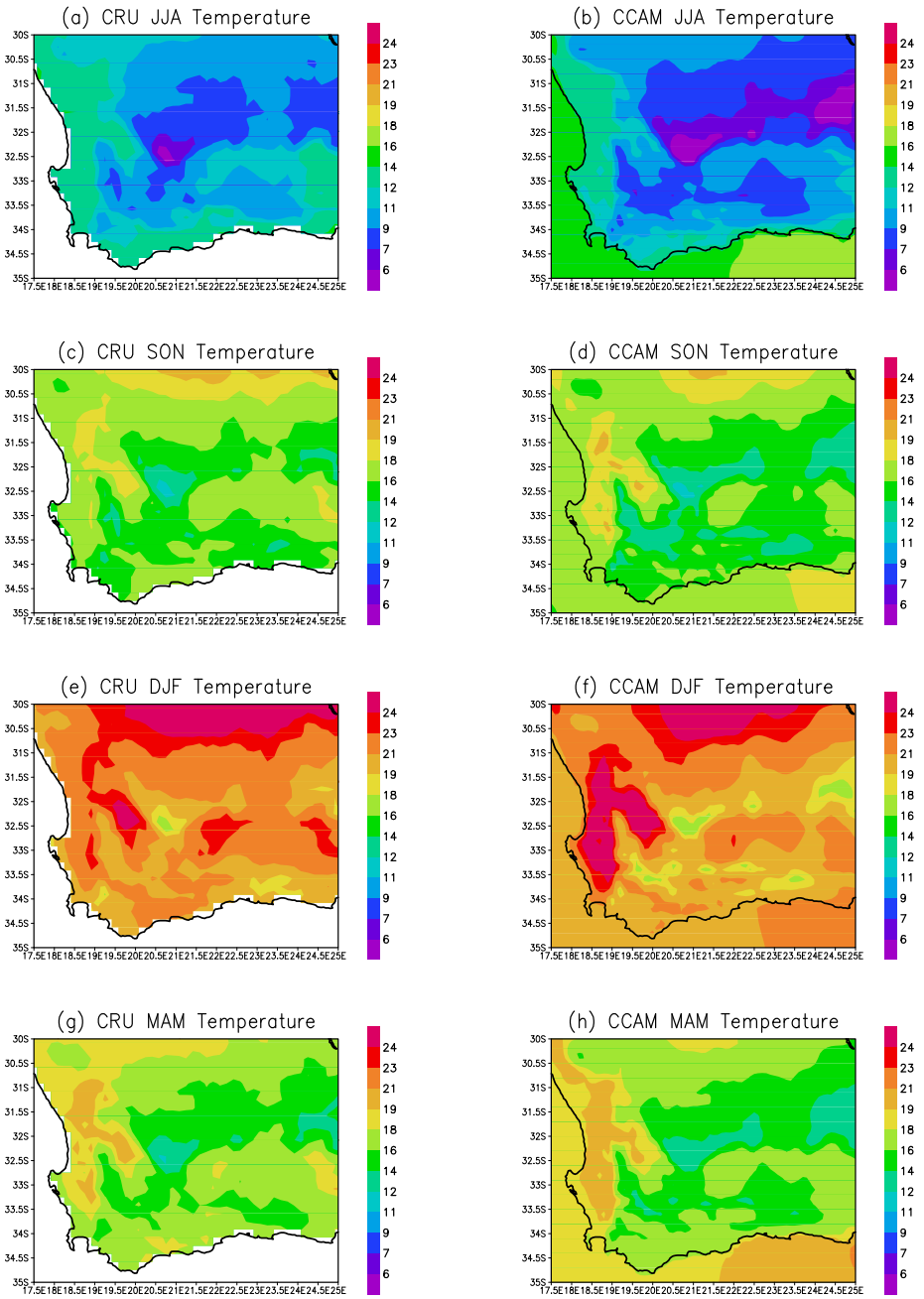

Figure 4.13: CRU observed and CCAM simulated seasonal temperature over the Western Cape for JJA (panels a and b); SON (panels c and d); DJF (panels e and f) and MAM (panels g and h)

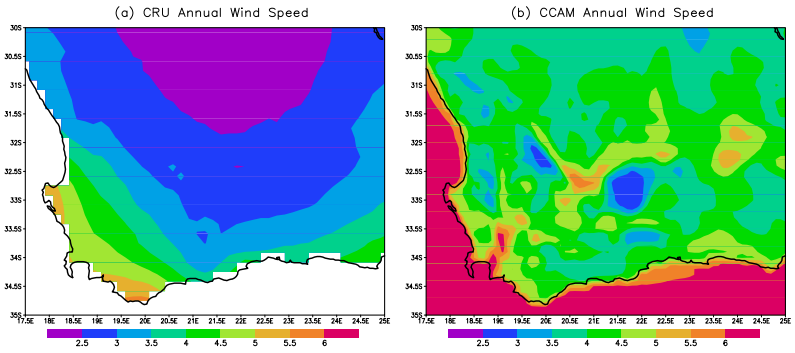

Figure 4.14: CRU observed (a) and CCAM simulated (b) annual 10 m wind speed over the Western Cape

overestimation of wind speed over the interior is the result of a model bias or the scarcity of observed data over this region.

Seasonal wind speed

During winter the 10 m wind speeds are relatively low (below 5 m/s) over the western Cape, with a maximum over the Cape Peninsula and minimum to the north (Figure 4.15 a). This basic pattern is not immediately evident from the CCAM simulation, which shows much more detail than the observed fields. In particular, wind maxima over the areas of high orography over the centre of the domain are simulated, with minima over the adjacent low-lying areas (Figure 4.15 b).

During spring (SON) the wind starts to increase in the southwestern coastal areas (Figure 4.15 c). This is also simulated by the model, with a local maximum on the mountainous area around Stellenbosch (Figure 4.15 d). The observed pattern is much the same in summer, with a further strengthening of the wind speed in the southwestern areas (Figure 4.15 e). CCAM accurately simulates this, with maximum wind speeds of more than 7 m/s over the Stellenbosch area (Figure 4.15 f).

The wind speed decreases in autumn (MAM), and the lowest wind speeds occur during this season in the domain (Figure 4.15 g). The model also show a decrease in wind speed from summer (Figure 4.15 h), although the areas of steep topography still has relatively high wind speeds (>5 m/s). CCAM generally overestimates the wind speed in the interior. This can either be a result of the scarce observations or maybe a bias in the model.

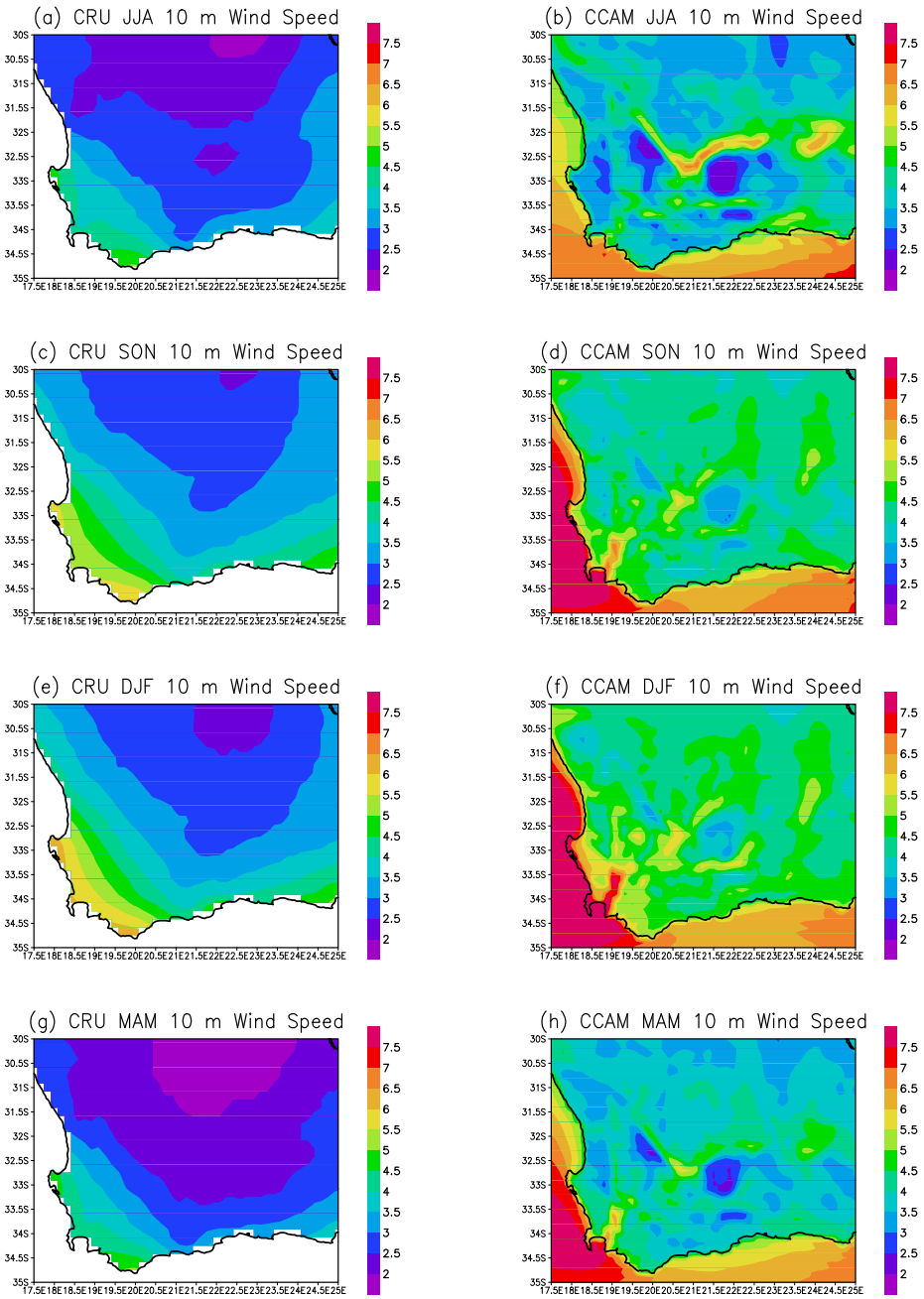

Figure 4.15: CRU observed and CCAM simulated seasonal 10 m wind speed over the Western Cape for JJA (panels a and b); SON (panels c and d); DJF (panels e and f) and MAM (panels g and h)

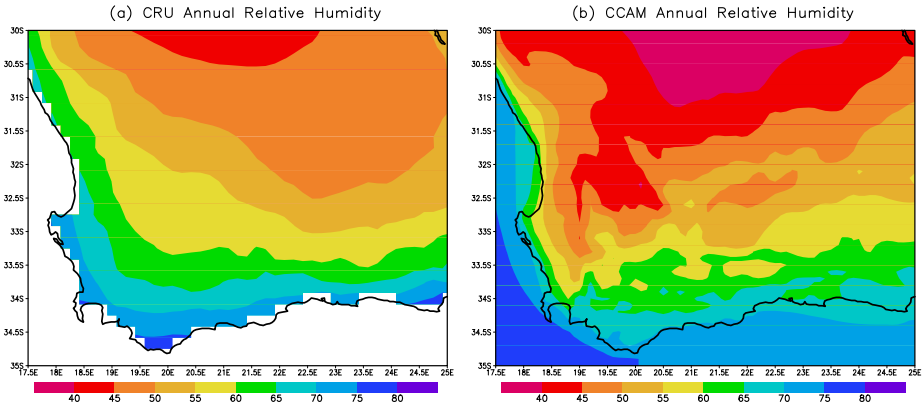

Figure 4.16: CRU observed (a) and CCAM simulated (b) yearly relative humidity over the Western Cape

4.3.5 Yearly and seasonal relative humidity

Yearly relative humidity

There is a well defined gradient in the observed average annual relative humidity, with maximum values (up to 80%) occurring over the coastal areas and decreasing to about 45 % over the northern interior regions (Figure 4.16 a). Again the observed relative humidity field appears smooth due to the relatively few stations absorbing this feature. The model correctly simulates the gradient in relative humidity between the coastal and inland areas. CCAM simulates a more detailed pattern however, with lower relative humidity values occurring over the high topography areas over the interior. The model's slight negative bias in relative humidity may be linked to the low rainfall being simulated.

Seasonal relative humidity

Winter is the season with the highest relative humidity in the Western Cape (Figure 4.17 a). This is consistent with the area receiving most of its rain and experiencing its lowest temperatures during this season. The highest relative humidity appears along the southwest and decreases towards the northeast as one moves inland. The model simulates this pattern, although the observed relative humidity is underestimated, especially in the southwestern Cape and in the northern parts of the domain (Figure 4.17 b).

During spring (SON) the area of high relative humidity reduces to the coastal areas (Figure 4.17 c). There is a well defined gradient from the coast (75%) to the inland areas (40%). The same pattern and intensities is observed during summer (Figure 4.17 e). The coastal band of high relative humidity is accurately simulated by the model during spring, but the intensity of the low relative

humidity to the north is a bit exaggerated (Figure 4.17 d). The orientation is different as well, as also observed in the yearly totals. The model preserves the same orientation and intensities of simulated relative humidity during summer (Figure 4.17 f), which is the same tendency as with the observed data.

The relative humidity is again starting to increase in autumn (MAM), as the rainy season approaches (Figure 4.17 g). The model accurately simulates the relative humidity at the coastal areas, but the northern parts of the domain is again too dry (Figure 4.17 h).

4.4 Verification of the micro-scale simulations

4.4.1 Intra-annual variation in the diurnal cycle of temperature and rainfall of the 1 km simulation

The monthly average diurnal temperature cycle described by the 1 km simulation is compared at a number of points against automatic weather station (AWS) data. The monthly averaged values of a number of variables were calculated at hourly time-intervals, for four stations over the five year period of 1995-1999. Ideally, a period of about 30 years or longer should be use to define climatological averages, but due to the limited availability of quality continuous AWS data, the analysis of the AWS data is constrained to the mentioned five year period. However, when comparing the corresponding simulated variables averaged over the full 30 year period or given five year period, little difference was found between the the averages obtained. The monthly average diurnal cycle is verified for the variables temperature, relative humidity and wind speed. The point of the simulation closest to the position of the station is used for the verification.

Goedehoop AWS is situated at 33.92° S, 18.76° E and is at 236 m above sea level. Figure 4.18 gives a monthly comparison between the CCAM 1 km simulation (averaged over 1995 - 1999) and Goedehoop AWS average over the same period. During the warmer months (November to March) the model gives a very good representation of the average diurnal cycle, although the daytime temperatures are somewhat overestimated. CCAM clearly displays a cold bias in the simulation of night-time, early morning and therefore also minimum temperatures. This is particularly evident for the colder months (April to October), with an underestimation of up to 6°C in July for early morning temperatures. However, the temperature amplitudes around midday are simulated with much greater accuracy. Note that the cold bias seems to be related to night-time cooling, perhaps suggesting that the model suffers a too big radiative heat loss within its boundary layer scheme during night-time. The model also seems to start warming up an hour earlier than the observations.

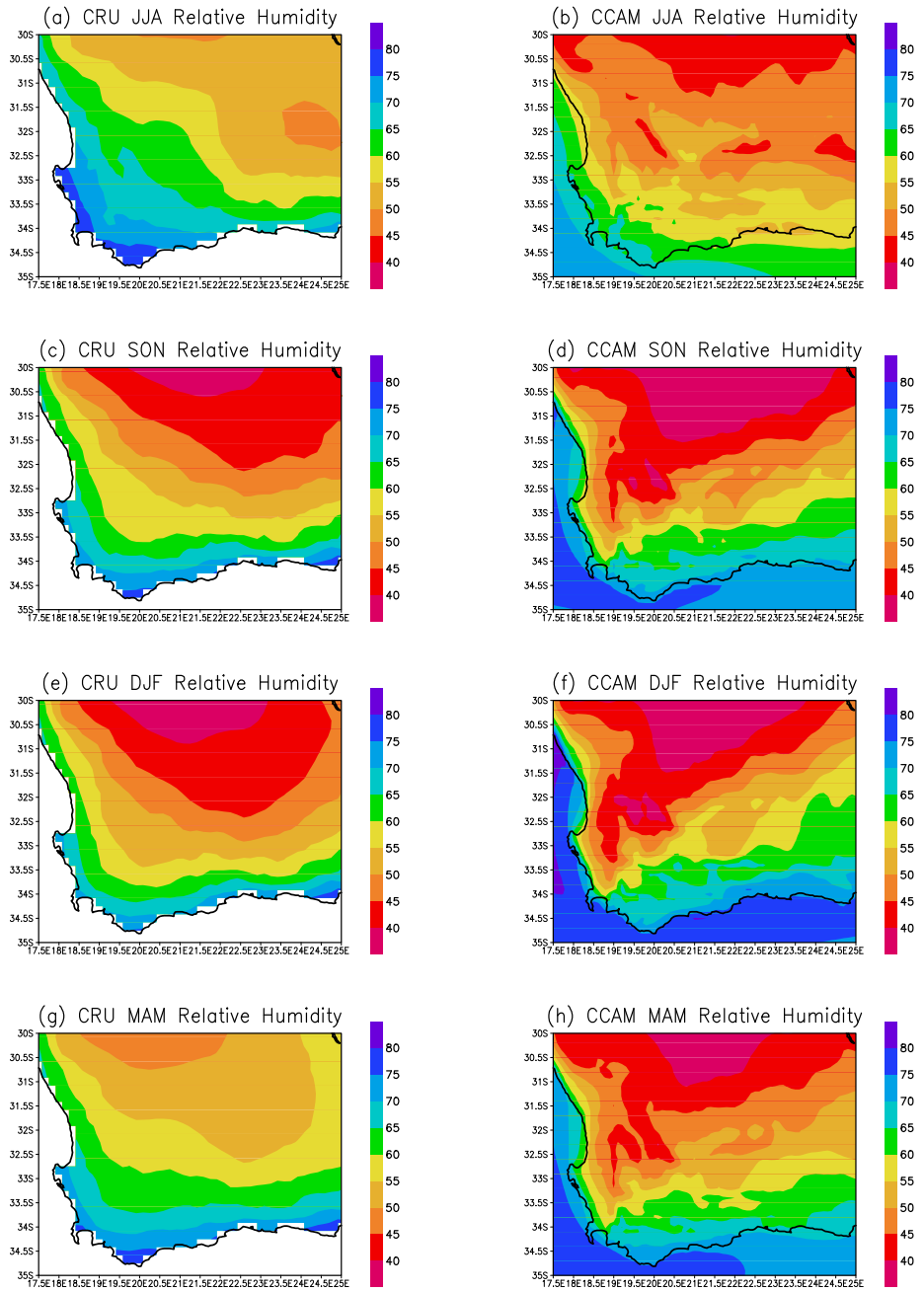

Figure 4.17: CRU observed and CCAM simulated seasonal relative humidity over the Western Cape for JJA (panels a and b); SON (panels c and d); DJF (panels e and f) and MAM (panels g and h)

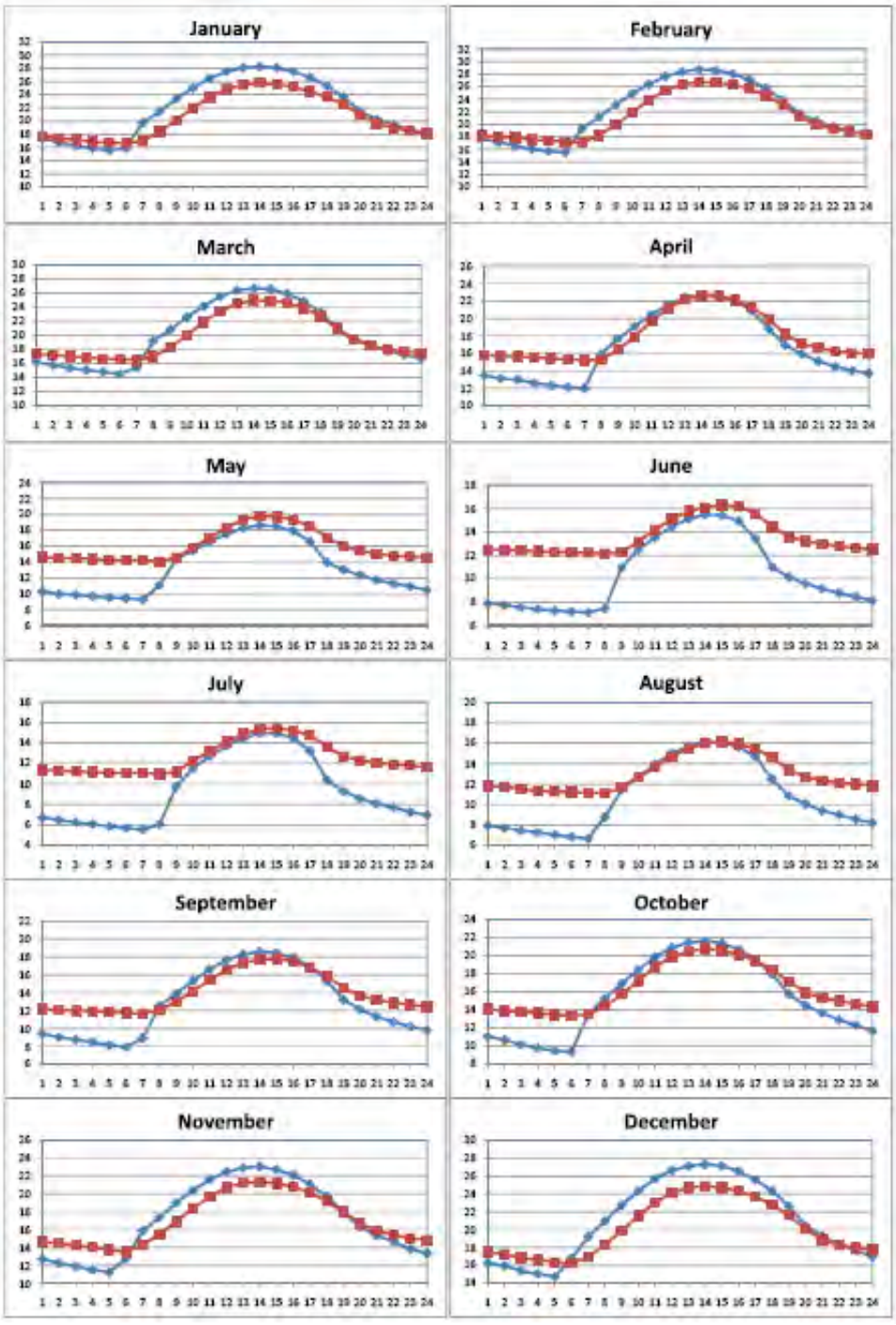

Figure 4.18: Comparison between the monthly diurnal temperature cycle of the 1 km simulation (blue) and the AWS Goedehoop (red) for the years 1995-1999

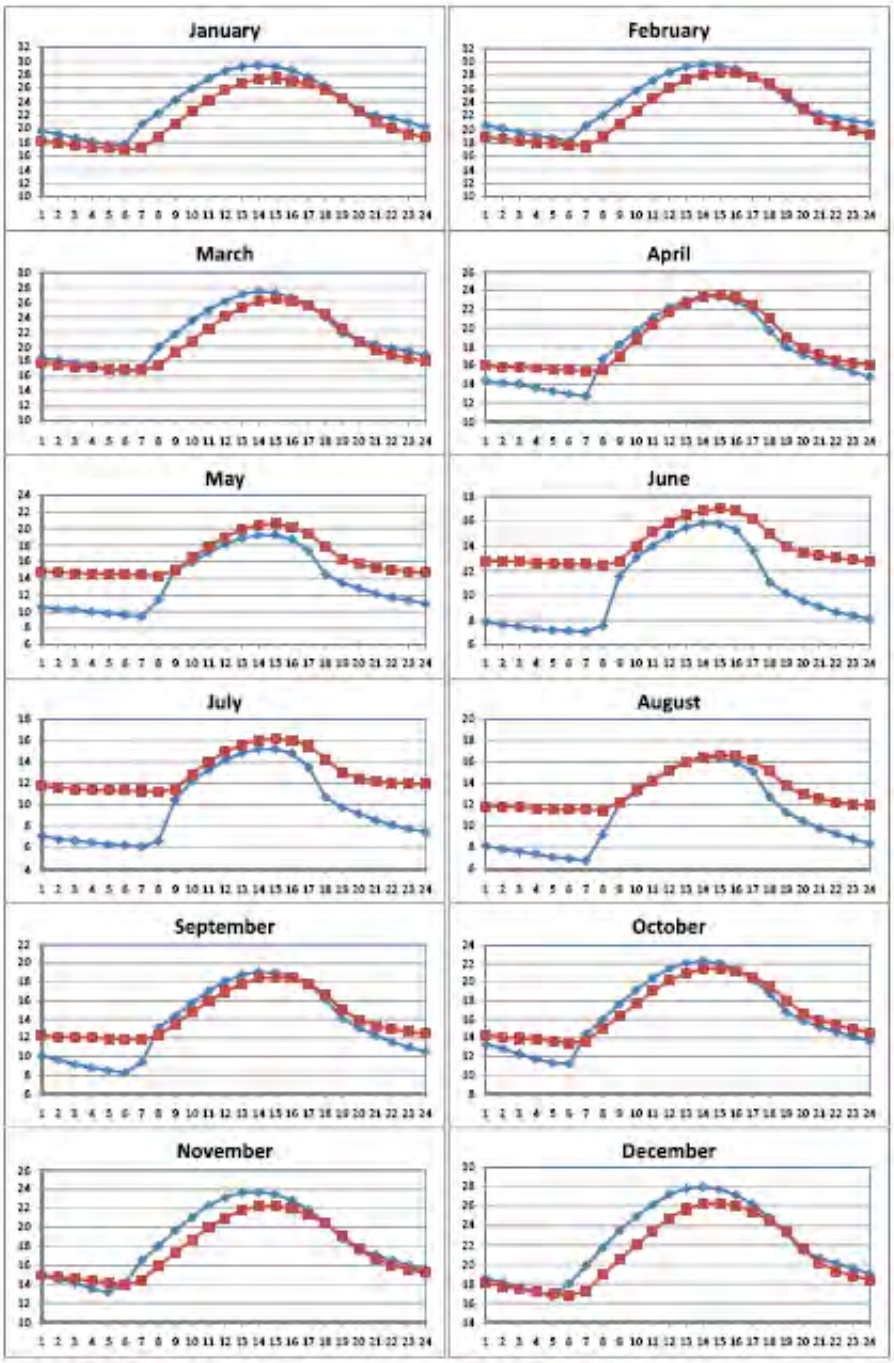

Figure 4.19: Comparison between the monthly diurnal temperature cycle of the 1 km simulation (blue) and the AWS Alto (red) for the years 1995-1999

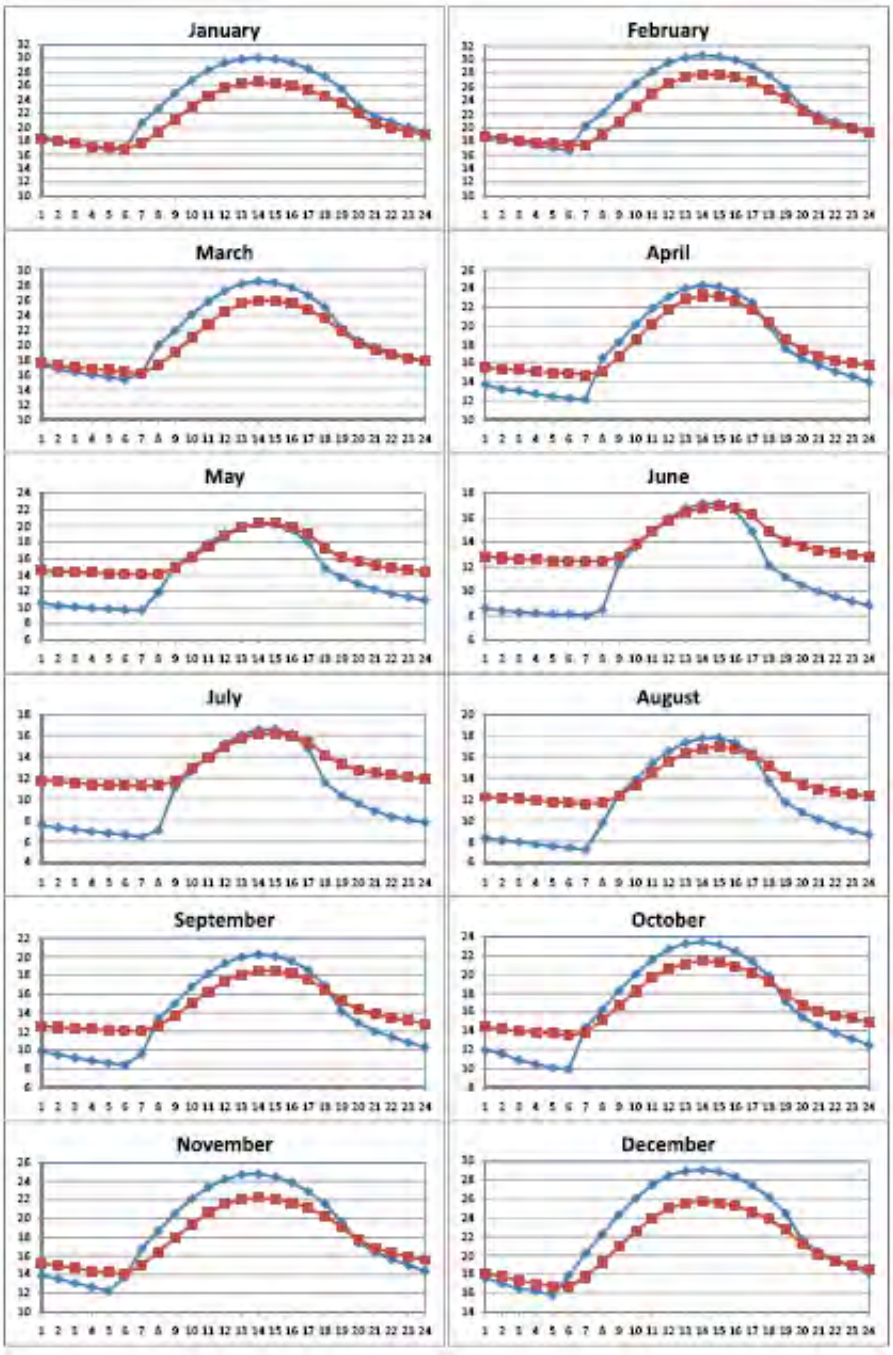

Figure 4.20: Comparison between the monthly diurnal temperature cycle of the 1 km simulation (blue) and the AWS Bonfoi (red) for the years 1995-1999

Alto AWS has an altitude of 245 m and is located at 34.01°S and 18.86°E. The comparison between CCAM and Alto (Figure 4.19) indicates that the model is capable of simulating the average diurnal cycle accurately during the warmer months. However, minimum temperatures are simulated to be lower than observed during the colder months, but to a lesser extent than those of Goedehoop. This station is the closest station to the ocean with its moderating effect on temperature which might contribute to the lesser cold bias.

Bonfoi is situated at 33.94°S and 18.78°E. With an altitude of only 153 m, it is the station closest to sea level. The simulated daytime temperatures are overestimated to a greater extent (up to around 4°C) during the warmer months (November to March) than at the other stations, but the diurnal cycle is still simulated relatively accurately (Figure 4.20). During the colder months the night temperatures are again simulated to be lower than observed.

Le Bonheur is located at 33.83°S, 18.87°E and has an altitude of 251 m. During summer the daytime temperatures are overestimated by the model by up to 3°C and during winter the night time temperatures are underestimated with up to 6°C (Figure 4.21), as for the other stations.

The average monthly rainfall totals calculated for the same stations and period as used in the temperature verification are shown in Figure 4.22. All four stations have an observed maximum rainfall during June and a minimum in January. This is consistent with the area-averaged observed rainfall over the southwestern Cape (Figure 4.7a and Figure 4.11). When considering the intra-annual cycle of the simulated rainfall of the 1 km simulation, the simulated rainfall at Goedehoop has a good correlation to the station rainfall (0.92), but rainfall is grossly underestimated during most of the year. This is consistent with the underestimation of rainfall in both the 8 km and 60 km simulations. The model also simulates the rainfall to peak in May rather than in June. Note that for the area-averaged rainfall of the 8 km and 60 km rainfall, the rainfall peak over the southwestern Cape is correctly simulated to occur in June. CCAM simulates the intra-annual cycle in rainfall at Alto quite accurately, with a correlation of 0.93 between the model and station. The simulation is close to the observed during most of the year, with the largest differences in November (up to 1.5 mm/day). The rainfall peak is correctly simulated to occur in June. Bonfoi and Le Bonheur are the two stations where the rainfall simulation is the furthest apart from the observed intra-annual cycle, with correlations of 0.8 and 0.75 respectively. During summer the simulated rainfall is close to the observed, but in winter there is a great deficit in simulated rainfall. Bonfoi has the greatest difference between observation and simulation with almost 5 mm/day more rainfall in June than what is simulated. The rainfall peak is also wrongly simulated to be in May, rather than June. It should be borne in mind that the period for which this comparison was made is only 5 years of observed data (and therefore the same 5 year simulated period is used). This is probably

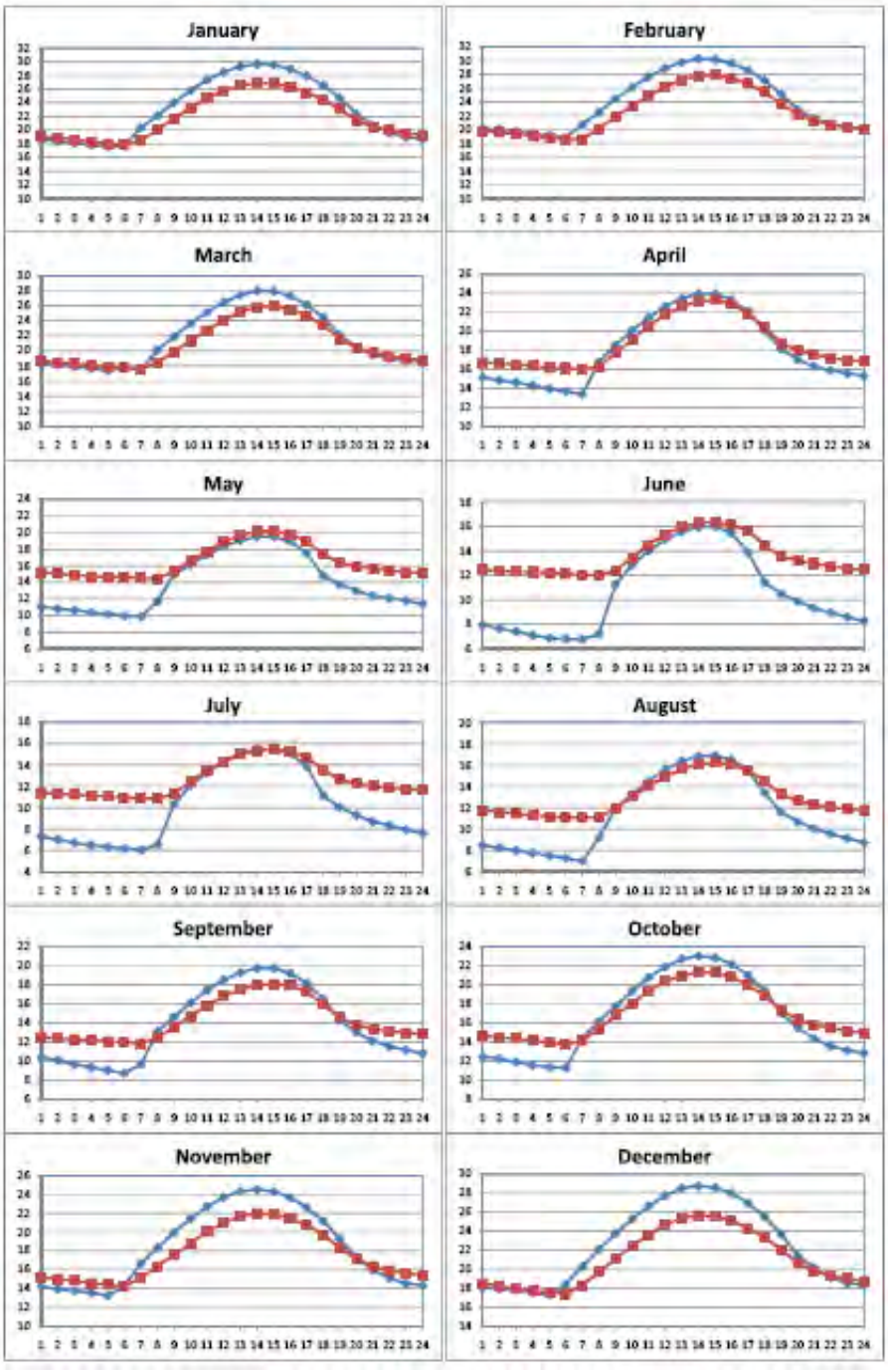

Figure 4.21: Comparison between the monthly diurnal temperature cycle of the 1 km simulation (blue) and the AWS Le Bonheur (red) for the years 1995-1999

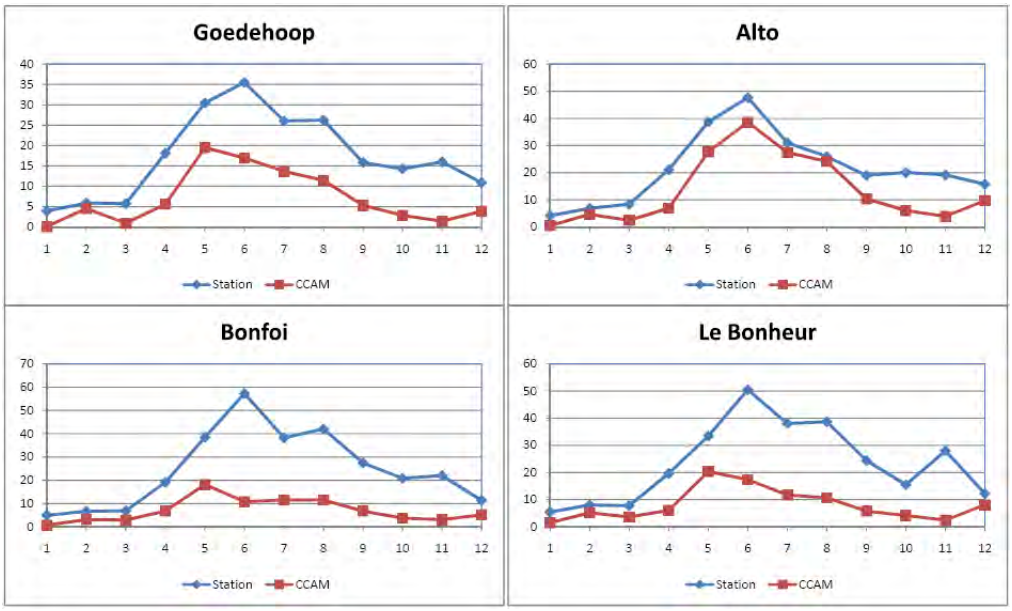

Figure 4.22: Comparison between the monthly rainfall totals (mm/day)*10 of the 1 km simulation and the automatic weather stations for the years 1995-1999

not adequate since the aim is to simulate a general climate and one big rainfall event that is missed by the model could make a huge difference in the validation during such a short period of time.

4.4.2 Ultra-high resolution verification for February

The average diurnal cycle in temperature of the 1 km and 200 m resolution simulations for February is compared to six automatic weather stations in Figure 4.23. The average was taken over the period 1996-2005. February is an important month for the wine industry as it is usually the harvesting month for the Stellenbosch wine producing region and the climate at harvesting has an important influence on the character of the wine (Carey et al, 2003). The correlation and root mean square error between the automatic weather station data and simulations (as well as between the simulations averaged over different periods) can be seen in Table 4.2. Notice the perfect correlation between different periods of simulation and how small the root mean square error is ($<0.5°C$). In the comparison between the model and AWS, both resolutions have a very good correlation with all of the stations and the root mean square error is also relative small (less than 2.5 degrees).

Overall the model simulates the diurnal temperature variation very well, with correlations between both the 1 km and 200 m simulations and observations

Table 4.2: The correlations and root mean square error between the automatic weather stations and simulations, as well as between the simulations of different periods for hourly February temperature

Station name		NIETVOORBIJ	LE BONHEUR	BONFOI	ALTO	JACOBSDAL	GOEDEHOOP
Correlation	1km 10y vs 30y	1.00	1.00	1.00	1.00	1.00	1.00
	station vs 1km	0.97	0.98	0.97	0.96	0.98	0.96
	station vs 200m	0.98	0.99	0.99	0.99	1.00	0.99
	200m 10y vs 30y	1.00	1.00	1.00	1.00	1.00	1.00
Root Mean Square Error	1km 10y vs 30y	0.38	0.41	0.39	0.40	0.39	0.42
	station vs 1km	2.43	1.41	1.73	1.40	1.57	1.56
	station vs 200m	2.19	1.43	1.23	1.86	1.55	2.16
	200m 10y vs 30y	0.32	0.32	0.30	0.31	0.27	0.29

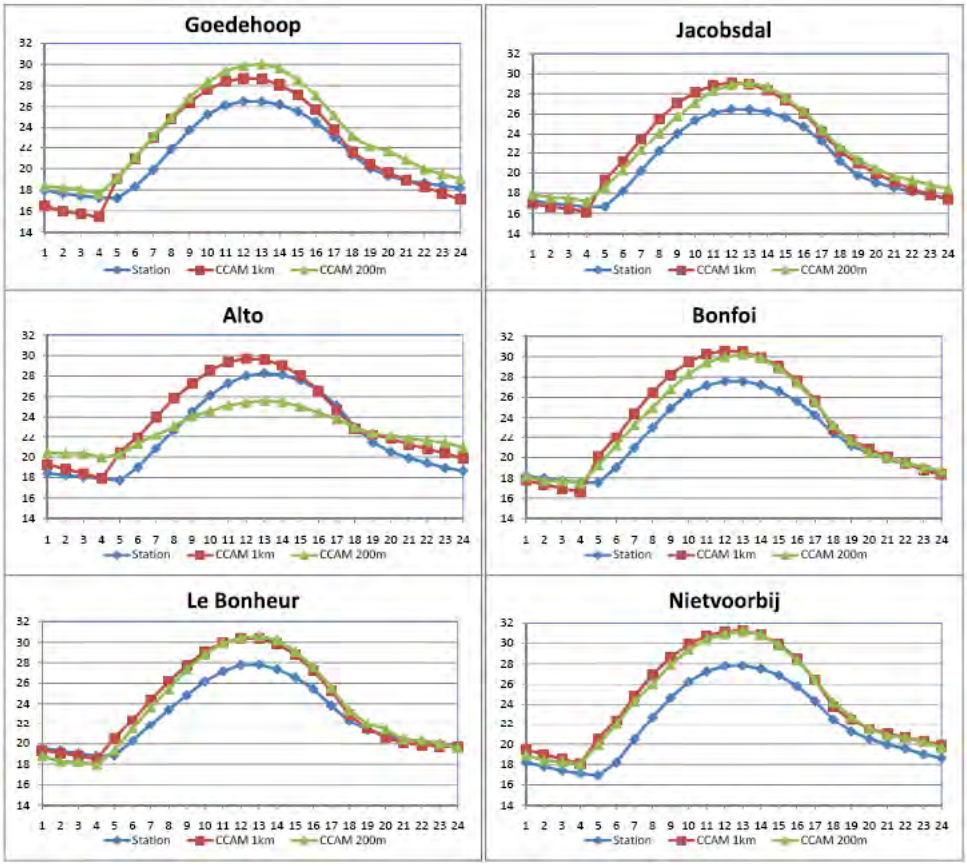

Figure 4.23: Comparison of February diurnal temperature range between AWS and CCAM simulations

Table 4.3: The correlations and root mean square error between the automatic weather stations, and simulations as well as between the simulations of different periods of the relative humidity

Station name		NIETVOORBIJ	LE BONHEUR	BONFOI	ALTO	JACOBSDAL	GOEDEHOOP
Correlation	1km 5y vs 30y	1.00	1.00	1.00	1.00	1.00	0.99
	station vs 1km	0.95	0.96	0.94	0.82	0.95	0.91
	station vs 200m	0.98	0.95	0.96	0.93	0.93	0.94
	200m 5y vs 30y	1.00	1.00	1.00	1.00	1.00	1.00
Root Mean Square Error	1km 5y vs 30y	0.76	0.47	1.18	0.67	1.24	1.35
	station vs 1km	17.20	17.26	20.75	21.90	16.04	16.87
	station vs 200m	16.04	16.09	18.28	20.43	14.90	17.99
	200m 5y vs 30y	0.55	0.50	0.72	0.40	0.75	0.56

above 0.95. For most of the points the 200 m simulation seem to be slightly closer to the observed, except for Alto, where the 200 m minimum temperatures are overestimated and the maximum temperatures are underestimated by about six degrees Celsius. The reason for this is that Alto falls outside the high-resolution panel of the 200 m simulation. Note in this regard that in the strongly stretched 200 m simulations the spatial resolution decreases rapidly as one moves away from the high-resolution panel. The simulation results at Alto illustrates that the 200 m simulations should not be used outside the high resolution panel, where the simulations are essentially driven by the 1 km run and the actual 200 m simulation is meaningless. The model generally overestimates the peak daytime temperatures but the night temperatures are very close to the observed. The 200 m simulation looks very realistic within the area of interest, and the downscaling seems to work. However, there is no sound evidence that the 200 m simulation has a greater accuracy than the 1 km simulation.

For the relative humidity, a five year average (1996 - 2000) was taken to compare the six weather stations with the simulations. The reason for this shorter period is limited availability of quality observed (weather station) data. Table 4.3 shows the correlations and root mean square error between the automatic weather stations and simulations, as well as between the simulations averaged over different periods. The correlation between the average diurnal cycle calculated for different periods of the same resolution simulations is again high. The comparison between the simulations and observations show a correlation that is lower than the temperature, but still generally above 0.9. The root mean square is as high as o 21.9%, which is expected from the graphs of diurnal variation (Figure 4.24).

The hourly comparison between the six AWS and the 1 km and 200 m average relative humidity for February (1996 - 2000), is shown in Figure 4.24. Again both the 1 km and 200 m simulations capture the pattern of the diurnal variation satisfactorily. The simulations display a dry bias - the 200 m and 1 km relative

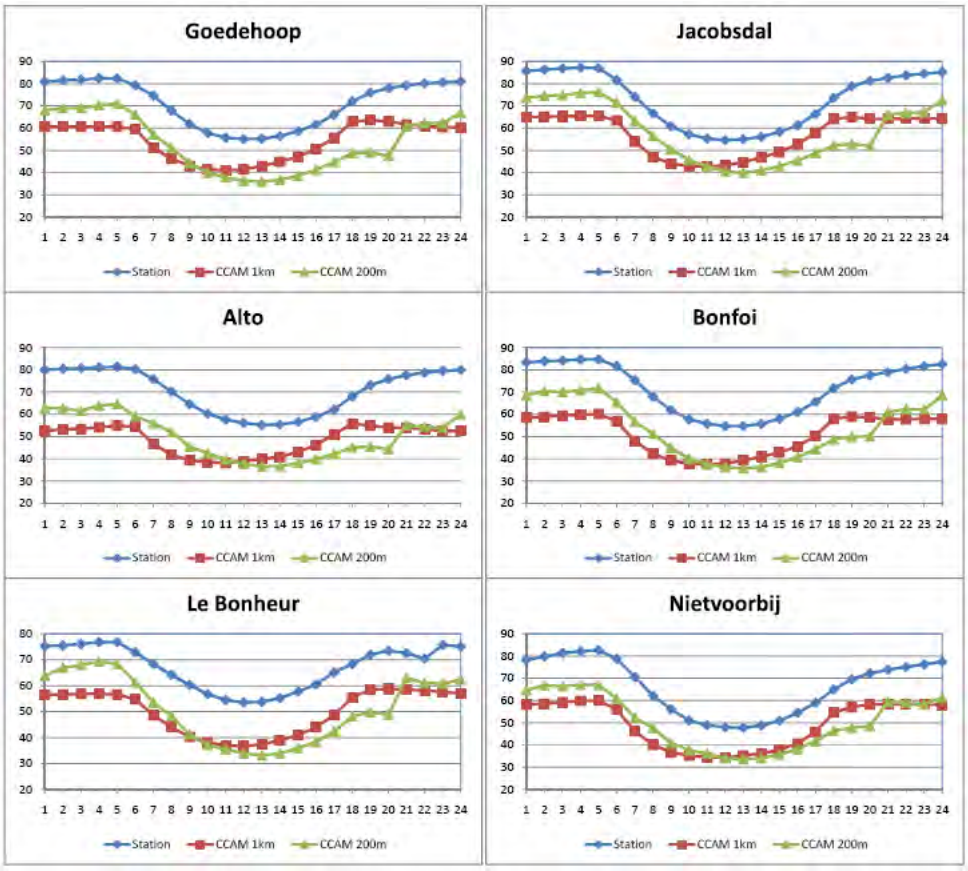

Figure 4.24: Comparison of February diurnal relative humidity between AWS and CCAM simulations

Table 4.4: the correlations and root mean square error between the automatic weather stations, and simulations as well as between the simulations of different periods for wind speed

Station name		NIETVOORBIJ	LE BONHEUR	BONFOI	ALTO	JACOBSDAL	GOEDEHOOP
Correlation	1km 5y vs 30y	1.00	0.99	1.00	1.00	1.00	1.00
	station vs 1km	0.98	0.96	0.99	0.74	0.99	0.99
	station vs 200m	0.95	0.94	0.95	-0.11	0.95	0.94
	200m 5y vs 30y	1.00	0.99	1.00	0.99	1.00	1.00
Root Mean Square Error	1km 5y vs 30y	0.23	0.44	0.05	0.32	0.05	0.08
	station vs 1km	0.42	1.28	0.54	2.57	0.64	0.45
	station vs 200m	0.43	0.76	0.39	3.54	0.31	0.62
	200m 5y vs 30y	0.25	0.20	0.07	0.49	0.13	0.16

humidity are both mostly between 5% and 20% below the the observed relative humidity. An interesting deviation from the generally well simulated pattern is found at 2000 Zulu, where the 200 m simulation shows a sudden decrease (or at least a zero trend) in relative humidity at all six stations, rather than an increase as in the observations. The reason for this irregularity in the simulations are unclear at this stage, and should be investigated further. The 200 m run is a bit closer to the observations in the cooler hours, and have a good correlation with the observations in spite of the irregularity that occurs at 2000 Z.

The average screen-height (2 m) wind speed for February is also validated using a five year period, as for the relative humidity. Figure 4.25 shows the CCAM screen-height wind speed (at 1 km and 200 m) against the observed wind speed at the six weather stations. The correlations and root mean square error between the automatic weather stations and simulations as well as between the simulations of different periods can be seen in Table 4.4. The correlation between the stations and both simulations are above 0.93, except for Alto, where the correlation between the 1 km simulation is 0.74 and the 200 m has a very poor correlation of -0.11. But as mentioned before, Alto is located quite far from the 200 m focus area and is not expected to show a good correlation with the 200 m simulation. Alto also has the largest RMSE (2.57 for the 1 km and 3.45 for the 200 m). Apart from that and the 1 km Le Bonheur RMSE of 1.28, all the other stations have a RMSE of less than 1 with both simulations.

CCAM seems to capture the wind speed for February exceptionally well in both the 1 km and 200 m simulations. Alto is the only station where the simulated wind speed does not reflect the true wind speed at the weather station. For the 1 km simulation the pattern of wind speed is satisfactorily, but the magnitude is simulated to be too high. The 200 m simulation of wind speed at that point deviates strongly from observations, once again indicating that the simulation should not be used outside the area of 200 m resolution. The 200 m simulation

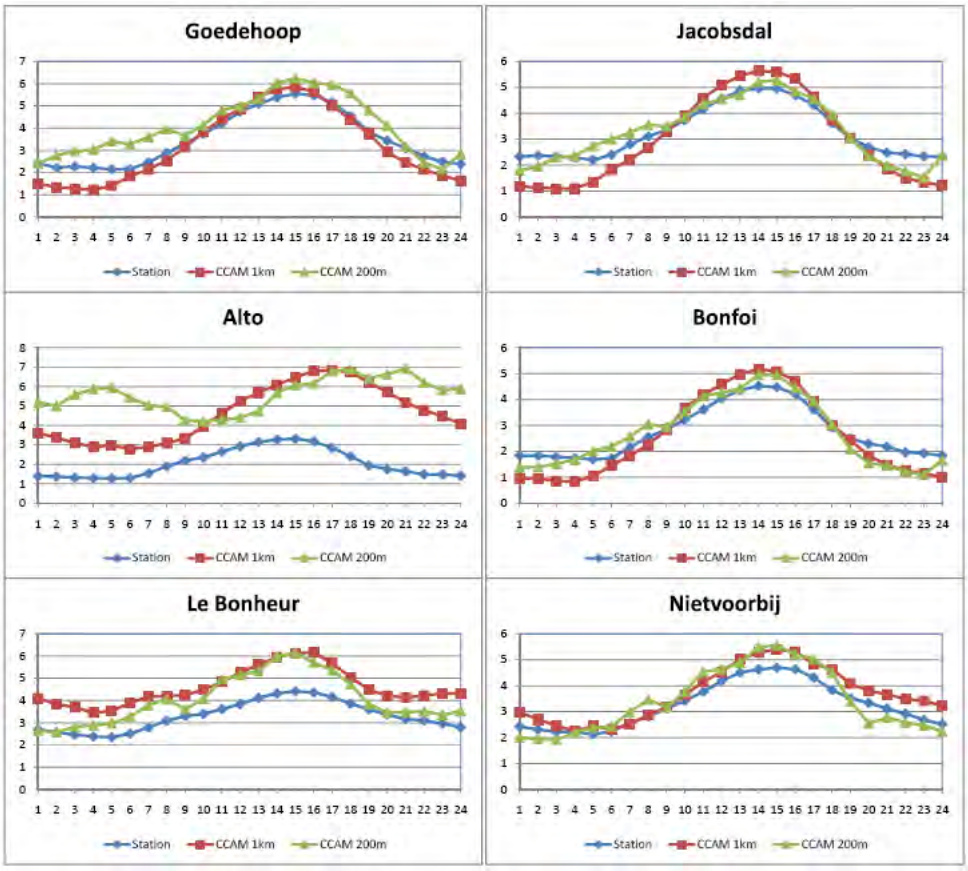

Figure 4.25: Comparison of February diurnal wind speed between AWS and CCAM simulations

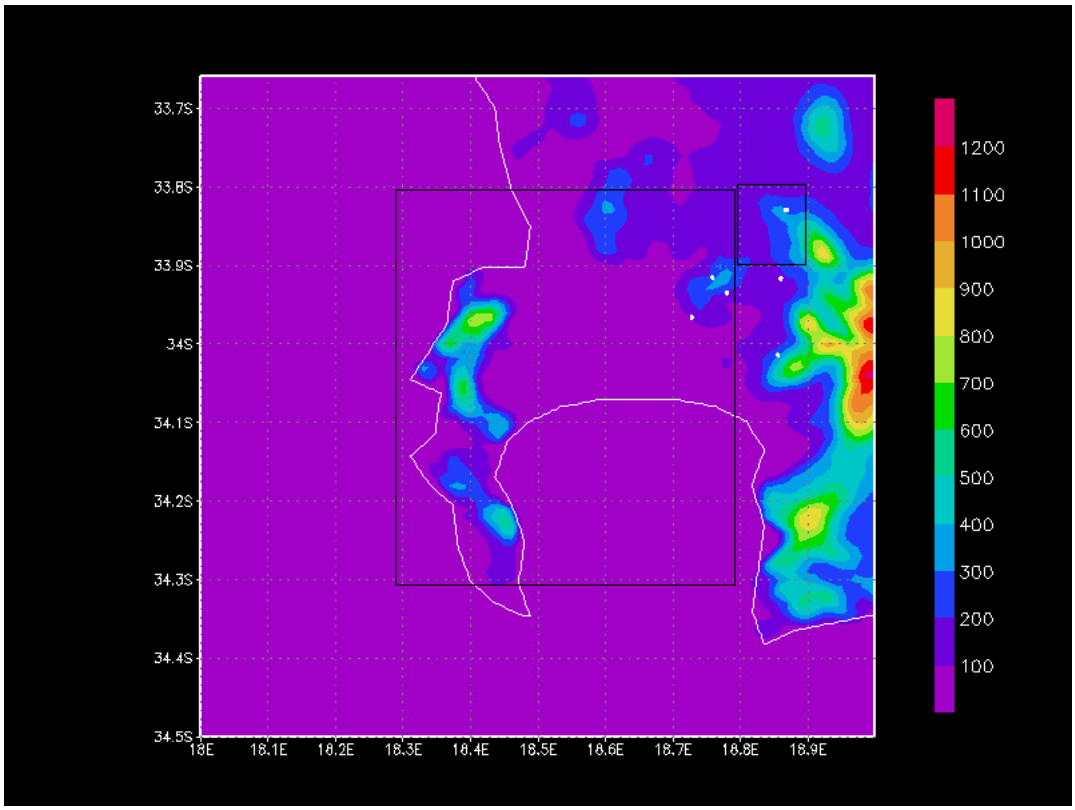

Figure 4.26: 1 km simulation area (big black rectangle), 200 m simulation area (small black rectangle) and AWS (white dots). The shades are representing the 1 km topography (m)

seems to be slightly noisy compared to the 1 km simulation, which have a better correlation to the automatic weather station data.

4.5 Climate parameter maps

Climate parameter maps are produced over the 1 km area (33.81°S to 34.31°S and 18.28°E to 18.78°E) as well as the 200 m area (33.79°S to 33.89°S and 18.79°E to 18.89°E). Figure 4.26 indicates the simulation areas, as well as locations of the automatic weather stations for reference. The location of the 200 m simulation high-resolution panel outside the 1 km high-resolution panel is not ideal, but it is sufficiently close to the 1 km high-resolution panel to be forced with data from the 1 km simulation that is of resolution close to 1 km. The same reasoning goes for the stations lying outside the 1 km resolution panel. Maps are shown of the highest and lowest hourly temperature, wind speed and relative humidity

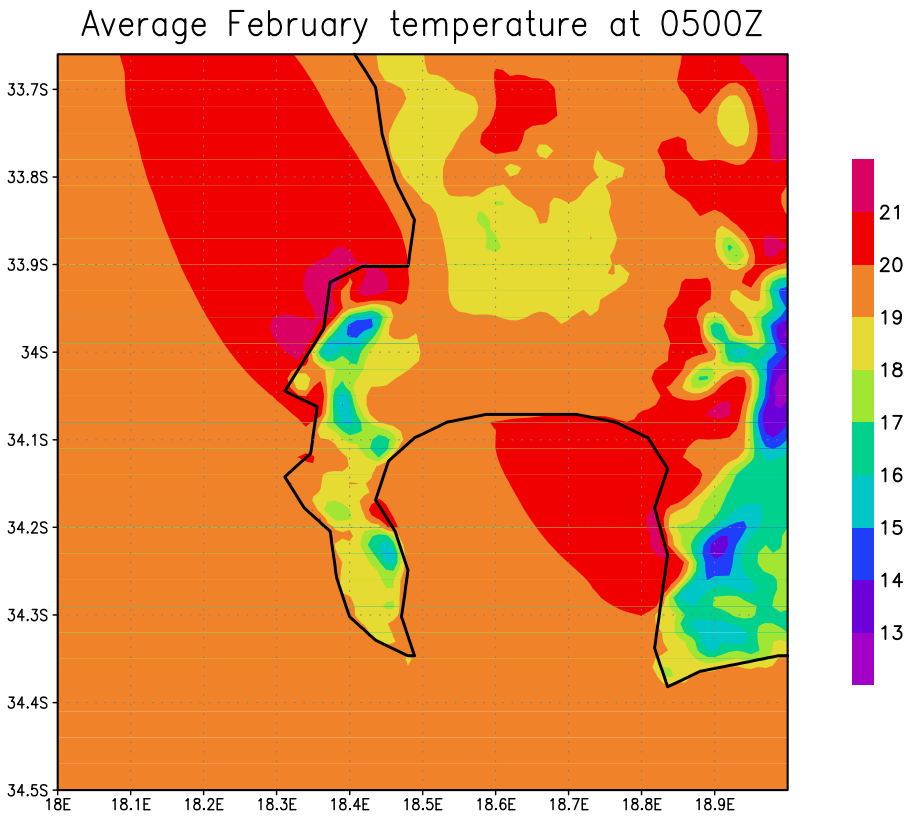

Figure 4.27: Temperature over the south-western Cape for 0500Z as simulated by CCAM for 1976-2005 at a resolution of 1 km

for February over the southwestern Cape as well as average temperature, wind speed and relative humidity over the Stellenbosch area, as simulated by the model for the climate period of 1976-2005. With 48 x 48 gridpoints on a panel, the 1 km simulation area is actually only about 50 x 50 km and the 200 m simulation area 10 x 10 km. Le Bonheur is actually the only weather station which is right inside of the 200 m focus area, with Goedehoop, Bonfoi and Nietvoorbij in the vicinity.

The temperature over the southwestern Cape for 0500Z as simulated by CCAM for 1976-2005 at a resolution of 1 km is given in Figure 4.27. The areas of high topography are clearly cooler than the surrounding areas, although the temperatures are above 10°C over the whole region, which is good for the growing of quality wines (Chapter 2). During this cool hour, average temperatures of up to 21°C can be found at the north-eastern corner of the simulation area, as well as on the coastal plains to the east of False Bay and at Cape Town, to the

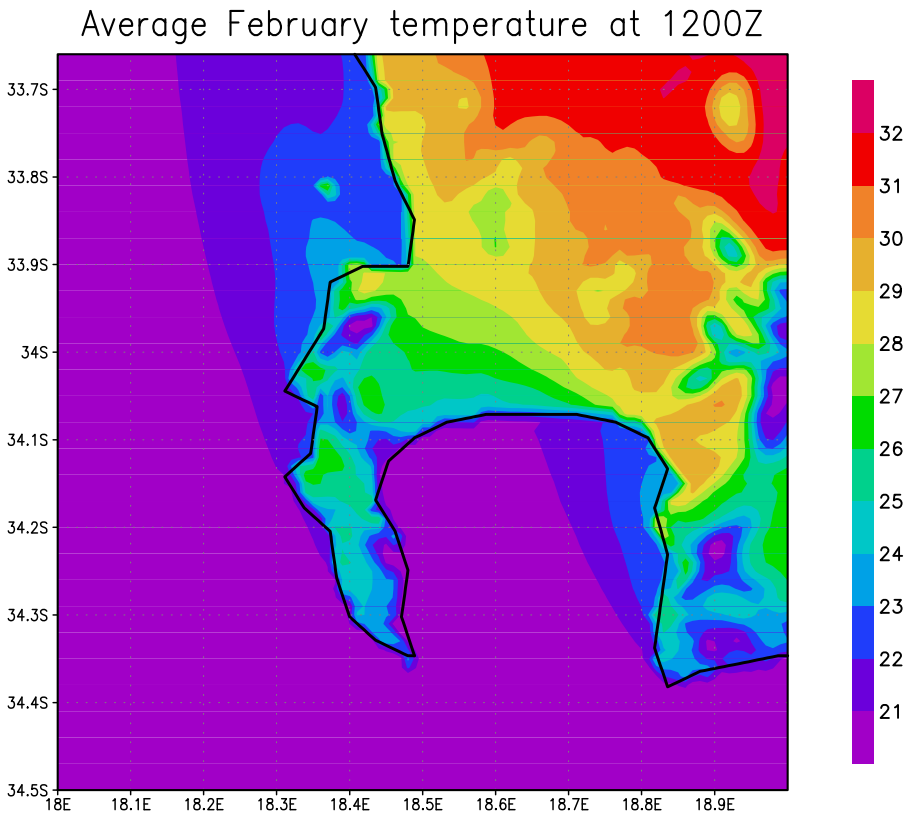

Figure 4.28: Temperature over the south-western Cape for 1200Z as simulated by CCAM for 1976-2005 at a resolution of 1 km

north-west of Table mountain.

Figure 4.28 shows the temperature over the south-western Cape for 1200Z as simulated by CCAM (1976-2005) at a resolution of 1 km. It is clear that the ocean have a cooling effect on the areas around False Bay, with temperatures hovering around the 23°C - 26°C in the south-west and southern part of the country. The coastal plain to the north east of False Bay (at about 34.1°S and 18.85°E) is warmer than the rest of the areas around the Bay, probably because of the shield against the winds an moderating effect of the ocean provided by the mountains to the south (around 34.25°S and 18.9°E). Another interesting feature is the diagonal gradient in which the temperatures increase towards the north east. The average temperature at midday gets up to 31°C in the north-eastern corner of the domain, with the Paarl Mountain having a temperature of 28°C at the top. The topography of the southwestern Cape can again clearly be spotted by the cooler temperatures at Table Mountain, the mountains around

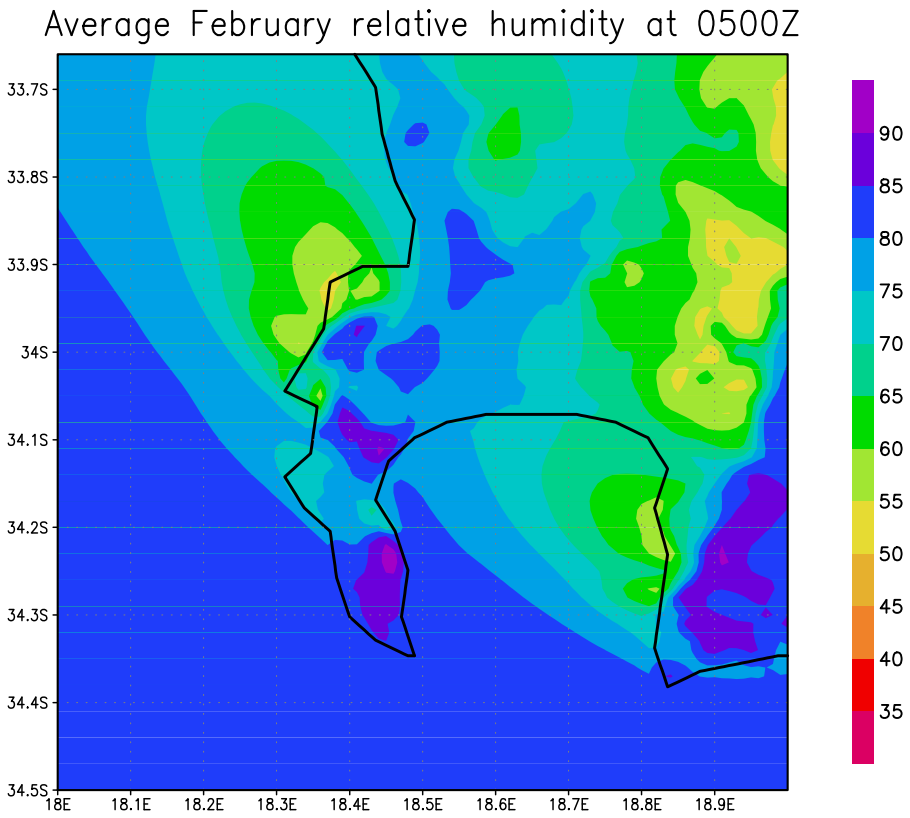

Figure 4.29: Relative humidity over the south-western Cape for 0500Z as simulated by CCAM for 1976-2005 at a resolution of 1 km

the Stellenbosch area and the mountains at the south-eastern part of False Bay.

The average relative humidity at 0500Z for February over the southwestern Cape is given in Figure 4.29. There is a band of high relative humidity (up to 90%) along the west coast as well as the south eastern corner of the domain. The lowest relative humidity (50%) can be found around Cape Town and at a band to the north east, especially around the Stellenbosch area. It is probably a positive feature for the wine regions of Stellenbosch, as too much moisture can cause diseases such as mildew and fungus in the grape (Chapter 2).

The average relative humidity at 1200Z exhibit the same diagonal gradient as observed in the 1200Z average temperature. The lowest relative humidity (less than 30%) is found in the northeastern corner of the domain, and it increases gradually towards the south western corner where a relative humidity of up to 85% can be found (Figure 4.30). Over the Stellenbosch wine producing region,

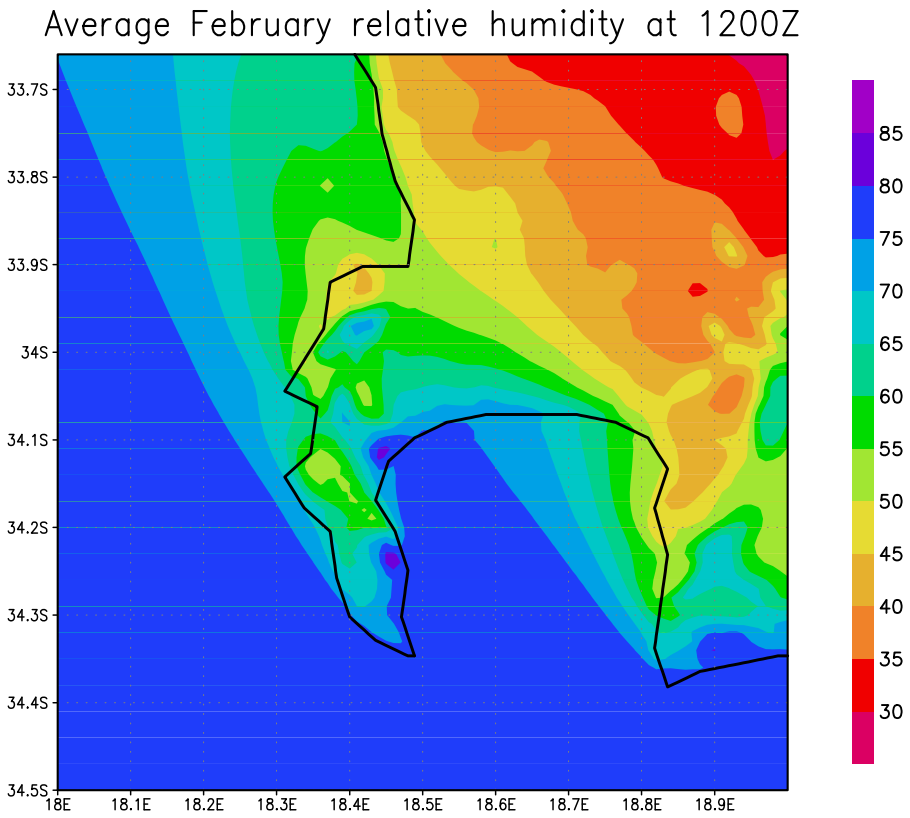

Figure 4.30: Relative humidity over the south-western Cape for 1200Z as simulated by CCAM for 1976-2005 at a resolution of 1 km

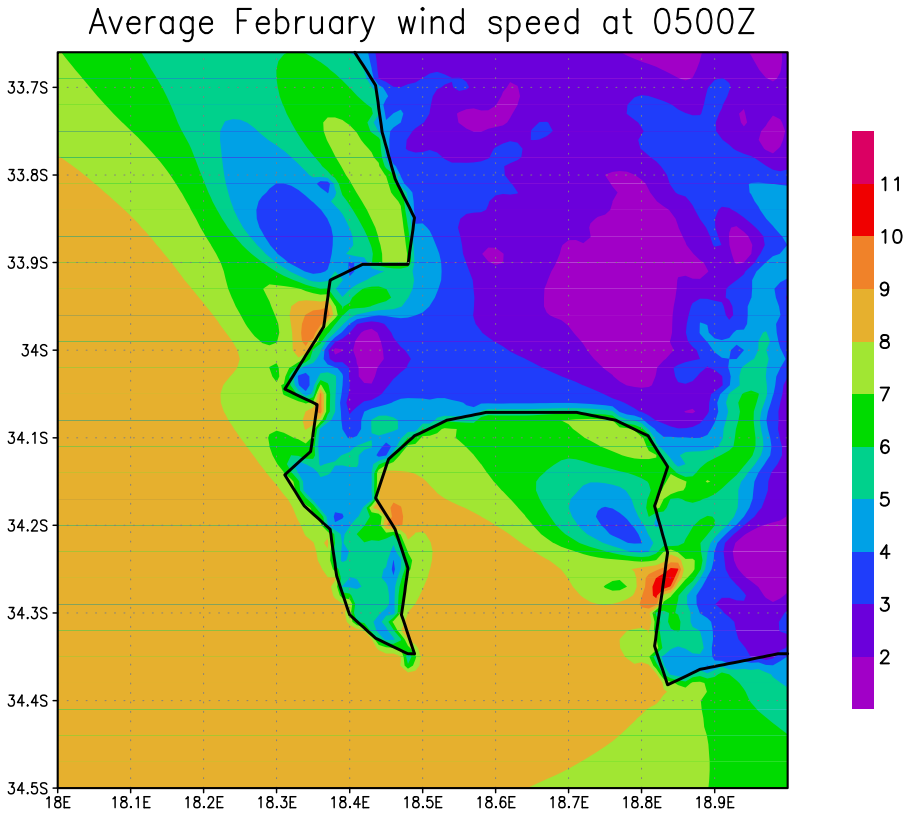

Figure 4.31: Screen-height wind speed in m/s over the south-western Cape for 0500Z as simulated by CCAM for 1976-2005 at a resolution of 1 km

the relative humidity is around 35%.

The average screen-height wind speed for February at 0500Z is given in Figure 4.31. The wind over most of the the southwestern Cape is below 4 m/s. One area where the average wind speed is very high (up to 11m/s) is at about 34.25°S and 18.82°E. From that point there's a tongue of stronger wind speeds (up to 7m/s) in a northeasterly direction, (between Somerset West and Grabouw). The Cape Peninsula and areas around Cape Town also receive higher wind speeds than the majority of the southwestern Cape.

Overall the winds over the southwestern Cape is much stronger at 1500Z than 0500Z, but some of the same features can be seen in this hour. One is the area of strong winds at 34.5°S and 18.82°E, followed by the tongue of stronger wind speed to the north-east (Figure 4.32). The south-western parts of the domain experience relative stronger wind speeds (6-7 m/s), with the exception of Table

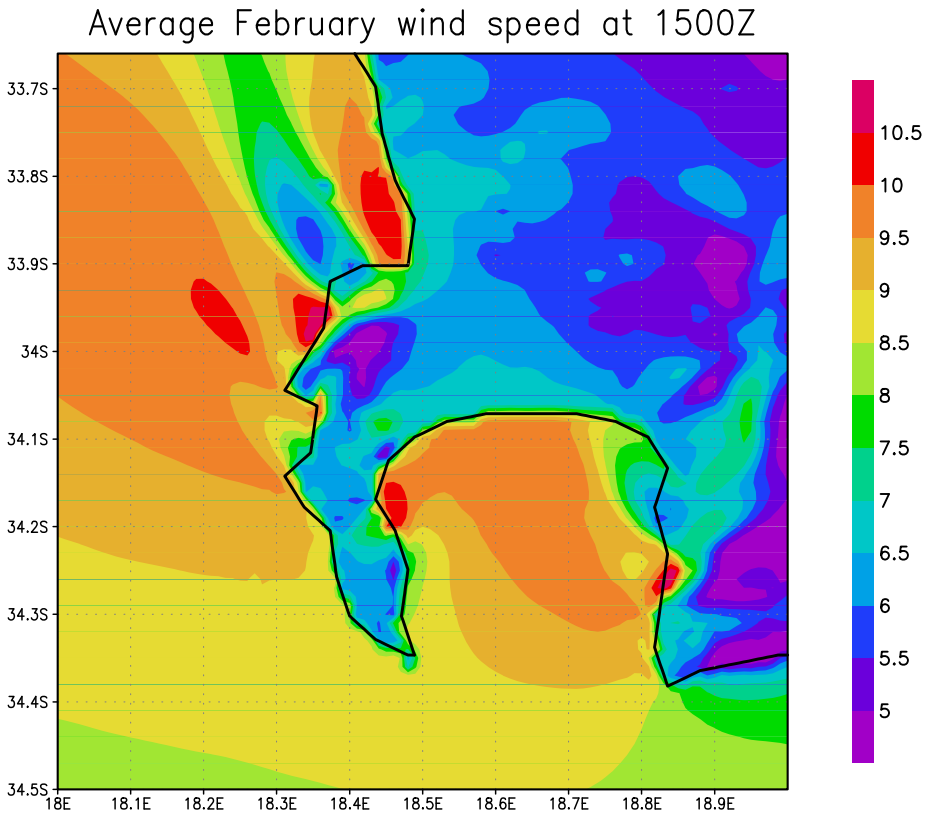

Figure 4.32: Screen-height wind speed in m/s over the south-western Cape for 1500Z as simulated by CCAM for 1976-2005 at a resolution of 1 km

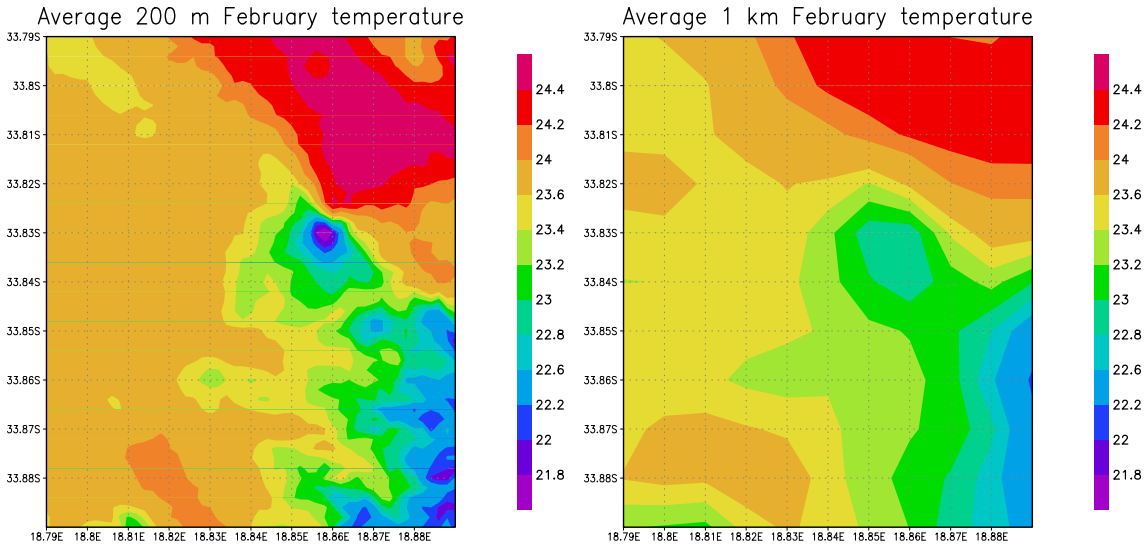

Figure 4.33: Average February temperature over the Stellenbosch area as simulated by CCAM at a 200 m (left) and 1 km (right) resolution for 1976-2005

Mountain, which is around 5 m/s. The average wind speed decrease towards the northeast, with Stellenbosch district and the north eastern corner (around Paarl) experiencing the lowest wind speeds of around 5 m/s as well.

The focus area of the 200 m resolution simulation is around the Stellenbosch district (33.79°S to 33.89°S and 18.79°E to 18.89°E). The monthly average temperature, relative humidity and wind speed for February over this area at both 1 km and 200 m resolution are shown in the following few figures. Figure 4.33 show the average temperature for February 1976-2005 as simulated by CCAM on a 200 m and 1 km resolution. Both maps show a similar pattern and temperature range, but the 200 m map has more detail. The temperature in the mountainous areas fell down to below 22°C while the hottest part reach up to 24.5°C. The majority of the area to the west is between 23.4°C and 24°C.

The average relative humidity of the area for February varies between 48% and 55% according to the simulations. There is not a big variation in the average February relative humidity over this (relative small) area. It should be borne in mind that the area is only about 10 km x 10 km. Overall the relative humidity decrease from the west (55%) to the east (48%) over the area (Figure 4.34).

Figure 4.35 gives the average screen-height wind speed for February as simulated by CCAM for 1976-2005 on a 200 m and 1 km resolution. The wind speed is between 2.8 m/s and 4.8 m/s. The wind speed increase from the south-west

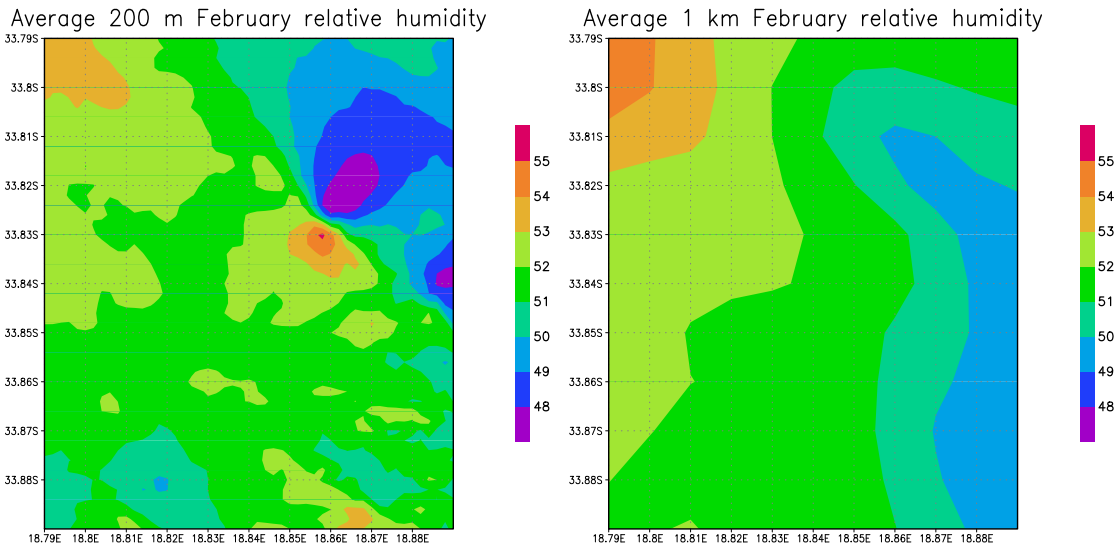

Figure 4.34: Average February relative humidity over the Stellenbosch area as simulated by CCAM at a 200 m (left) and 1 km (right) resolution for 1976-2005

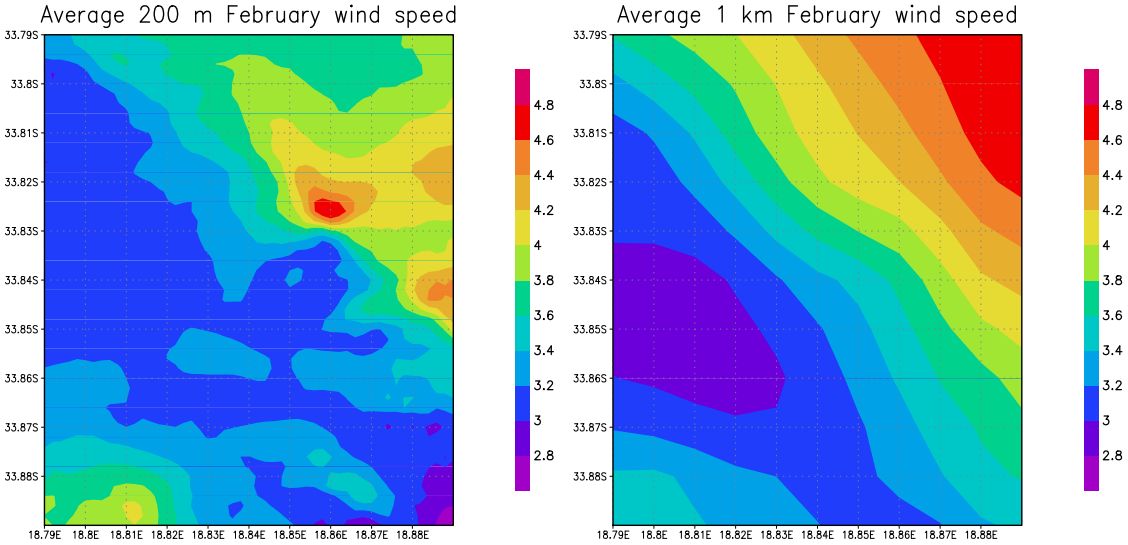

Figure 4.35: Average February wind speed in m/s over the Stellenbosch area as simulated by CCAM at a 200 m (left) and 1 km (right) resolution for 1976-2005

to the north-east, with the exception of slightly higher wind speeds in the very south-western corner of the domain.

Chapter 5

Conclusion

An ultra high-resolution climatology has been produced over the southwestern Cape of South Africa and for the Stellenbosch wine producing region in particular. Simulations at such high resolution are unexplored in climate modelling and need to be verified thoroughly against observations before being applied. The ultra high-resolution simulations was achieved by dynamically downscaling CCAM simulations from 60 km to 8 km to 1 km and finally to 200 m resolution. The 60 km simulation was obtained by nudging the model in NCEP reanalysis data. This is a very suitable way to start the downscaling process, as the model is forced to simulate realistic synoptic-scale weather patterns and frequencies. The 8 km simulation was then nudged within the 60 km output to obtain a meso-scale climatology, after which the 1 km simulation was nudged within the 8 km run, and the 200 m was in turn driven by the 1 km simulation.

In the 60 km simulation CCAM simulates the west-east gradient in rainfall over South Africa satisfactorily, although rainfall over Lesotho is overestimated rather severely. The features of the extremely dry Namibian coast, wet tropics, relatively dry East Africa and the band of drier conditions from 25°S to 15°S are simulated remarkably well by the model. Rainfall totals over the Mozambique coast and eastern South Africa are overestimated, however, the model in general simulates rainfall totals realistically. A small part of the southwestern Cape receives a high annual rainfall which is not simulated by CCAM, but overall the model gives an excellent representation of the synoptic-scale distribution and amplitude of annual rainfall over tropical and southern Africa. The 60 km resolution simulated seasonal patterns of rainfall percentages show a good comparison with the 0.5^oCRU CL1.0 dataset. For most regions over southern Africa the simulated and observed intra-annual rainfall cycles also compared well. The southwestern Cape (Region A) had the largest difference between observations and simulation, with CCAM underestimating the winter rainfall by up to 1.2 mm/day during June. The rainfall peak in June is captured by the model, although the second peak (in August) is not captured. The regional circulation patterns were simulated remarkably well, and the seasonal circulation

anomalies were very close to the observed NCEP reanalysis data throughout the atmosphere. This suggested that driving the model through the wind nudging has been successful.

The 8 km simulation was compared to the observed high-resolution 10' CRU gridded dataset to determine whether the model can also capture the characteristics of the mesoscale climate of the region. CCAM simulates the temperature patterns very well and the effects of topography can clearly be seen in the simulation. This includes cooler mountain tops with warmer valleys and adiabatic heating to the west of the mountains that form part of the escarpment. CCAM also simulates the seasonal temperature cycle over the Western Cape remarkably well. The model indeed produces more a more detailed climate for variables such as relative humidity, that are not observed at the same spatial resolution as as temperature and rainfall. CCAM does however again underestimate the rainfall over the southwestern Cape (by up to 1.2 mm/day in June) and this matter should probably be investigated during future research. The rainfall maximum in June is captured, in spite of the underestimation, but the second maximum in August is again not simulated. The high rainfall along the south coast of the Western Cape (23°E-25°E) is successfully captured by the model. CCAM generally captures the pattern of the seasonal rainfall cycle over the Western Cape well.

Four automatic weather stations with data from 1995-1999 were used to examine the simulated monthly temperature and rainfall of the 1 km run. It was found that CCAM provides a good representation of the diurnal temperature cycle, especially in the warmer months. The minimum temperatures were however under estimated quite severely (up to 6°C) during winter and the maximum temperatures slightly over estimated during summer. The model clearly has a cold bias in simulating minimum temperatures. The intra-annual rainfall cycle was simulated accurately for the AWS Alto, and reasonable at Goedehoop AWS. Both stations had a correlation of above 0.9 with the simulation. The winter rainfall were underestimated to a great extent at the other two stations (Bonfoi and Le Bonheur), but the lowest correlation between a station and simulation was 0.75. The model usually wrongly simulates the peak in rainfall to be in May rather than June, as observed by the stations. The 200 m and 1 km simulations for February was compared to 6 automatic weather stations. For temperature a 10 year period is used (1996-2005) for verification, but due to a lack of station data the period for the relative humidity and wind speed verification was again 5 years (1996-2000). For the hourly February temperature the 200 m and 1 km simulation were very close to each other and both simulations compared well with the weather stations. The 200 m and 1 km simulations of relative humidity had a good correlation with the stations, although both estimated the relative humidity to be too low. The two simulations of wind speed were again both similar, and close to observations, although the 200 m wind speed seem a bit erratic. Although the downscaling to 200 m simulation seems to be

successful in the sense of producing physically meaningful fields, there does not seem to be any gain over the results provided by the 1 km simulation if one look at the correlations and magnitude between the 1 km and 200 m simulations. However, the 200 m simulation provide much more spatial detail over a small area, although the accuracy of this data can not sufficiently be tested.

Climate parameter maps were produced for the temperature, relative humidity and wind speed using the 1 km and 200 m climate simulations for 1976-2005. The minimum and maximum values of variables derived from the hourly intervals during the month of February are shown for the southwestern Cape using the 1 km simulation. More detail over the Stellenbosch area is given in maps of average February temperature, wind speed and relative humidity, using the 200 m simulation as well as the 1 km simulation.

In what may be a world-first in the history of numerical atmospheric modelling, the CCAM climate simulations were performed seamlessly on the CSIR Cluster Computing Center (C4). Seamless climate simulation may be defined as the simulation of climate at spatial resolutions ranging from the global to the micro-scale, using a single model code. What makes the simulations seamless (and unique), is the ultra-high resolution (200 m) of the finest-scale simulations, and the fact that the same model code was used in the downscaling procedure from the global to the micro-scale. From an atmospheric modelling point of view, the CCAM simulations are satisfactory. To complete an ultra high-resolution climate simulation on a local computer cluster in South Africa within a reasonable time frame represents a huge leap for modelling capacity in the country. The simulations compared well observations at all the different spatial scales, although a number of model biases have been identified. Unfortunately the wine industry sometimes need more accuracy (e.g. simulated temperatures need to be within one degree Celsius of observations) for certain highly accuracy-sensitive studies. However, at this point in time there is not another dynamic model or statistical method available that can supply that kind of accuracy in a climate simulation at such a fine resolution in a computationally feasible way. However, it may be expected that through model improvements a higher accuracy ultra high-resolution climatology can be obtained in future. For CCAM, higher accuracy simulations may follow from using a nonhydrostatic version of the model, by improving the rainfall and moisture scheme (to address the underestimation of rainfall over the southwestern Cape), removing apparent biases from the boundary layer scheme (to remove the cold bias in simulating night time temperatures) and by improved nudging techniques. In their present form, the CCAM simulations have value to give a reasonable indication of the spatial variation in meso- and microscale climate over the southwestern Cape, and in particular the Stellenbosch wine region, at ultra high resolution. This should aid the wine industry to make more informed decisions when it comes to the interaction in climate and the location of vineyards.

Bibliography

[1] AGIS, 2007. Agricultural Geo-Referenced Information System, accessed from www.agis.agric.za on 22 April 2009

[2] American Meteorological Society (AMS), 1986: Glossary of Meteorology (1986) accessed from http://amsglossary.allenpress.com/glossary on 22 April 2009.

[3] Bonnardot V., Carey V.A., Strydom J., 2004: Weather stations: Applications for viticulture, Wynboer. http://www.wynboer.co.za/recentarticles/0405weather.php3

[4] Bonnardot V.M.F., Cautenet S., Du Preez C.B., Planchon O. & Cary V.A., 2002: Atmospheric Modeling: A tool to assess the sea breeze effect in the south-western Cape winegrowing area, Proc. 27th World congress of vine and wine, OIV, Bratislava, Slovakia, June 2002

[5] Carey V.A., Archer E. and Saayman D., 2002: Natural terroir units: What are they? How can they help the wine farmer?, Wynboer

[6] Cary V.A., Bonnardot V.M.F., Schmidt A., Theron J.C.D., 2003: The interaction between vintage, vineyard site (mesoclimate) and wine aroma of Vitis vinfera L.cvs, Sauvignon Blanc, Chardonnay and Cabernet Sauvignon in the Stellenbosch-Klein Drakenstein wine producing area, South Africa (1996-2000), Bulletin De L'OIV, 2003, 863-864.

[7] Champagnol F., 1984: Elements de Physiologie de la Vigne et de la Viticulture Generale, François Champagnol, Saint-Gely-du-Fesc, France, 351pp.

[8] Clarke R.H., 1955: Some observations and comments on the sea breeze, Australian Meteorological Magazine, 32, 207-226.

[9] Crimp S.J., Lutjeharms J.R.E. and Mason S.J., 1998: Sensitivity of a tropical-temperate trough to sea surface temperature anomalies in the Agulhas retroflection region, Water SA 24, 39-100.

[10] Crimp S.J., Van den Heever S.C., D'Abreton P.C., Tyson P.D. and Mason S.J., 1997: Mesoscale modelling of tropical-temperate throughs and

associated systems over southern Africa, WRC Report 595/1/97. Water Research Commision, Pretoria

[11] Christensen J.H., Hewitson B., Busuioc A., Chen A., Gao X., Held R., Jones R., Kolli R.K., Kwon W.K., Laprise R., Magana Rueda V., Mearns L., Menendez C. G., Räisänen J., Rinke A., Sarr A., Whetton P., 2007: Regional climate projections. In Climate Change, 2007: The Physical Science Basis. Contribution of working group I to the fourth assessment report of the intergovernmental panel on climate change, University press, Cambridge, Chapter 11, 847-940.

[12] Clarke O., 2001: Encyclopedia of Grapes, Harcourt Books, 2001, p 130 – 131, ISBN 0151007144 Du Preez C. B., 2006: A mesoscale investigation of the sea breeze in the Stellenbosch Winegrowing district, Msc Thesis, University of Pretoria, pp 98.

[13] Davies H.C., 1976: A lateral boundary formulation for multi-level prediction models, Quart. J. Roy. Met. Soc., 102, 405-418

[14] De Coning E. and Adam B.F., 2000: The tornadic thunderstorm events during the 1998-1999 South African summer, Water SA 26, 361-376.

[15] De Coning E., Adam B.F. and Banitz L., 2000: A severe weather event on 29 December 1997: synoptic and mesoscale perspectives, Water SA 26, 137-146.

[16] Defant F., 1951: Compendium of Meteorology, 655–672.

[17] Du Toit S. and Joubert S., 2005: Guidelines for Pinotage vineyards, Published by the Pinotage Association, PO Box 204, Stellenbosch 7599, South Africa, pp 16, www.pinotage.co.za

[18] Engelbrecht F.A., 2005: Simulations of climate and climate change over southern and tropical Africa with the conformal-cubic atmospheric model. In: Schulze, R.E. (Ed) Climate Change and Water Resources in Southern Africa: Studies on Scenarios, Impacts, Vulnerabilities and Adaptation. Chap. 4. Water Research Commission Report 1430/1/05

[19] Engelbrecht F.A., 2006: Theory and application of quasi-elastic equations in terrain following coordinates based on the full pressure field, Ph.D Thesis, University of Pretoria, South Africa.

[20] Engelbrecht F.A., McGregor J.L. and Engelbrecht C., 2009: Dynamics of the Conformal-Cubic Atmospheric Model projected climate change signal over southern Africa, Intl. J. Climatol., 29, 1013-1033.

[21] Engelbrecht F.A., McGregor J.L. and Rautenbach C.J.deW., 2007: On the development of a new atmospheric model in South Africa, South African Journal of Science, In Press.

[22] Engelbrecht F.A. and Rautenbach C.J.deW., 2000: Perspektief vir genestelde klimaatmodellering oor suidelike Afrika, Tydskrif vir Natuurwetenskap en Tegnologie, 19, no.2.

[23] Engelbrecht F.A., Rautenbach C.J. deW., McGregor J.L. & Katzfey J.J., 2002: January and July climate simulations over the SADC region using the limited-area model DARLAM. Water SA, 28, 361-374.

[24] Fox-Rabinovitz M., Côte J., Dugas B., Déqué M., McGregor J.L., 2006: Variable-Resolution GCMs: Stretched-Grid Model Intercomparison Project (SGMIP), J. Geophys. Res., 111, D16104, doi:10.1029/2005JD006520.

[25] Fu C., Wang S., Xiong Z., Gutowski W.J., Lee D.-K., McGregor J.L., Sato Y., Kato H., Kim J.-W. and Suh M.-S. 2005: Regional Climate Model Intercomparison Project for Asia. Bull. Amer. Meteor. Soc., 86, 257-266.

[26] Gazendam A.D., 2008: Building and refining general purpose computing clusters in an emerging HPC oriented research environment, in Proc. of the 22nd International Symposium on High Performance Computing Systems and Applications (HPCS 2008), Quebec City, Canada, 2008, ISBN 978-0-7695-3250-9 (CD).

[27] Gladstones J., 1992: Viticulture and environment, Winetitles, Adelaide, 310pp.

[28] Gordon, H.B., Rotstayn L.D., McGregor J.L., Dix M.R., Kowalczyk E.A., O'Farrell S.P., Waterman L.J., Hirst A.C., Wilson S.G., Collier M.A., Watterson I.G. and Elliott T.I., 2002: The CSIRO Mk3 Climate System Model, CSIRO Atmospheric Research technical paper, 60, 130pp.

[29] Grogan T., 2001: The concept of terroir and wine composition: correlating soil and topography with organoleptic properties of wine, Ven124/Spring 2001 Research Report, UC Davis University of California, http://listproc.ucdavis.edu/archives/ven124-1/log0107/att-0004/04-Grogan_Terroir_Research_Report.doc

[30] Giorgi F. and Mearns, L.O., 1991: Approaches to the simulation of regional climate change: A review, Rev. Geophys., 29, 191-216.

[31] Hamilton R.P., 1989: Wind and its effects on viticulture, Austr. Grapegr. Winemaker, March 16-17.

[32] Happ E., 1999: Indices for exploring the relationship between temperature and grape and wine flavour, The Australian and New Zealand Wine Industry Journal, 14, 4, 1-6.

[33] Hansingo K. and Reason C.J.C., 2006: Sensitivity of the atmospheric response to sea-surface temperature forcing in the South West Indian Ocean: a regional climate modelling study, South African Journal of Science, 102, 137-143.

[34] Hewitson B.C., Crane R.G., 2006: Consensus between GCM climate change projections with empirical downscaling: precipitation downscaling over South Africa, Int. J. Climatol. 26: 1315–1337

[35] Hope P.k., Nicholls N and McGregor J.L., 2004: The rainfall responce to permanent inland water in Australia, Australian Meteorological Magazine 53, 251-262.

[36] Joubert A.M., Katzfey J.J., McGregor J.L. and Nguyen K.C., 1999: Simulating mid-summer climate over southern Africa using a nested regional climate model, J. Geophys. Res. 104, 19015-19025.

[37] Joubert S.J., 2007: High resolution climate variable generation for the Western Cape. MSc thesis, University of Stellenbosch. In review.

[38] Kalnay E., Kanamitsu M., Kistler R., Collins W., Deavan D., Gandin L., Iredell M., Saha S., White G., Woollen J., Zhu Y., Chelliah M., Ebisuzaki W., Higgens W., Janowiak J., Mo K.C., Ropelewski C., Wang J., Leetmaa A., Reynolds R., Jenne R., and Joseph D., 1996: The NCEP/NCAR 40-year reanalysis project, Bull. Amer. Meteorol. Soc., 77, 437-472.

[39] Kistler R., Kalnay E. and Collins W., 2001: The NCEP-NCAR 50-year reanalysis; Monthly means CD-ROM and documentation, Bulletin of American Meteorology Society 82(2): 247-267.

[40] Kleynhans T.E. and Opperman J.M., 2005: Determination of priorities of buyers regarding value contributing characteristics of farm land in the Stellenbosch district, South Africa, Agrekon, vol. 44, no 4, p 496 – 510.

[41] Kruger A.C., 2004: Climate of South Africa, Climate Regions, WS45, South African Weather Service, Pretoria, South Africa.

[42] Kruger A.C., 2006: Observed trends in daily precipitation indices in South Africa: 1910-2004, Int. J. Climatol., 26, 15, 2275-2285

[43] Kruger A. C., and Shongwe S., 2004: Temperature trends in South Africa: 1960–2003, Int. J. Climatol., 24, 1929– 1945.

[44] Lal M., McGregor J.L. and Nguyen K.C., 2008: Very high resolution climate simulationover Fiji using a global variably resolution model, Climate Dynamics 30, 293-305.

[45] LaMar, J., 2002: Professional Friends of Wine, Professional Friends of Wine, 642 West Harvard, Fresno, CA 93705, Retrieved on 2007-06-25 http://www.winepros.org/wine101/grape_profiles/chenin.htm

[46] LaMar, J., 2003: Professional Friends of Wine, Professional Friends of Wine, 642 West Harvard, Fresno, CA 93705, Retrieved on 2007-07-10 http://www.winepros.org/wine101/grape_profiles/

[47] LaMar, J., 2005: Professional Friends of Wine, Professional Friends of Wine, 642 West Harvard, Fresno, CA 93705, Retrieved on 2007-07-10 http://www.winepros.org/wine101/grape_profiles/

[48] Landman W.A., Botes S., Goddard L. and Shongwe M.E., 2005: Assessing the predictability of extreme rainfall seasons over southern Africa, Geophys. Res. Lett. 32, L23818, doi:10.1029/2005GL023965.

[49] MacKellar N.C., Tadross M.A. and Hewitson B.C., 2008: Effects of vegetation map change in MM5 simulations of southern Africa's summer climate, Int. J Clim., 29, 6, 885 - 898

[50] New, M., Hulme, M. and Jones, P.D., 1999: Representing twentieth century space-time climate variability. Part 1: development of a 1961-90 mean monthly terrestrial climatology. Journal of Climate 12, 829-856

[51] New M., Lister D., Hulme M. and Makin I., 2002: A high-resolution data set of surface climate over global land areas. Climate Research 21:1-25

[52] McGregor J.L., 1997: Regional Climate Modelling, Meteorol. Atmos. Phys. 63, 105-117

[53] McGregor J.L., 2005: C-CAM: Geometric aspects and dynamical formulation. Technical Report 70, CSIRO Atmospheric Research, 43 pp.

[54] McGregor J.L. & Dix M.R., 2001: The CSIRO conformal-cubic atmospheric GCM. IUTAM Symposium on Advances in Mathematical Modelling of Atmosphere and Ocean Dynamics, P.F. Hodnett, Ed., Kuwer, 197-202.

[55] McGregor J.L. & Nguyen K.C., 2003: Simulations of the East Asian and Australian monsoons using a variable-resolution model, Proceedings of the 2nd Workshop on Regional Climate Modeling for Monsoon System, GAME Publication No 39, Yokohama, March 2003, 117-120.

[56] McGregor J.L., Nguyen K.C. and Katzfey J.J., 2002: Regional climate simulations using a stretched-grid global model. Research Activities in Atmospheric and Oceanic Modelling Report No. 32 (ed. H. Ritchie), WMO/TD-No. 1105, 3. 15–3. 16.

[57] McGregor J.L., Walsh K.J. and Katzfey J.J., 1993: Nested Modelling for Regional Climate Studies, Modelling Change in Environmental Systems, Jakeman A.J. et. al. (eds), John Wiley, 367-386.

[58] Moran W., 2001: Terroir – the human factor, Proceedings of the Pinot Noir New Zeeland 2001Conference, 25-28 January 2001, Michael Flower Centre, Wellington.

[59] Nunez M and McGregor J.L., 2007: Modelling future water environmnets of Tasmania, Australia, Climate Research 34, 25-37.

[60] Olwoch J.M., Rautenbach C.J.de W., Erasmus B.F.N., Engelbrecht F.A. and van Jaarsveld A.S., 2003: Simulating tick distributions over sub-Saharan Africa: the use of observed and simulated climate surfaces, Journal of Biography, 30, 1221-1232.

[61] Olwoch J.M., Reyers B., Engelbrecht F.A. and Erasmus B.F.N. 2007: Climate change and the tick-borne disease, Theileriosis (East Coast fever) in sub-Saharan Africa. Journal of Arid Environments. In press.

[62] Potgieter C.J., 2006: Accuracy and skill of the Conformal-Cubic Atmospheric Model in short range weather forecasting in South Africa, Msc Thesis, University of Pretoria, pp 172.

[63] Rancic M., Purser R.J. and Mesinger F., 1996: A global shallow-water model using an expanded spherical cube: Gnomic versus conformal coordinates, Quart. J. Roy. Meteor. Soc., 122, 959-982.

[64] Rautenbach C.J. deW., Engelbrecht F.A., Engelbrecht C.J., Ndarana T. and McGregor J.L., 2005: Regional model development for simulating atmospheric behavior and rainfall over southern Africa. Water Research Commission Report 1261/1/05, 121 pp. Water Research Commission, Pretoria.

[65] Reason C.J.C., Engelbrecht F., Landman W.A., Lutjeharms J.R.E., Piketh S., Rautenbach C.J.de W. and Hewitson B.C., 2006: A review of South African research in atmospheric science and physical oceanography during 2000 – 2005, South African Journal of Science, 102, 35-45.

[66] Reason C.J.C. and Jagadheesha D., 2005: Relationships between South Atlantic SST variability and atmospheric circulation over the South African region during austral winter, Journal of Climate 18, 3059-3075.

[67] Riphagen H.A., 1984: The implementation of a split explicit weather prediction model for the Southern Hemisphere, M.Sc. dissertation, University of Pretoria, South Africa.

[68] Riphagen H.A. and Burger A.P., 1986: Comments on the computational stability of Gadd's adjustment and advections schemes in a numerical weather prediction model, Q. J. R. Met. Soc. 112, 276–282.

[69] Riphagen H.A. and Van Heerden J., 1986: Comparative trials of a semi-Lagrangian advection scheme in a numerical weather prediction model. In Proc. 12th South African Symposium on Numerical Mathematics, Umhlanga Rocks, pp. 139–153.

[70] Rivest C., Staniforth A. and Robert A., 1994: Spurious resonant response of semi-Lagrangian discretizations to orographic forcing: Diagnosis and solution, Mon. Wea. Rev., 122 366-376.

[71] Robinson J., 1986: Vines, Grapes & Wines, Mitchell Beazley, 1986, pp 280, ISBN 1-85732-999-6

[72] Robinson J., 1996: Guide to Wine Grapes, Oxford University Press, 1996, Oxford, New York.

[73] Robinson J., 1999: Jancis Robinson's wine course, BBC Worldwide Ltd, London, ISBN 0 563 55131 3

[74] Robinson J., 2006: The Oxford Companion to Wine (3rd Ed.), Oxford University Press, ISBN 0-19-860990-6

[75] Roberts D., 1999: From soil to glass, 1999 Bragato Address, 5th Annual Conference of New Zealand Grape Growers Council, Auckland, New Zealand, August 1999

[76] Rotstayn, L.D., 1997: A physically based scheme for the treatment of stratiform clouds and precipitation in large-scale models. I: Description and evaluation of the microphysical processes. Q. J. R. Meteorol. Soc., 123, 1227-1282.

[77] Saayman D., 2003: The South African vineyard and wine landscapes: Heritage and development, International Symposium on Landscapes of vines and wines, Loire Valley, 2 - 4 July 2003, Wynboer. http://www.wynboer.co.za/recentarticles/0405landscape.php3

[78] S A Wine Industry Information &Systems, 2007: South African Wine Industry Statistics, Paarl, South Africa. www.sawis.co.za

[79] South African Weather Service (SAWS), 2003: Climate Data (1961-1990) for Cape Town, extracted from SAWS website on 22 April 2009 http://www.weathersa.co.za/Climat/Climstats/CapeTownStats.jsp

[80] Schmidt F., 1977: Variable fine mesh in spectral global model, Beitr. Phys. Atmos., 50, 211-217.

[81] Schulze G.C., 1996: The weather and climate of the extreme south-western Cape, South African Weather Bureau, Department of Environmental Affairs and Tourism.

[82] Schulze R.E., 1997: South African Atlas of Agrohydrology and –Climatology, Water Research Commission, Pretoria, Report TT82/96.

[83] Schulze R.E., 2007: Updated South African Atlas of Agrohydrology and –Climatology, Water Research Commission, Pretoria. In press.

[84] Singleton A.T. and Reason C.J.C., 2006: Numerical simulations of a severe rainfall event over the Eastern Cape coast of South Africa: sensitivity to sea surface temperature and topography, Tellus 58A, 355-367.

[85] Smart R.E., 2002.: New world responses to old world terroir, Australian and New Zealand Wine Industry Journal, The Institute of Masters of Wine, ©1999 -2007, http://www.masters-of-wine.org/Resources/CoursePDF/Session2-1.pdf

[86] Smith L., 2002: Site selection for establishment & management of vineyards, Proceedings of the 14th Annual Colloquium of the Spatial Information Research Centre, University of Otago, Dunedin, New Zealand, 3-5 December 2002.

[87] Smith L. & Whigham P., 1999: Spatial aspects of vineyard management and wine grape production, Proceedings of the 11th Annual Colloquium of the Spatial Information Research Centre, University of Otago, Dunedin, New Zealand, 13-15 December 1999.

[88] South African Weather Service (SAWS), 2009: Climate Data (1961-1990) for Cape Town, extracted from SAWS website on 22 April 2009 http://www.weathersa.co.za/Climat/Climstats/CapeTownStats.jsp

[89] Schwarzkopf, M. D., and Fels S.B., 1991: The Simplified Exchange Method Revisited: An Accurate, Rapid Method for Computation of Infrared Cooling Rates and Fluxes, J. Geophys. Res., 96(D5), 9075–9096.

[90] Tadross, M.A., Gutowski W.J. Jr., Hewitson B.C., Jack C.J., New M., 2006: MM5 simulations of interannual change and the diurnal cycle of southern African regional climate. Theoretical and Applied Climatology, 86, 63-80. DOI 10.1007/s00704-005-0208-2

[91] Tadross M.A., Jack C. & Hewitson B.C. 2005: On RCM-based projections of change in southern African summer climate. Geophys. Res.Lett. 32, L23713, doi: 10.1029/2005GL024460.

[92] Taljaard J.J., 1967: Development, Distribution and Movement of Cyclones and Anticyclones in the Southern Hemisphere During the IGY. J. Appl. Meteor., 6, 973–987.

[93] Tennant W., 2004: Considerations when using pre-1979 NCEP/NCAR reanalyses in the southern hemisphere, Geophys. Res. Lett., 31, L11112, doi:10.1029/2004GL019751.

[94] Triegaardt D.O., 1965: The application of dynamic methods of weather prediction to the South African forecasting problem: a progress report, South African Weather Bureau News Letter, No 201, 187-188.

[95] Tyson, P.D. and Preston-Whyte R.A., 2000: The Weather and Climate of Southern Africa, 2nd edition, Oxford University Press South Africa, Cape Town, ISBN 0195718062.

[96] Van Leeuwen C., Friant P., Chone X., Tregoat O., Koundouras S. & Dubourdieu D., 2004: Influence of climate, soil and cultivar on terroir, American Journal of Enology and Viticulture, 55 (3), 207-217.

[97] Van Rooy M.P., 1936: Influence of berg winds on the temperatures along the west coast of South Africa, Published Online: 10 Sep 2007, The Quarterly Journal of the Royal Meteorological Society Volume 62 Issue 267, Pages 528 - 537

[98] Wang Y., Leung R.L., McGregor J.L., Lee D.K., Wang W.C., Ding Y. & Kimura F., 2004: Regional Climate Modelling: Progress, Challenges and Prospects, Journal of the Meteorological Society of Japan, 82, 6, 1599-1629.

[99] Winetech, 2007: Wine Grape Terroir Research Programme, Research Abstracts booklet for the South African Wine Industry, © Winetech 2007.

[100] Winkler A.J., Cook J.A., Kliewer W.M. and Lider L.A., 1974: General Viticulture, 2nd ed. University of California Press, California, 710 pp.